中尺度氣象學

(Mesoscale Meteorology)

授課老師: 游政谷

Cheng-Ku Yu

Mesoscale(3): Concept of Atmospheric Convection

Mesoscale(4): Mesoscale Convective Systems

Consider an isolated body of density ρ_1 immersed in a fluid of density ρ_2

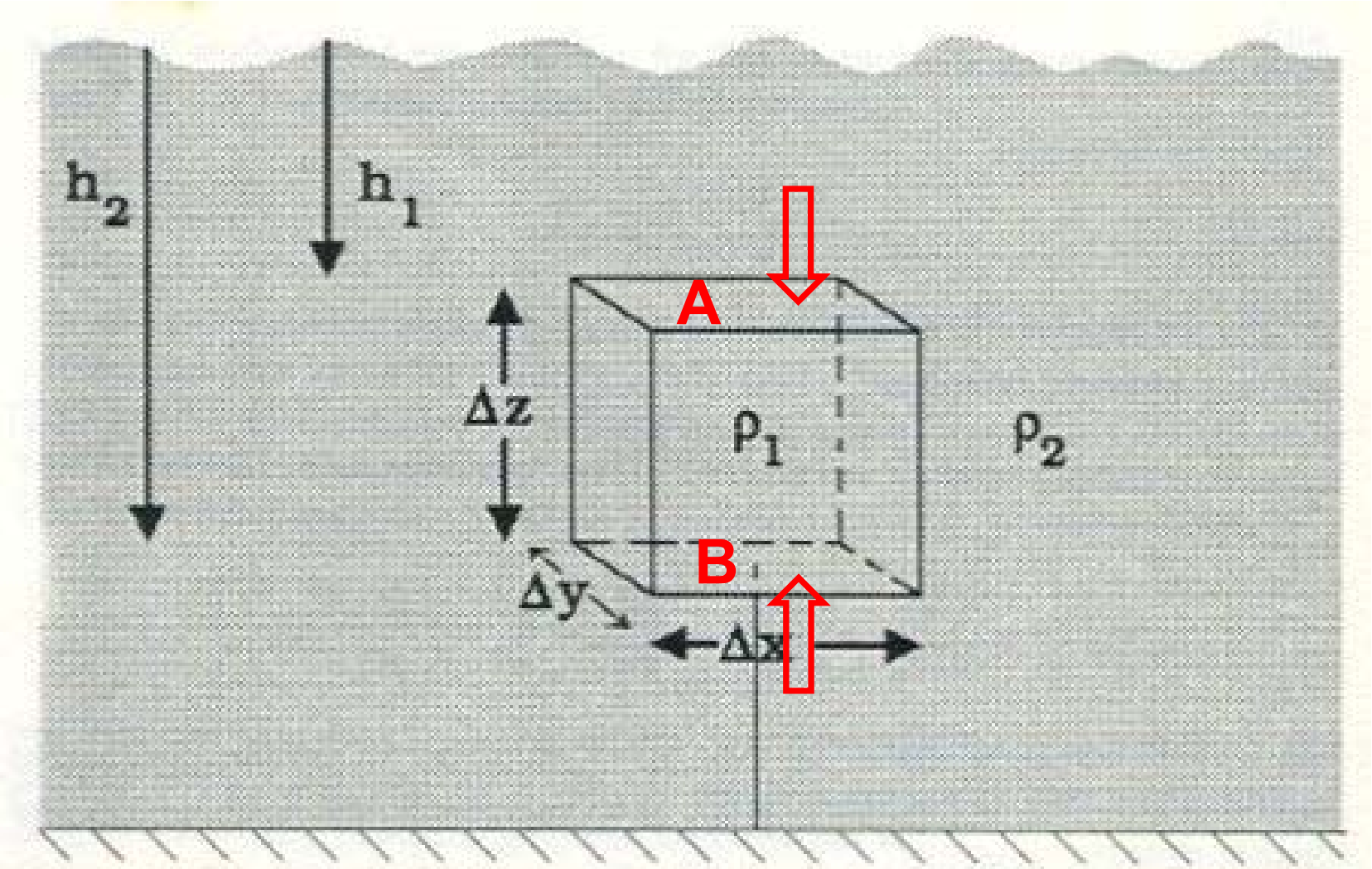

Fig. 1.1 Buoyancy force acting upon a submerged body.

Hot air ballon

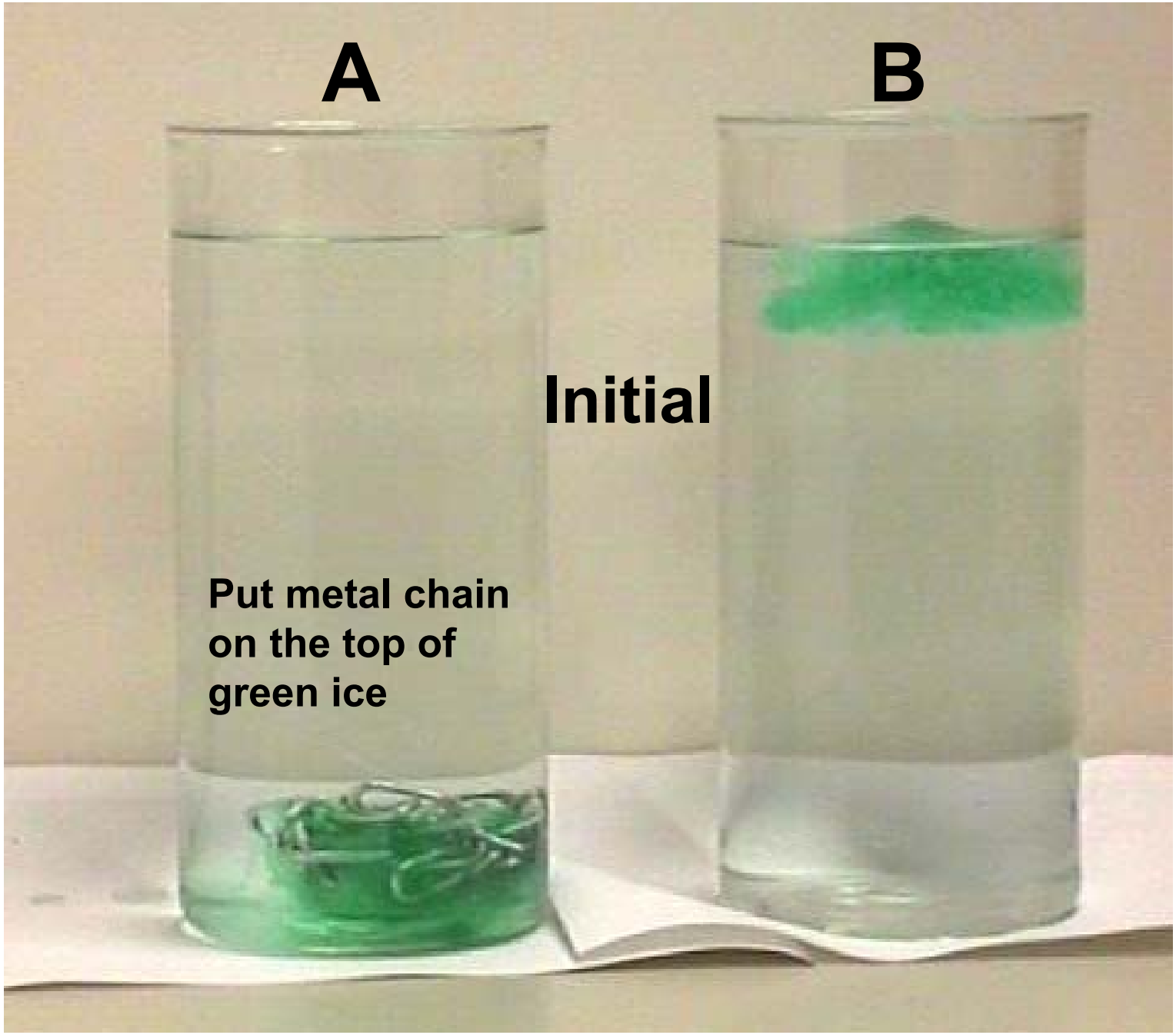
A
B
Initial
Put metal chain on the top of green ice

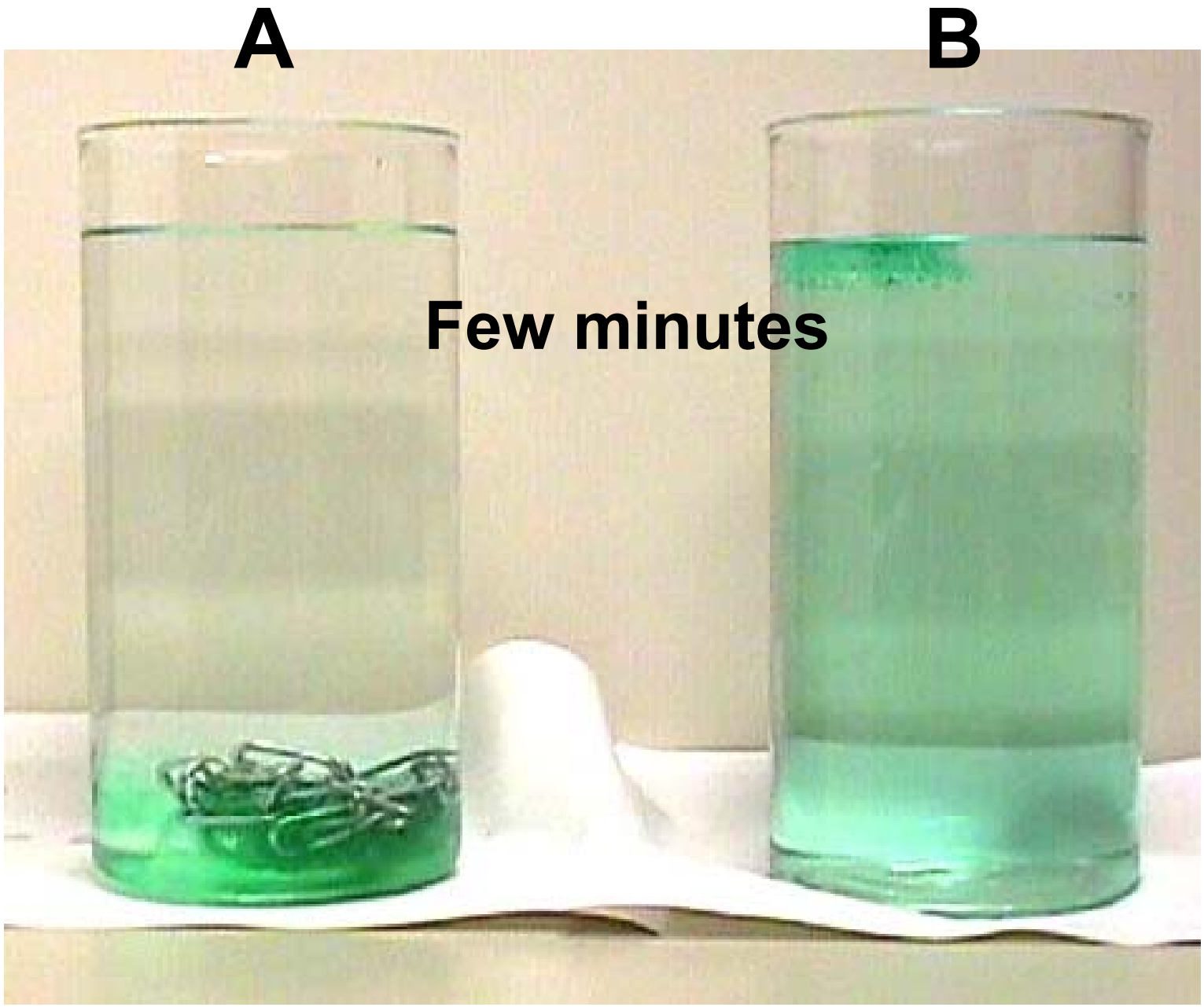
A
B
Few minutes

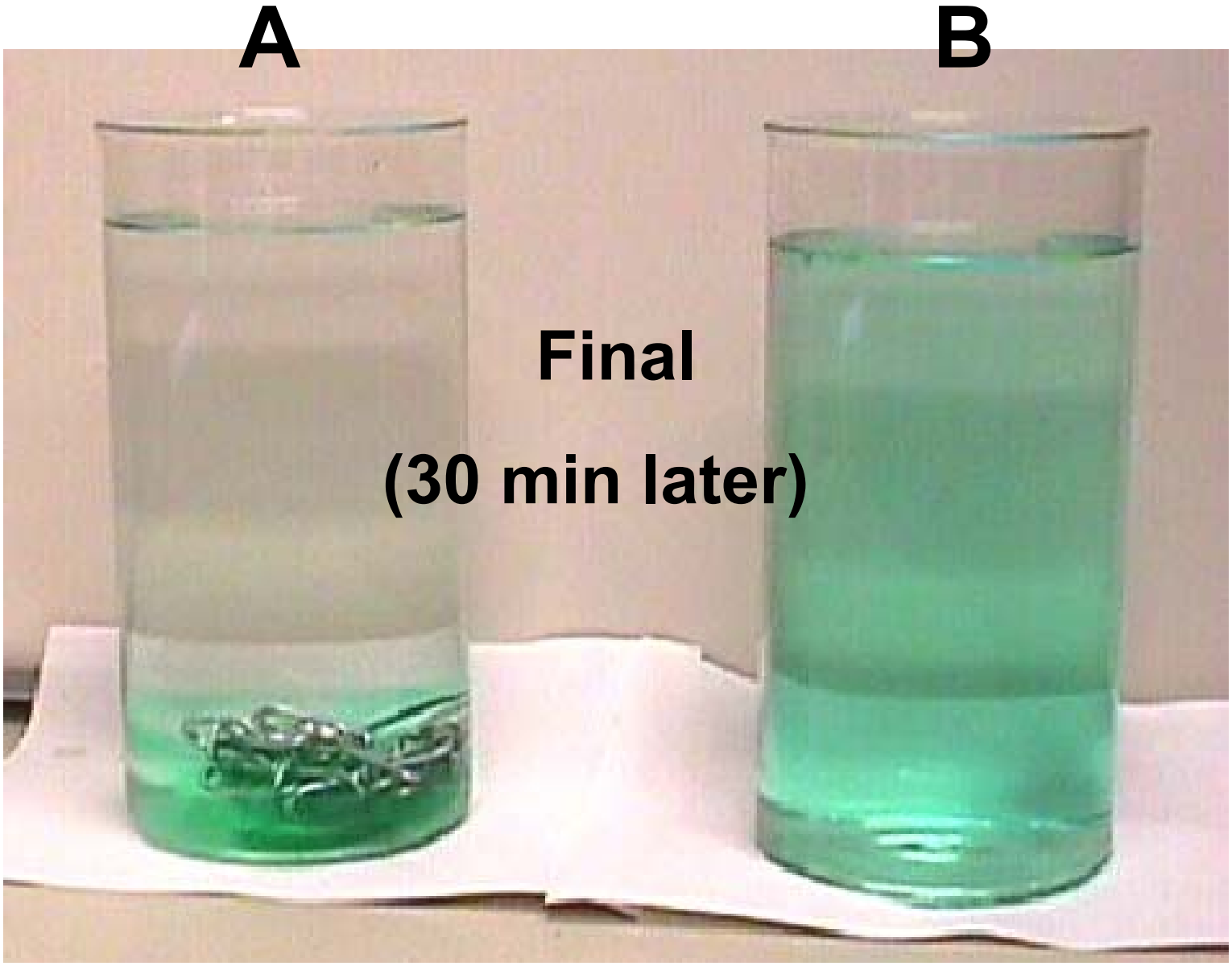
A
B
Final
(30 min later)

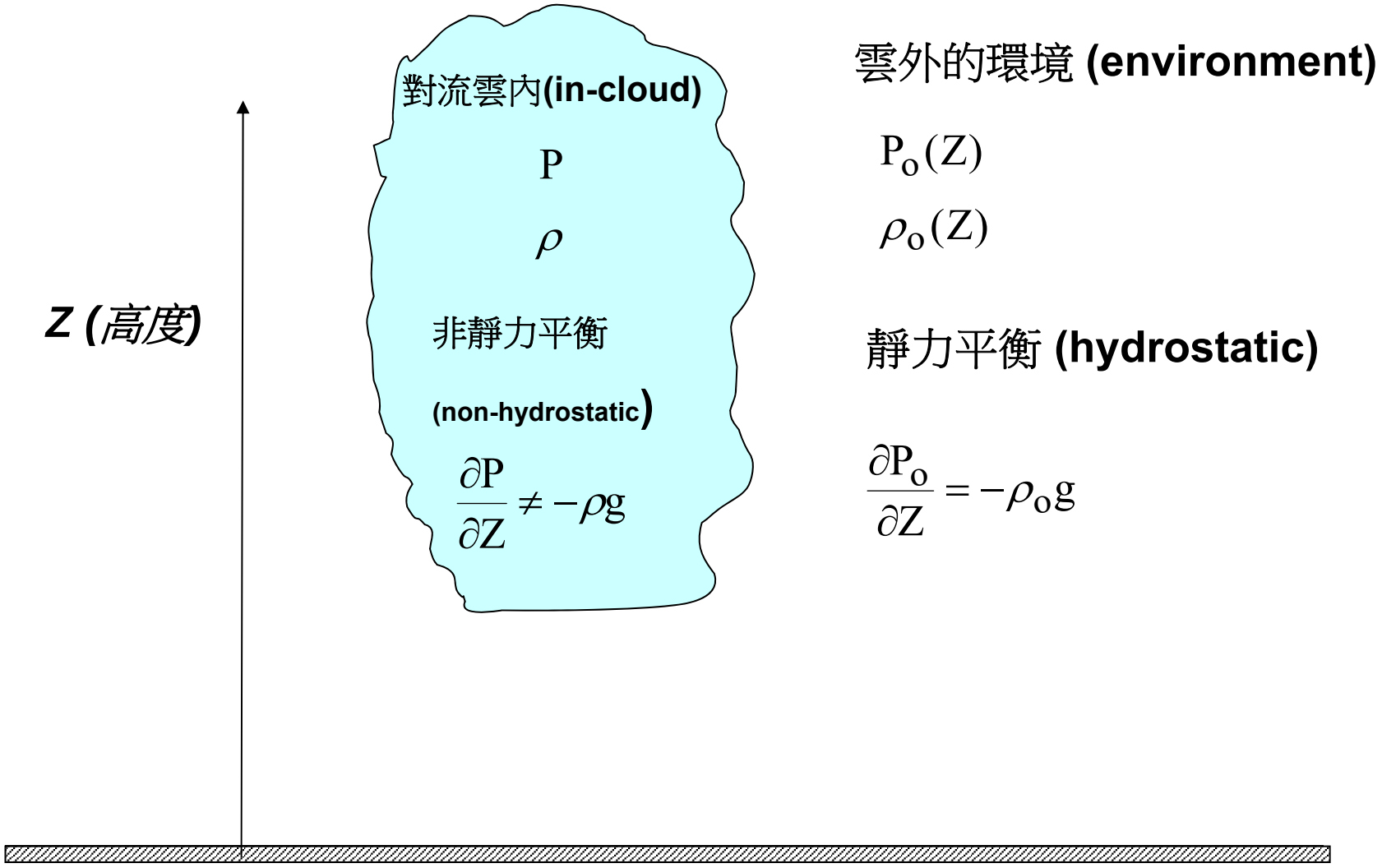
對流雲內(in-cloud)
P
ρ
非靜力平衡
(non-hydrostatic)
∂P/∂Z ≠ −ρg
Z (高度)
雲外的環境 (environment)
P_o(Z)
ρ_o(Z)
靜力平衡 (hydrostatic)
∂P_o/∂Z = −ρ_o g

實際探空觀測斜溫圖 (Skew T - log P diagram)

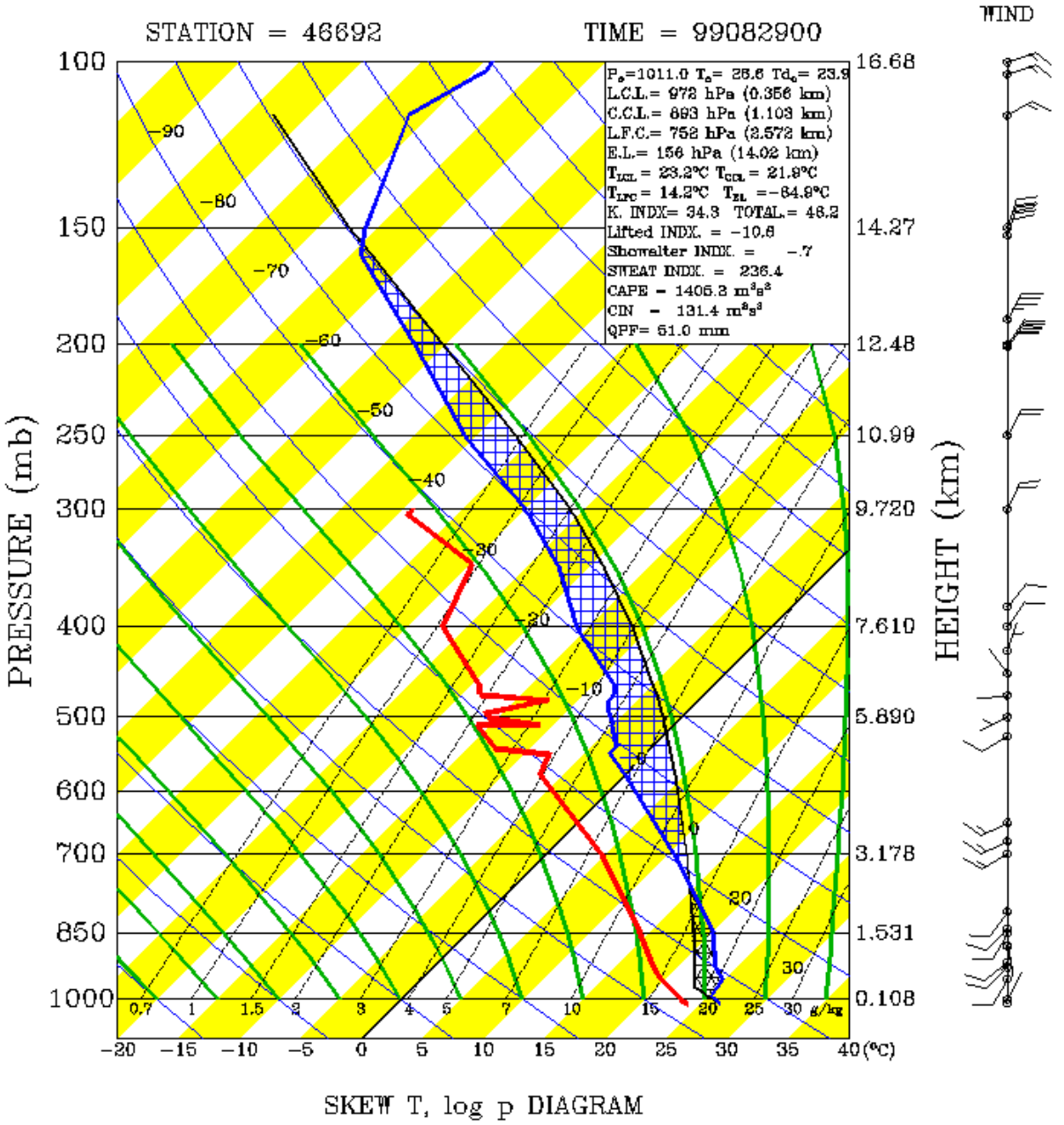

環境溫度線 (藍線)

(T, blue curve)

環境露點溫度線 (紅線)

(Td, red curve)

地面空氣塊絕熱舉升 (黑線)

(air parcel, black curve)

Compensating downward motions (D1 and D2) adjacent to the major updraft (U) (Yu and Jou 2005, MWR)

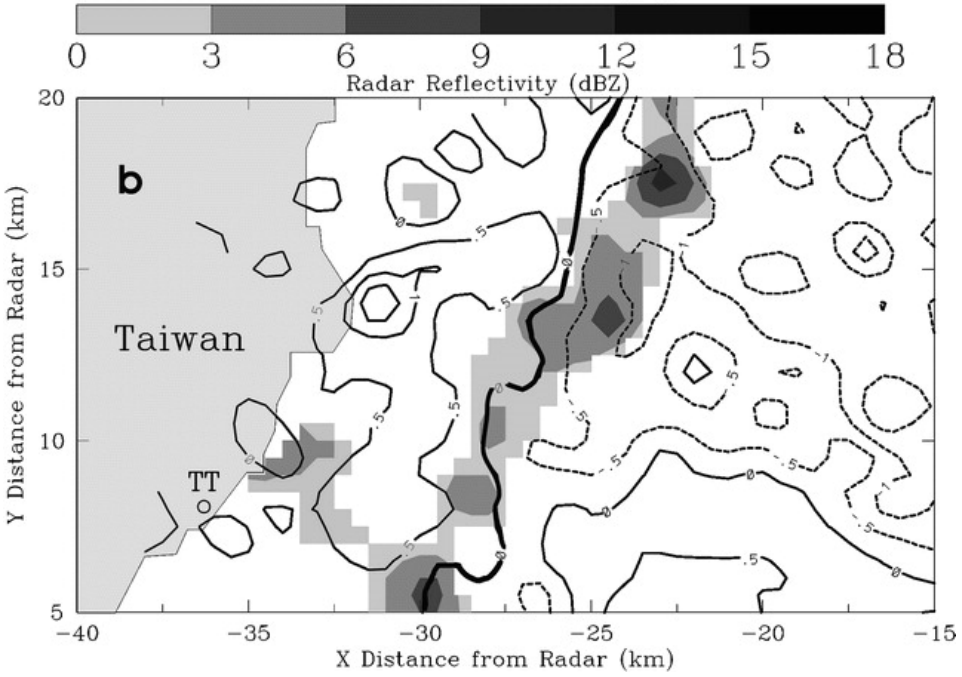

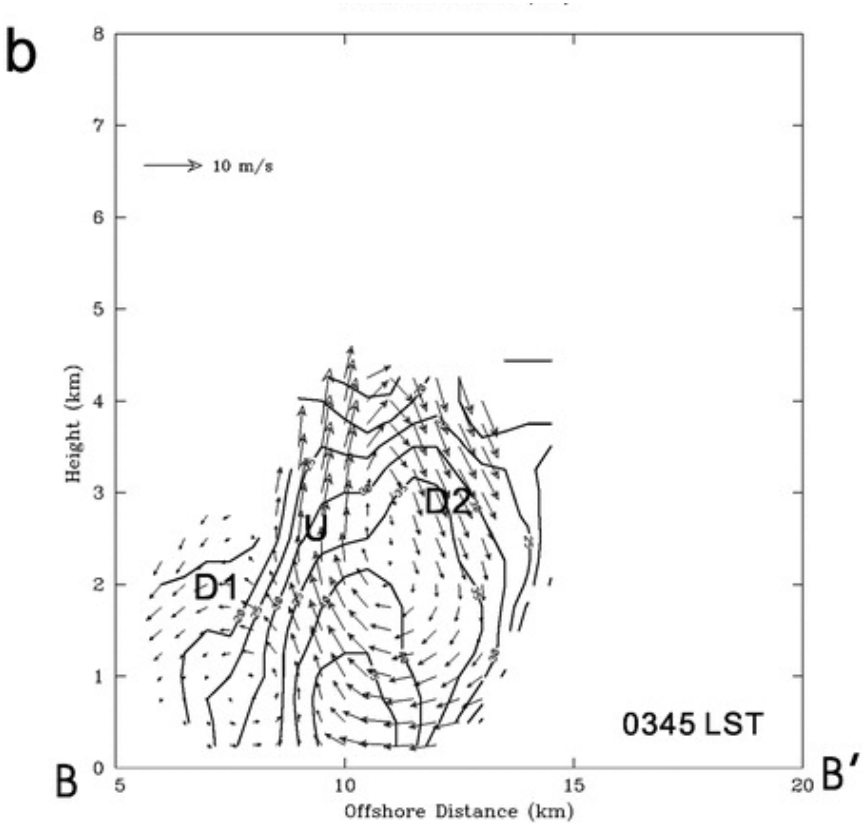

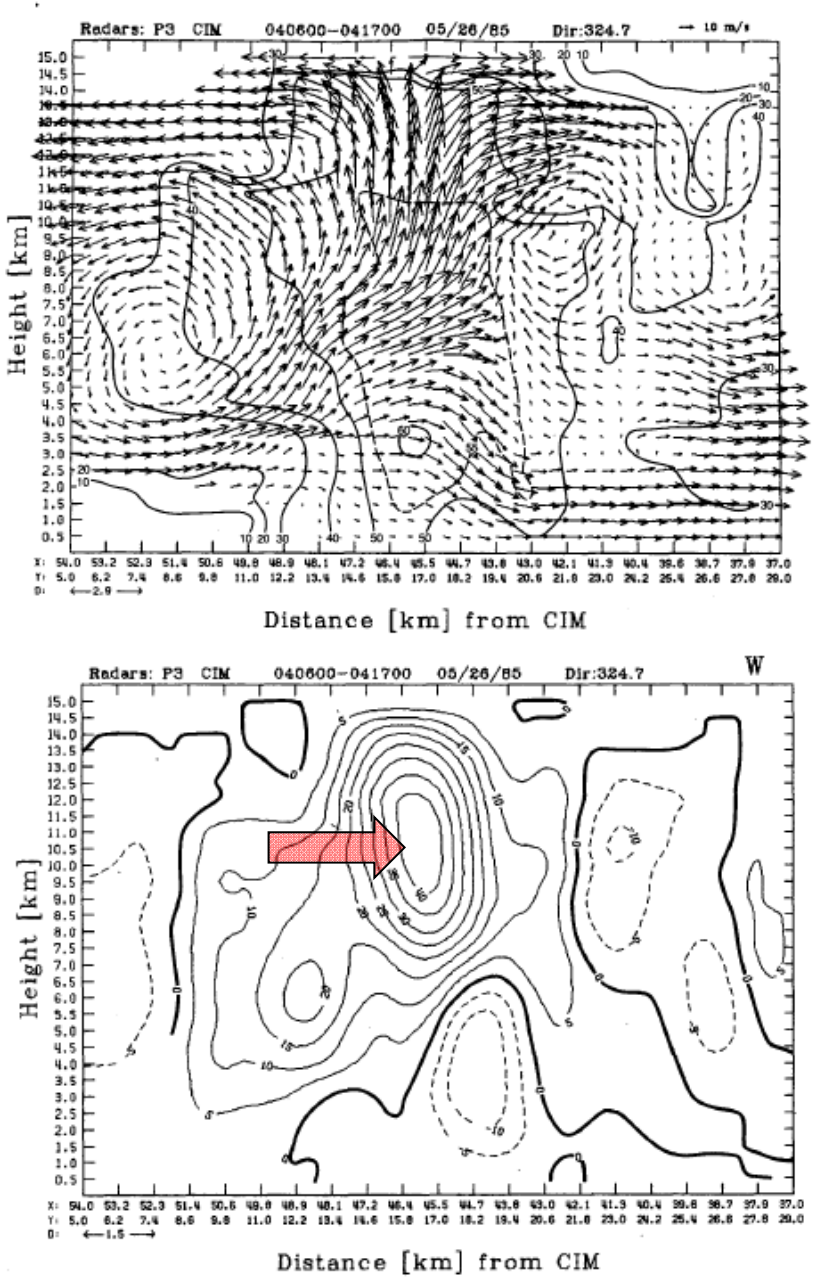

FIG. 11. As in Fig. 10, except for the NRO-CIM synthesis.

Perhaps the strongest updraft (> 40 m s^{-1}) seen from dual-Doppler Observations for a supercell case (Ray and Jorgensen 1988)

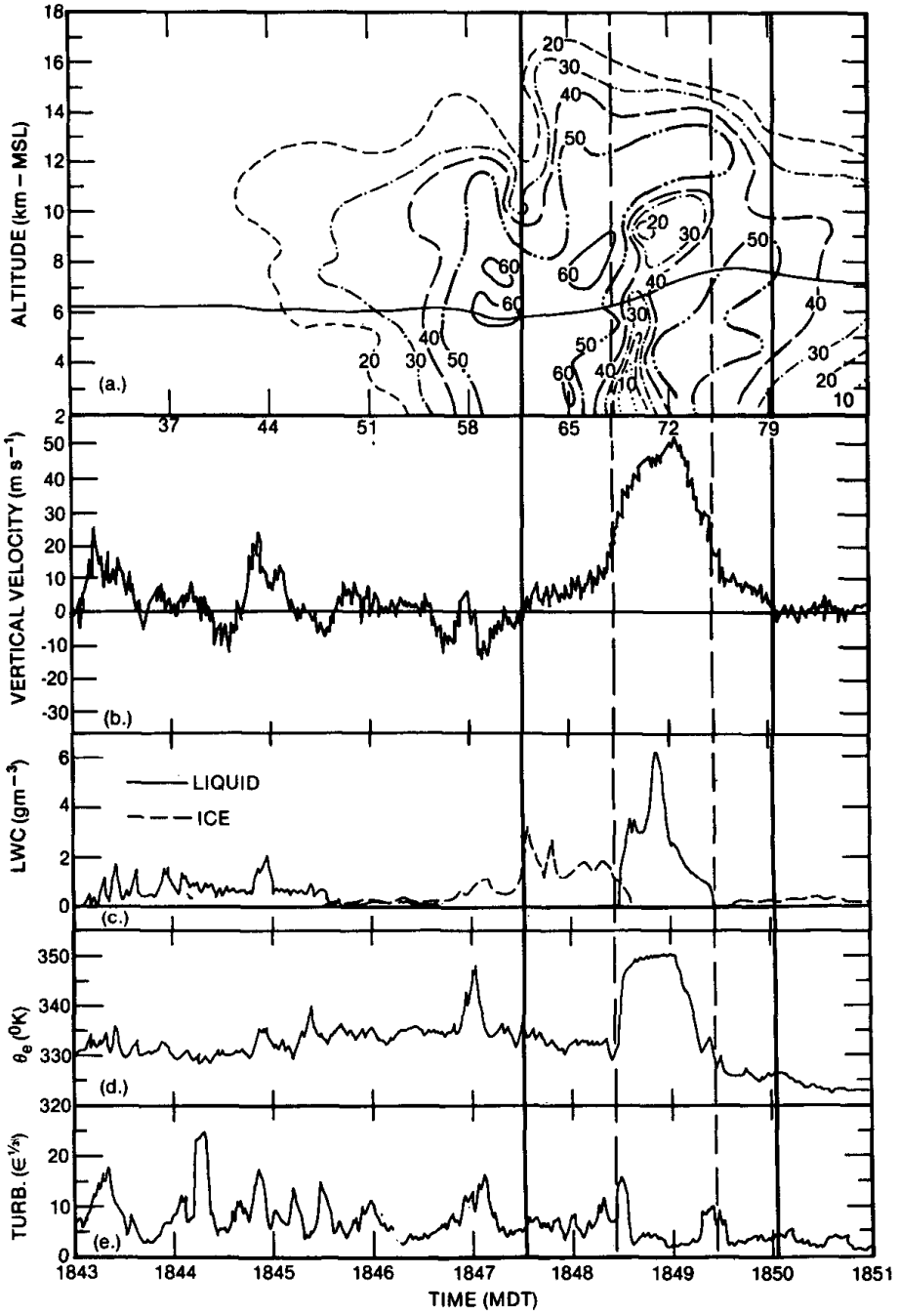

Perhaps the strongest updraft (50 m s^{-1}) seen from in-situ observations (Musil et al. 1986)

Various effects contributing to the pressure perturbation (Jorgensen et al. 1991)

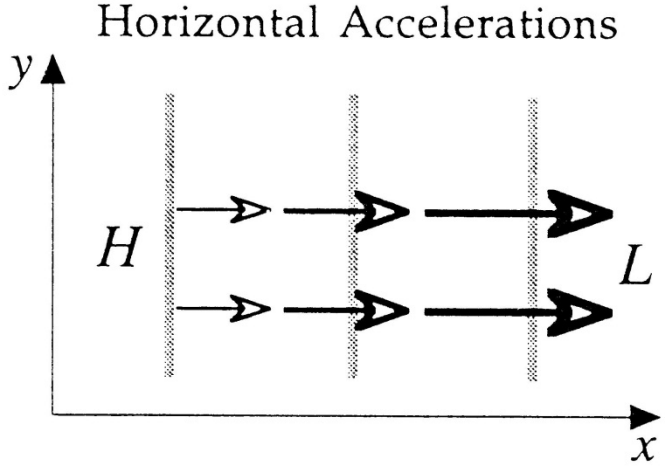

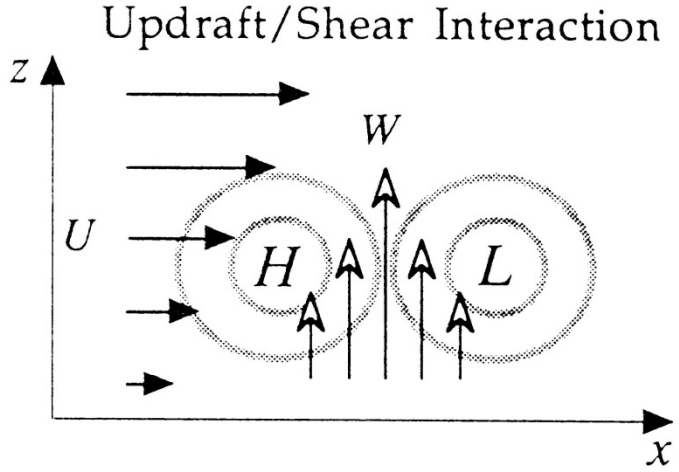

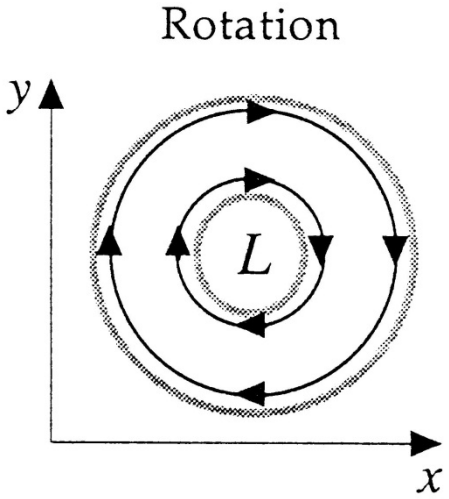

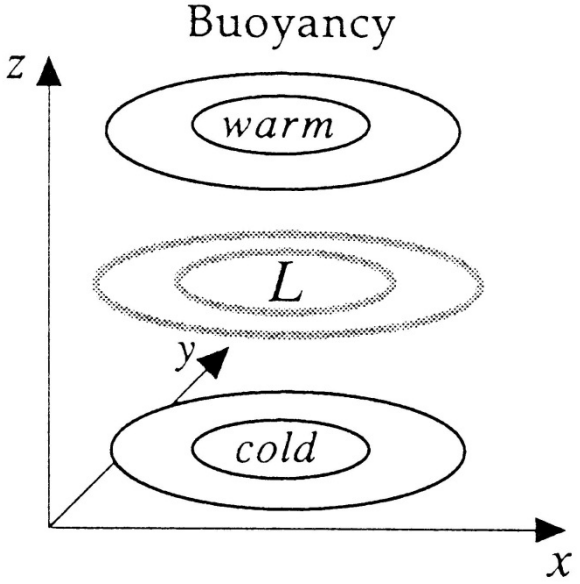

$$\nabla^2 p' \propto -2\rho_0 \left(\frac{\partial w}{\partial x}\frac{\partial u}{\partial z} + \frac{\partial w}{\partial y}\frac{\partial v}{\partial z} \right)$$

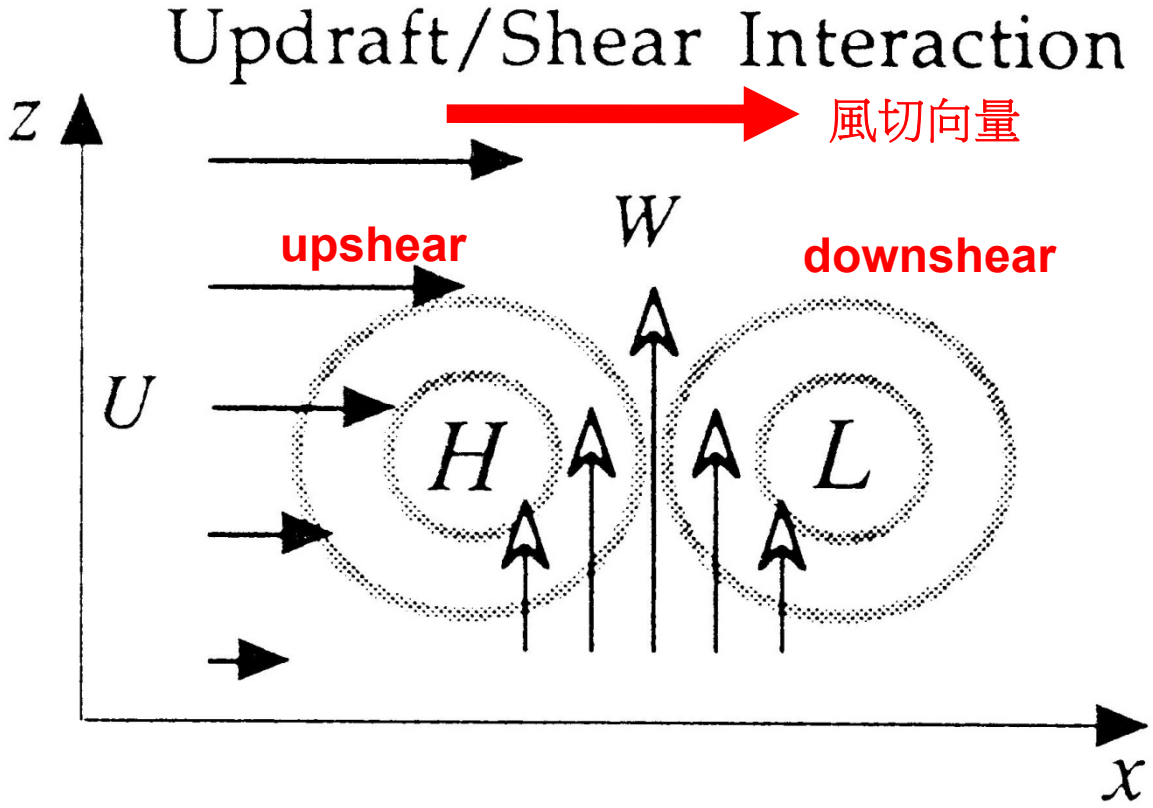

$$\frac{\partial w}{\partial x}\frac{\partial u}{\partial z}$$

風切向量

(shear vector)

$$\vec{s} \equiv \frac{\partial u}{\partial z}\hat{i} + \frac{\partial v}{\partial z}\hat{j}$$

$$\frac{\partial w}{\partial x}\frac{\partial u}{\partial z} + \frac{\partial w}{\partial y}\frac{\partial v}{\partial z} = \vec{s} \cdot \nabla w$$

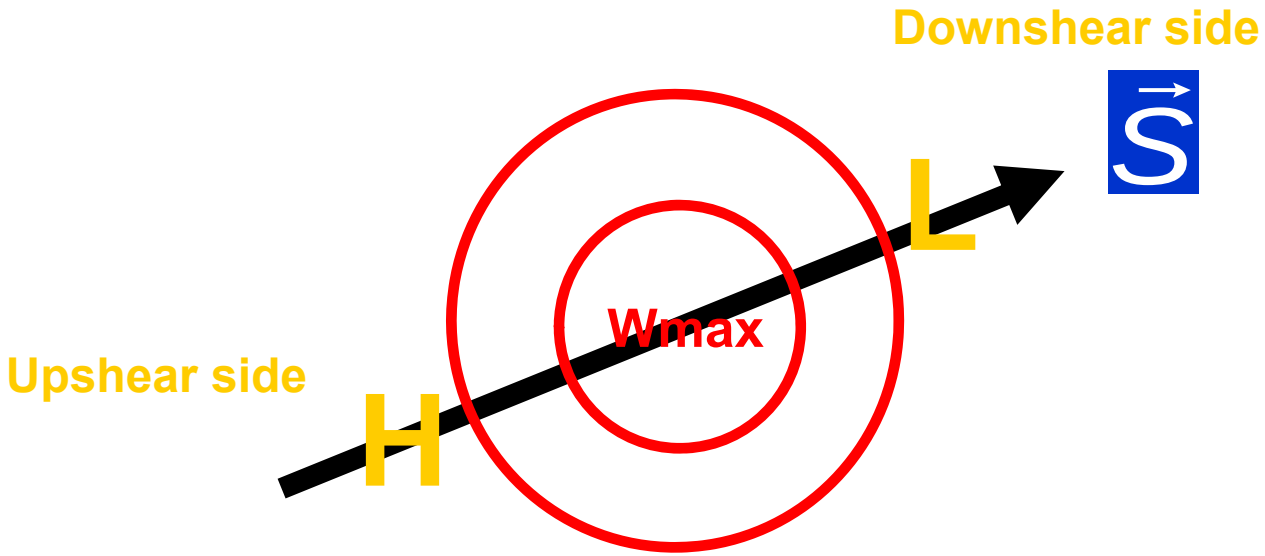

Hodography of environmental wind for a TAMEX convective line (Yu et al. 2001)

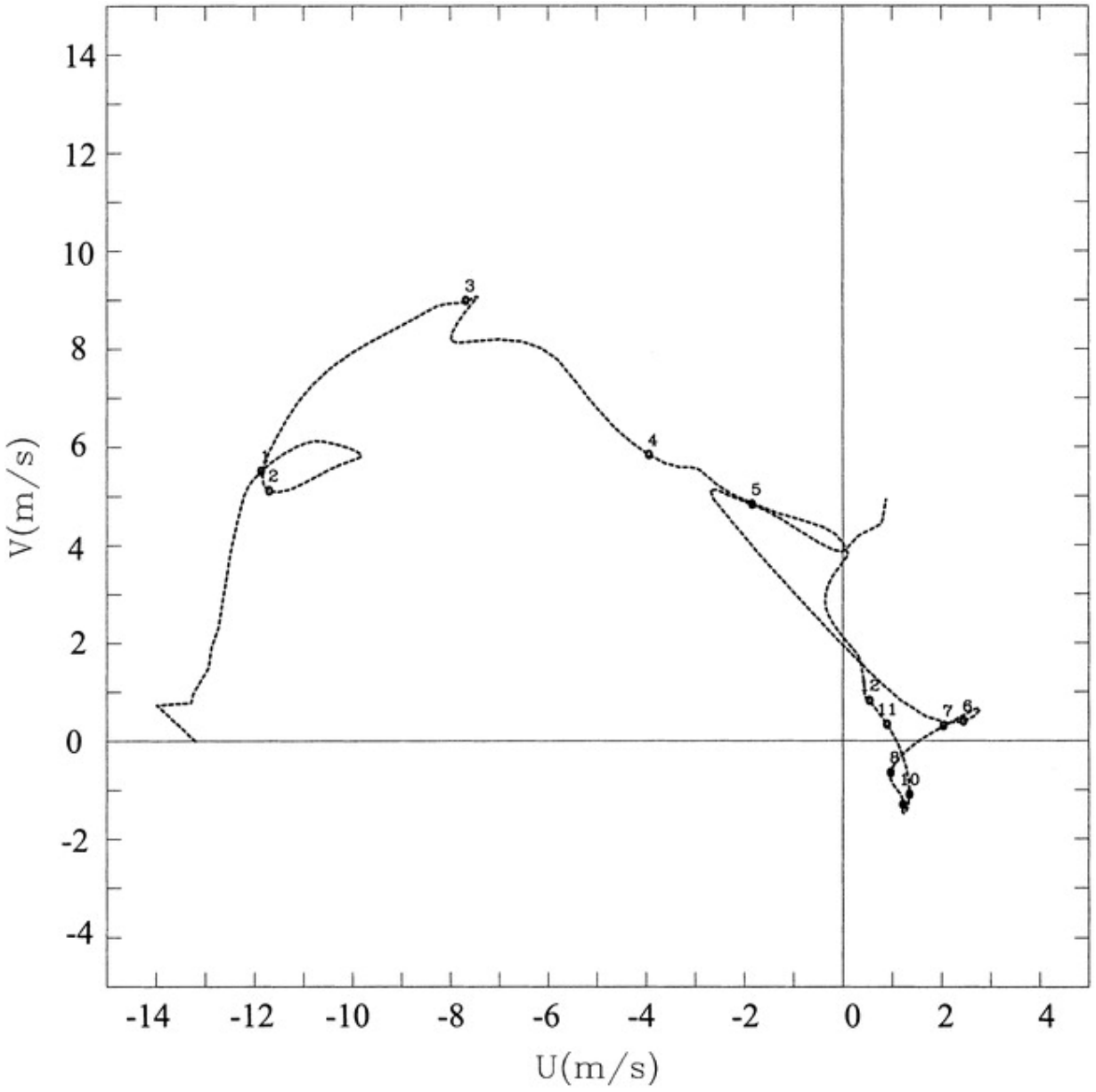

Kinematic and retrieval fields of the TAMEX convective line at 5.5 km (MSL) (Yu et al. 2001)

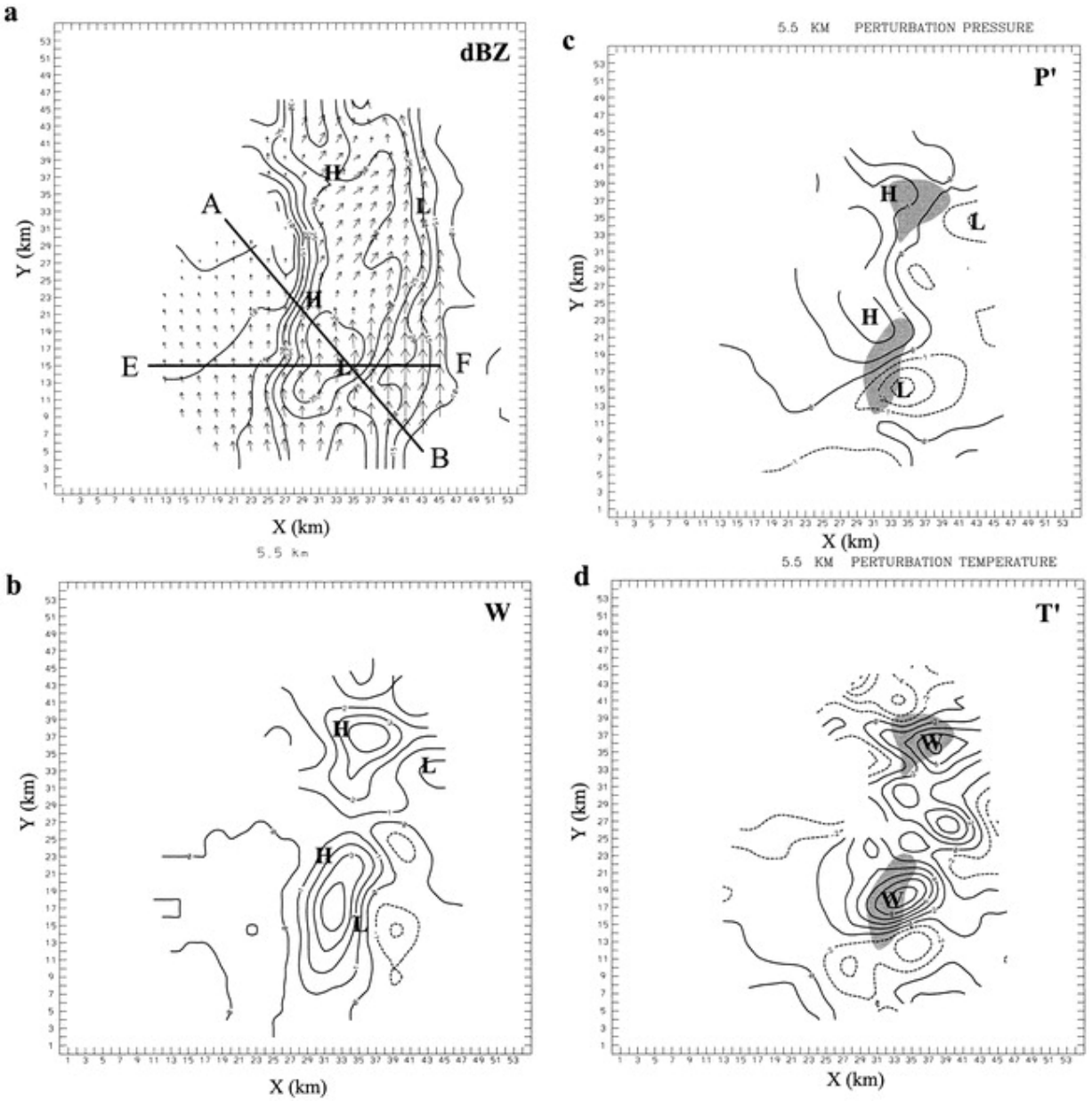

Kinematic and retrieval fields of the TAMEX convective line at 2.5 km (MSL) (Yu et al. 2001)

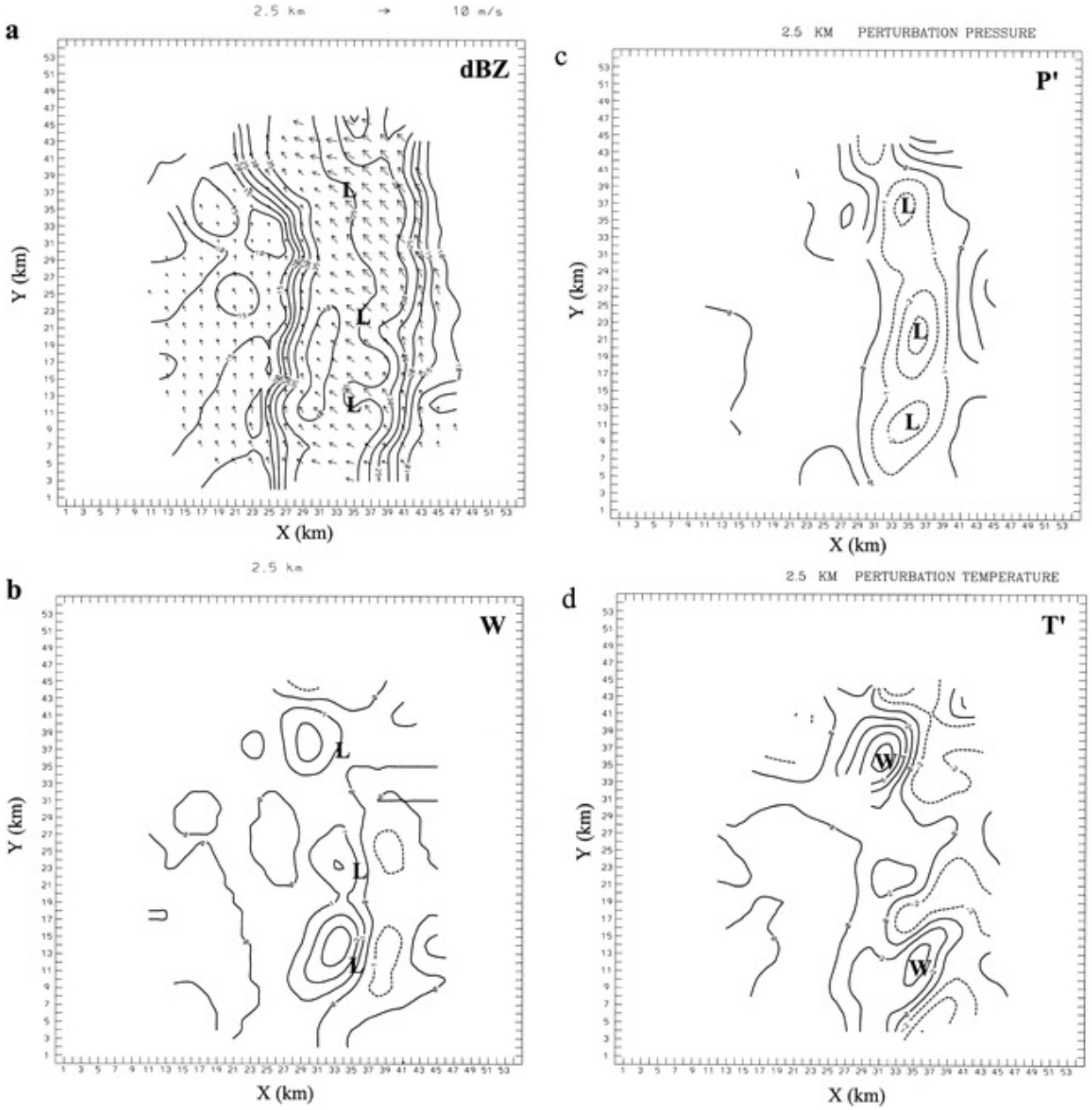

Vertical cross section of kinematic and retrieval fields for the TAMEX convective line (Yu et al. 2001)

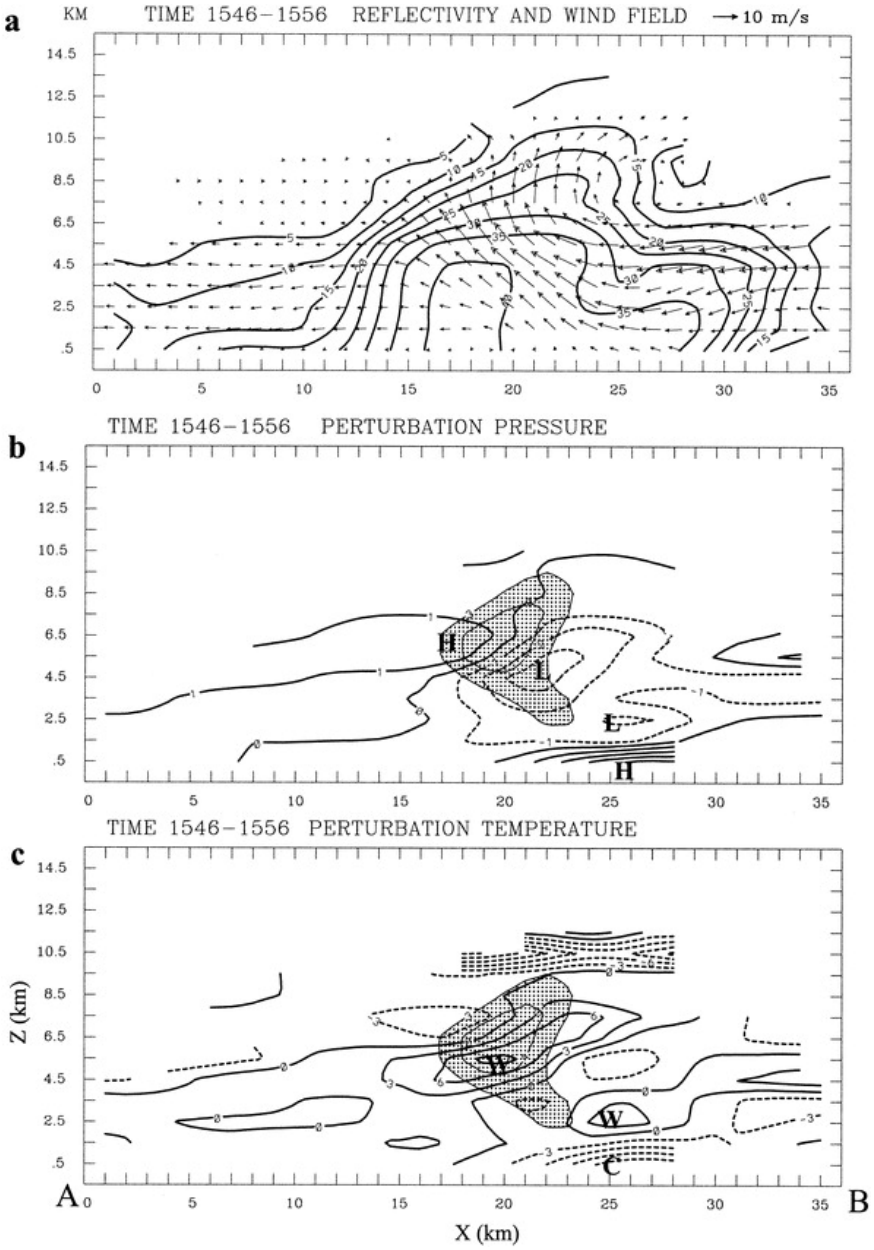

Schematic diagram showing patterns of perturbation pressure and airflow within the TAMEX convective line (Yu et al. 2001)

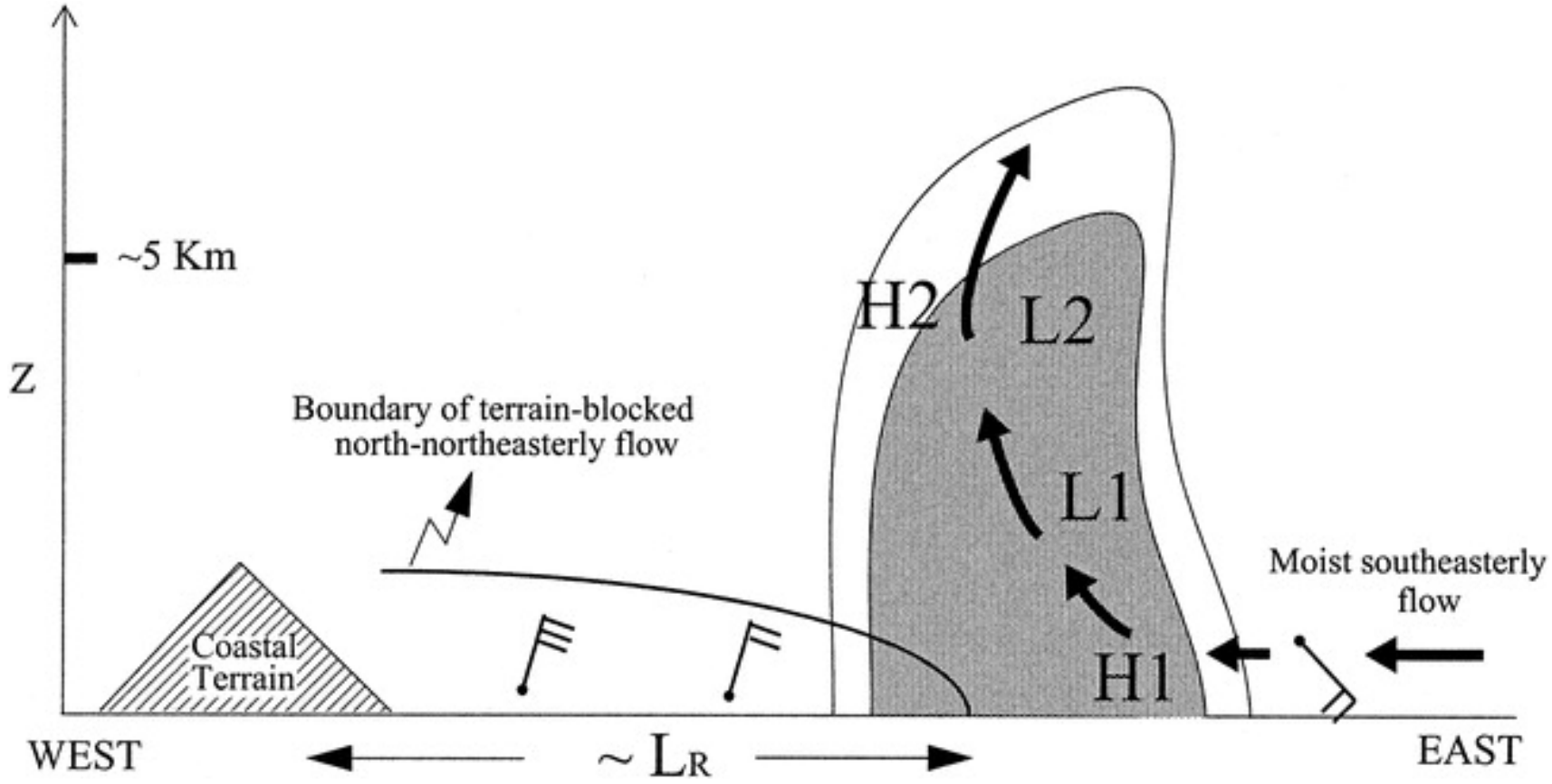

The classification of storm types

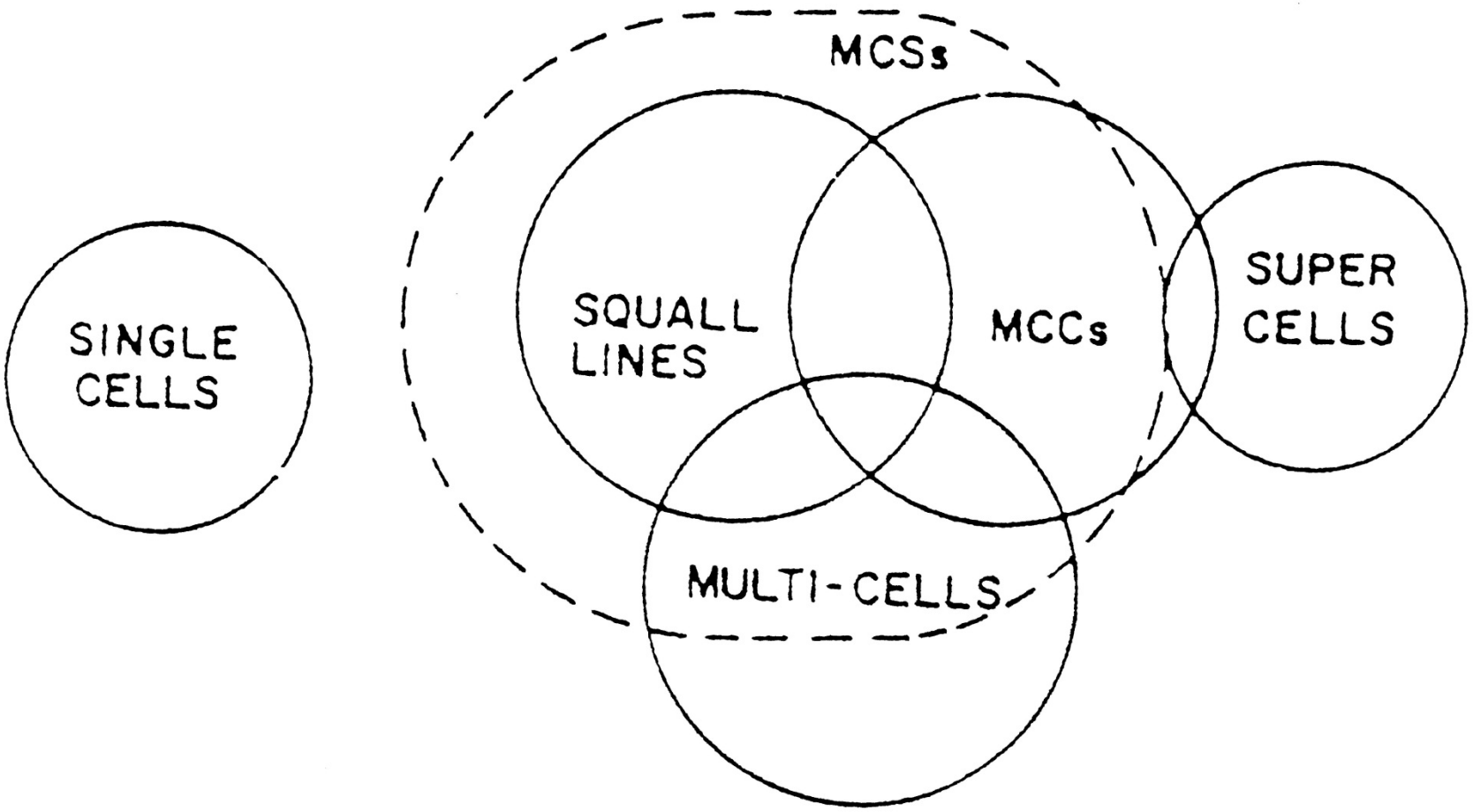

Different stages of a short-lived convective cell

(Byers and Braham 1949)

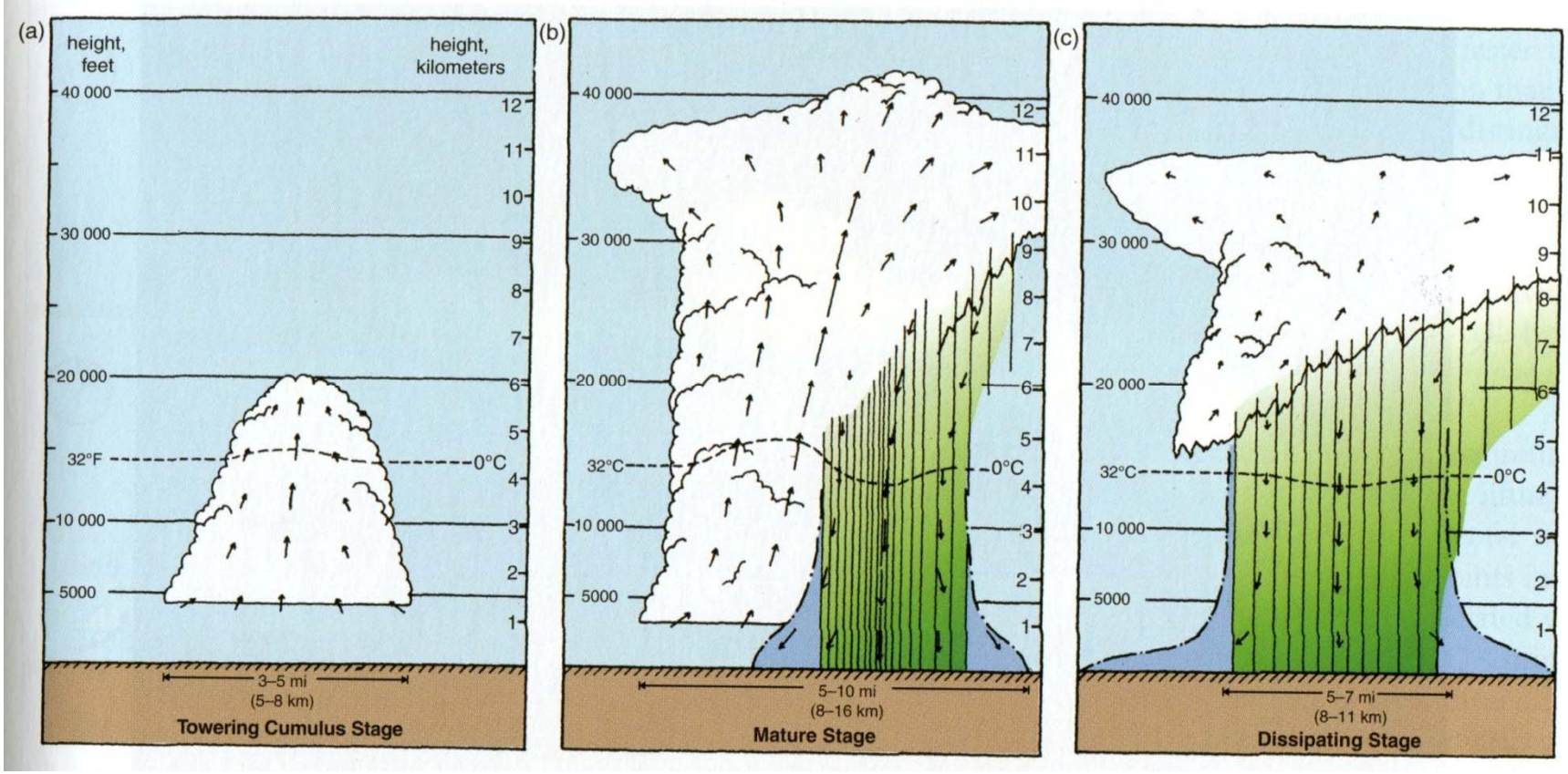

Different stages of a severe airmass storm (from Kingsmill and Wakimoto 1991)

Cumulus stage

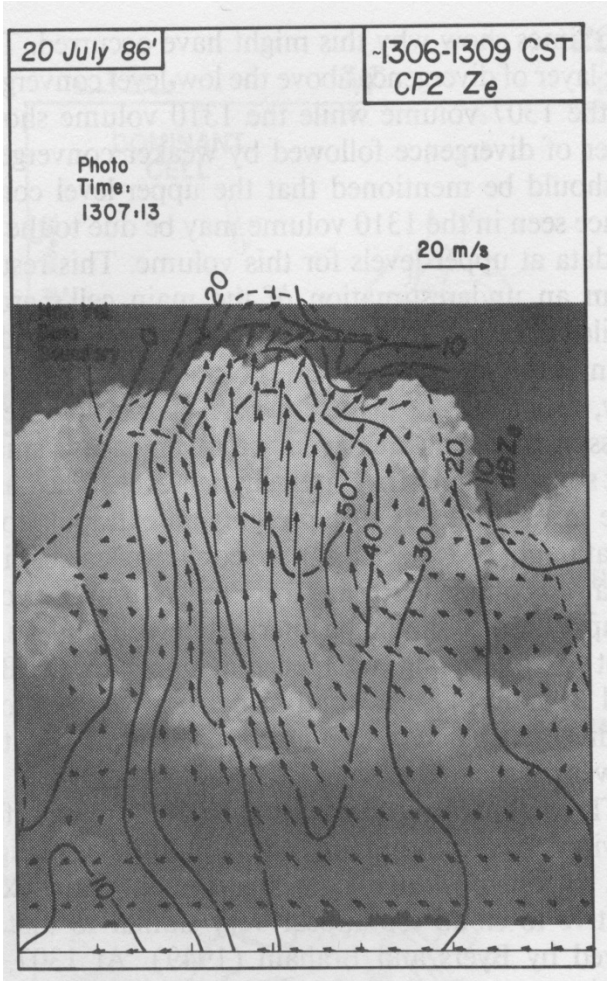

Developing stage

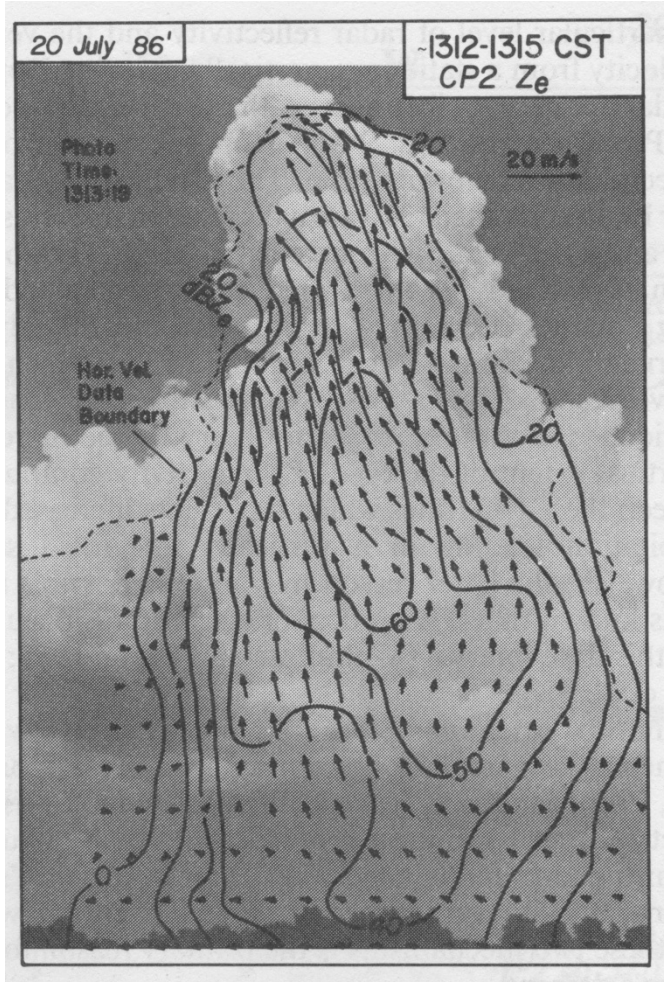

Mature-to-dissipating stage

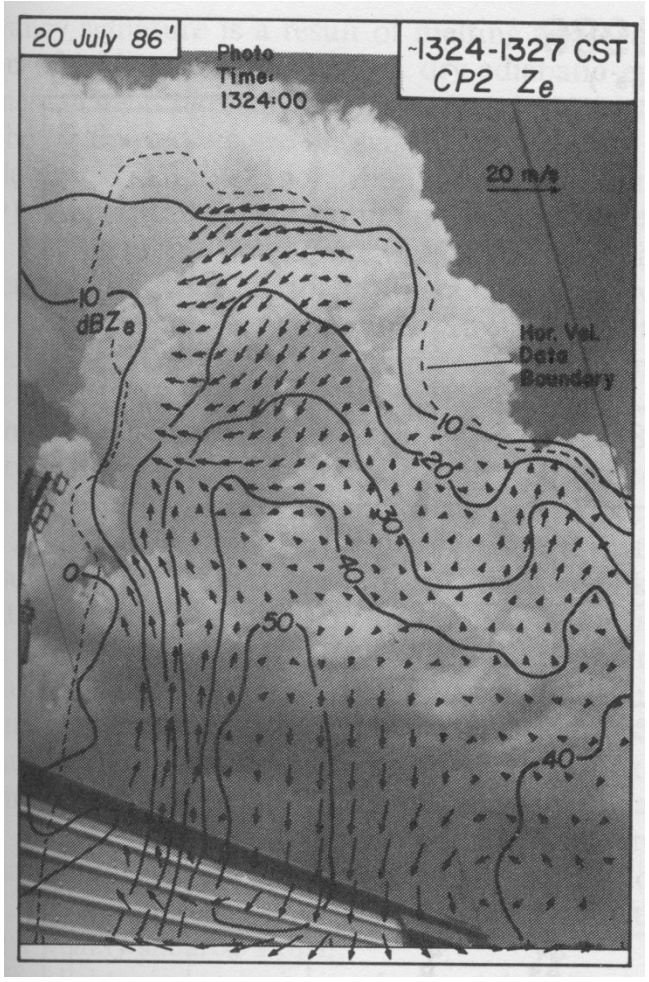

Plan view of a multicell storm (Byers 1959)

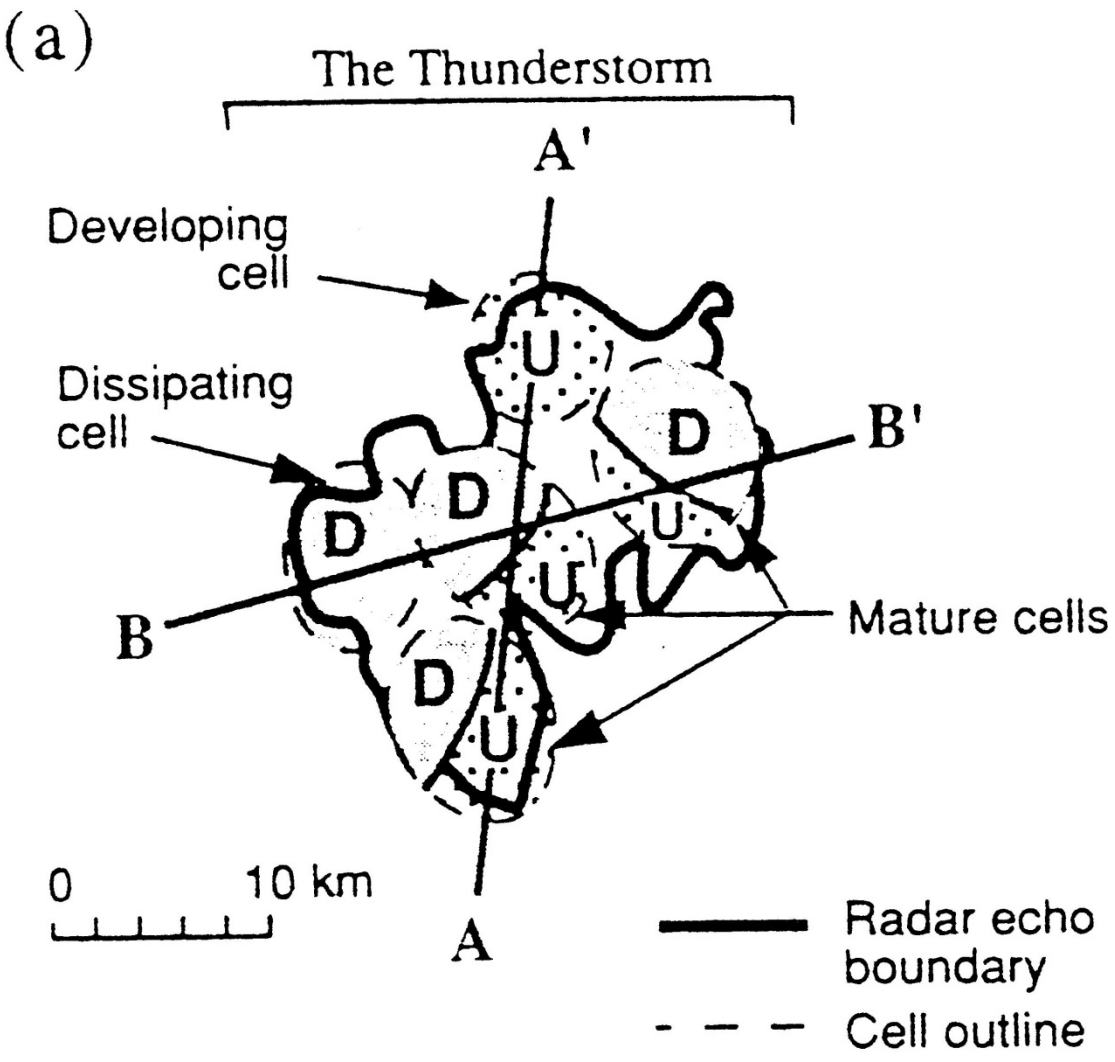

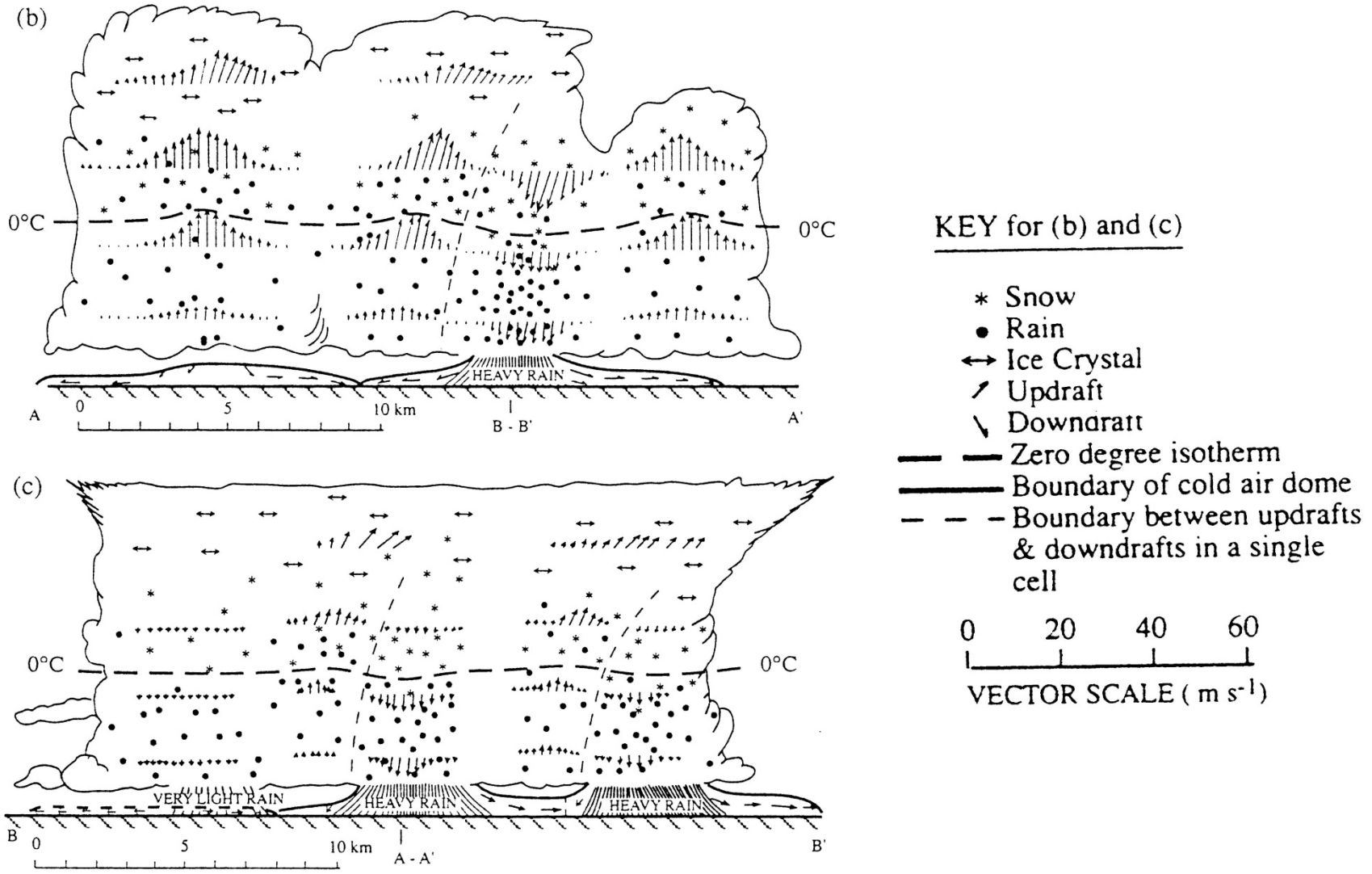

Figure 8.5 Schematic of a multicell thunderstorm in Ohio observed in the Thunderstorm Project. The storm consisted of cells in various stages of development. (a) Plan view. (b) Vertical cross section along A–A′. (c) Vertical cross section along B–B′. (From Byers, 1959. Reproduced with permission from McGraw-Hill, Inc.)

Schematic model of a multicell thunderstorm (Browning et al., 1976)

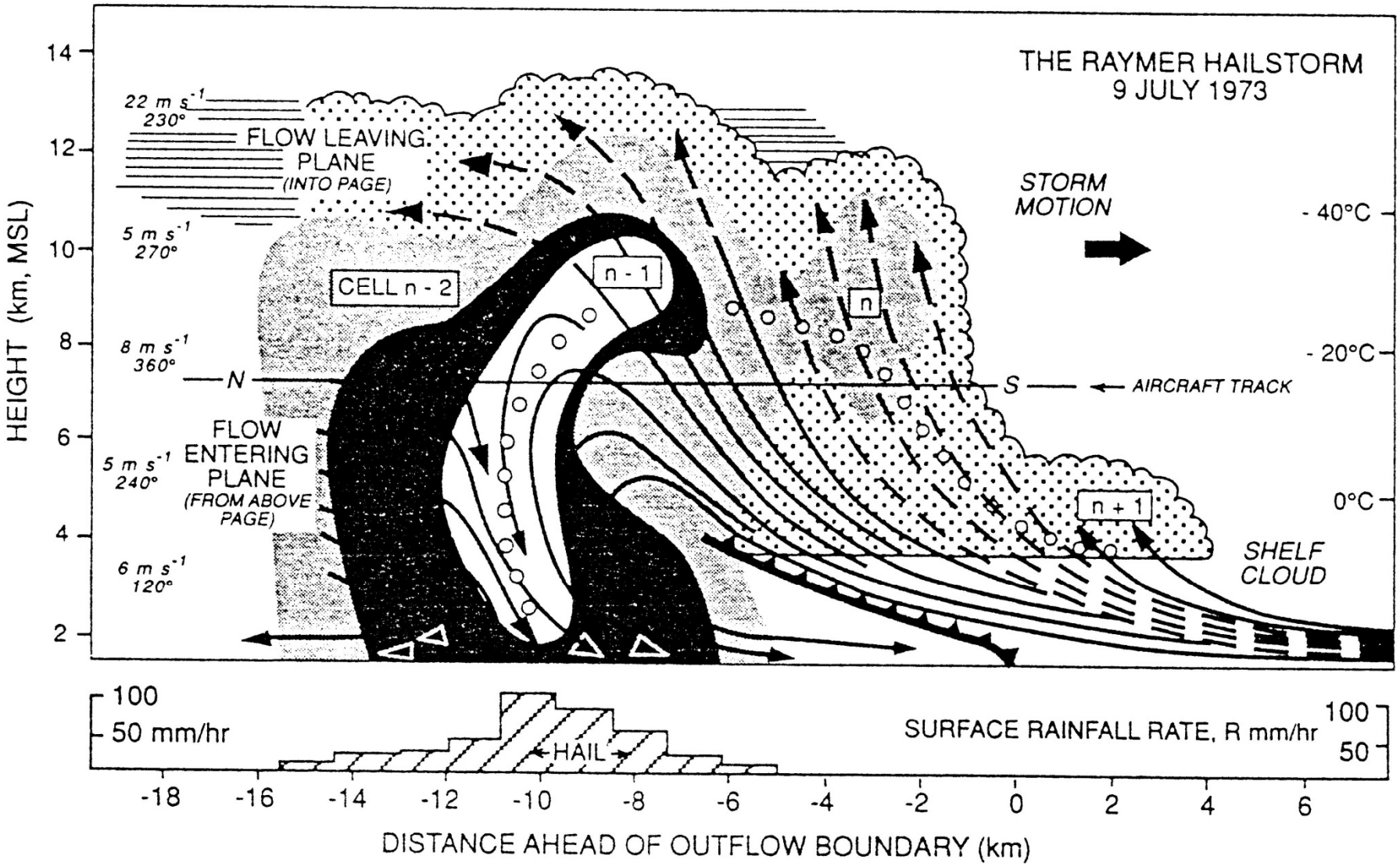

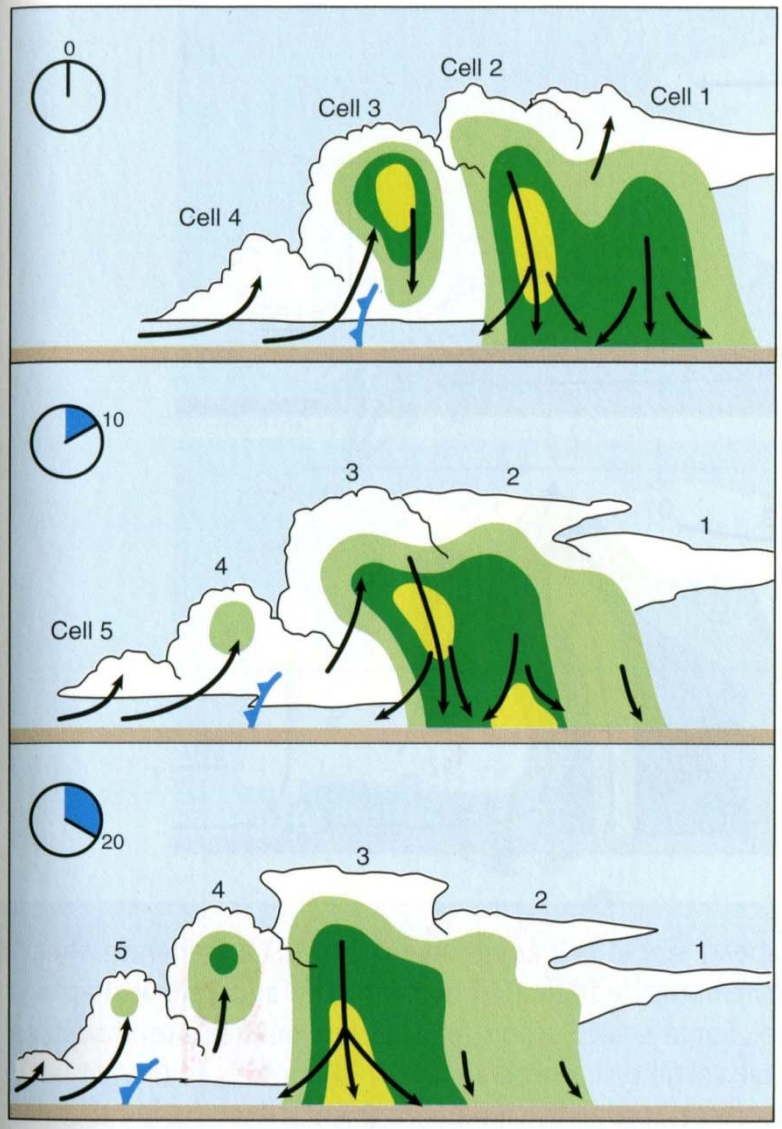

Figure 8.11 Schematic of the evolution of multicellular convection. Refer to the text for details. (Adapted from Doswell [1985].)

Possible arrangements of cells in multicell storms (Houze 1993)

Vc: velocity of individual cell

Vp: storm propagation velocity due to new cell development

Vs: velocity of storm as a whole (if Vs ~0, a quasi-stationary storm)

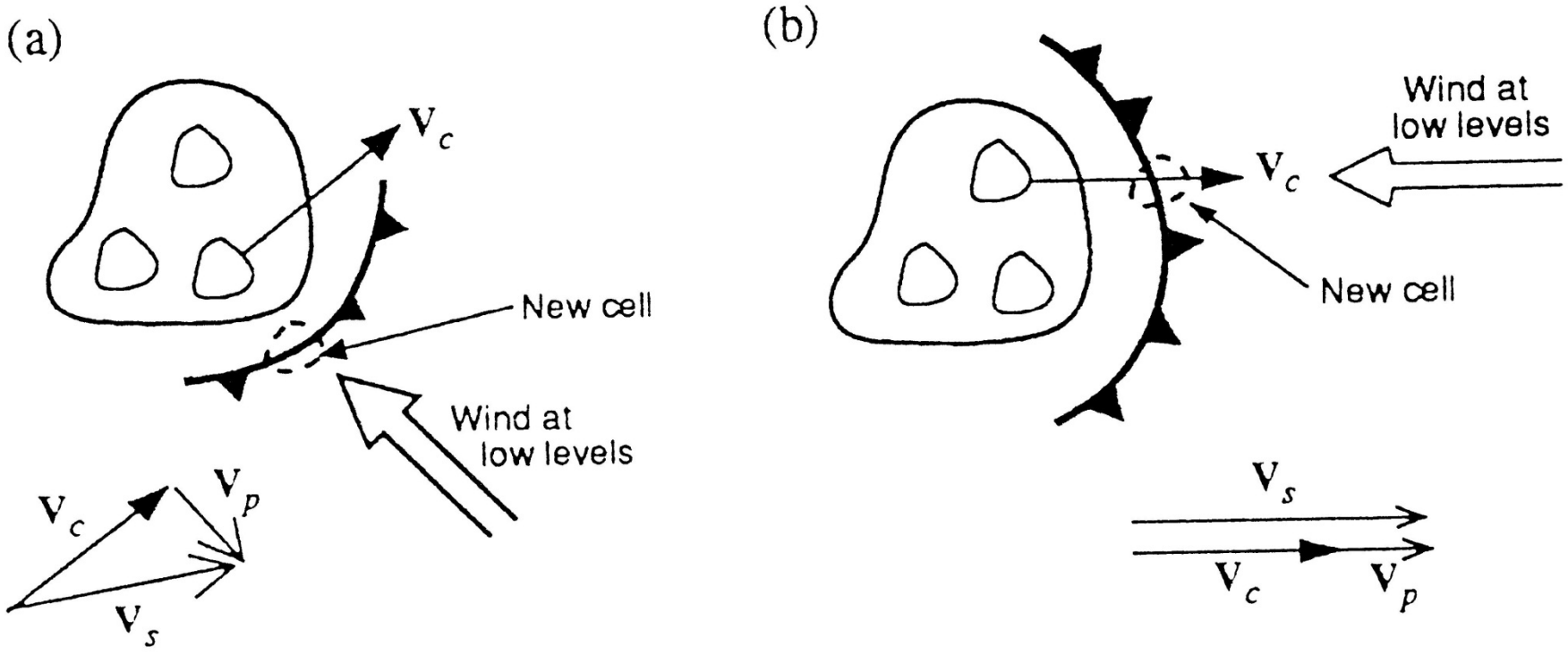

Propagation of a gust front from cell B and a number of the initiated cells (Mueller and Carbone 1987)

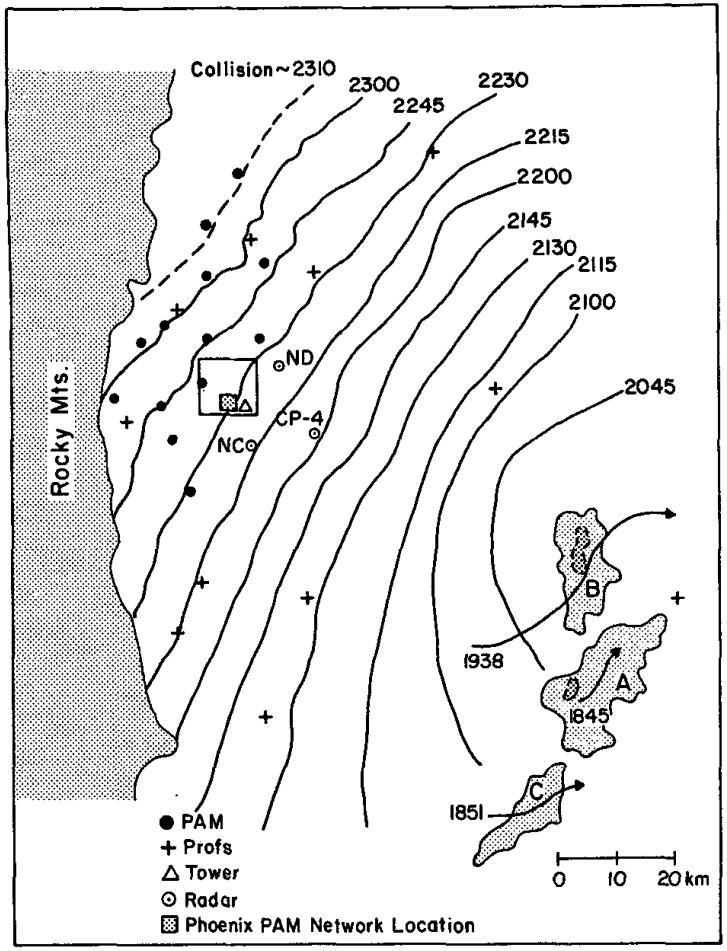

FIG. 2. The gust front's location at 15 min intervals are shown by solid lines. The location was determined from the CP4 radial velocities, radar reflectivity data and the mesonet data. Cell A, B and C are shown at 2039 Z. Low-level reflectivity contours are at 30 and 50 dBZ_e. The arrows show the movement of the cells, and the time that the cell was first detected at 2 km. The location of the dual-Doppler analyses is shown as a box. The WPL NOAAC (NC), NOAAD (ND), and NCAR CP4 radars are labeled.

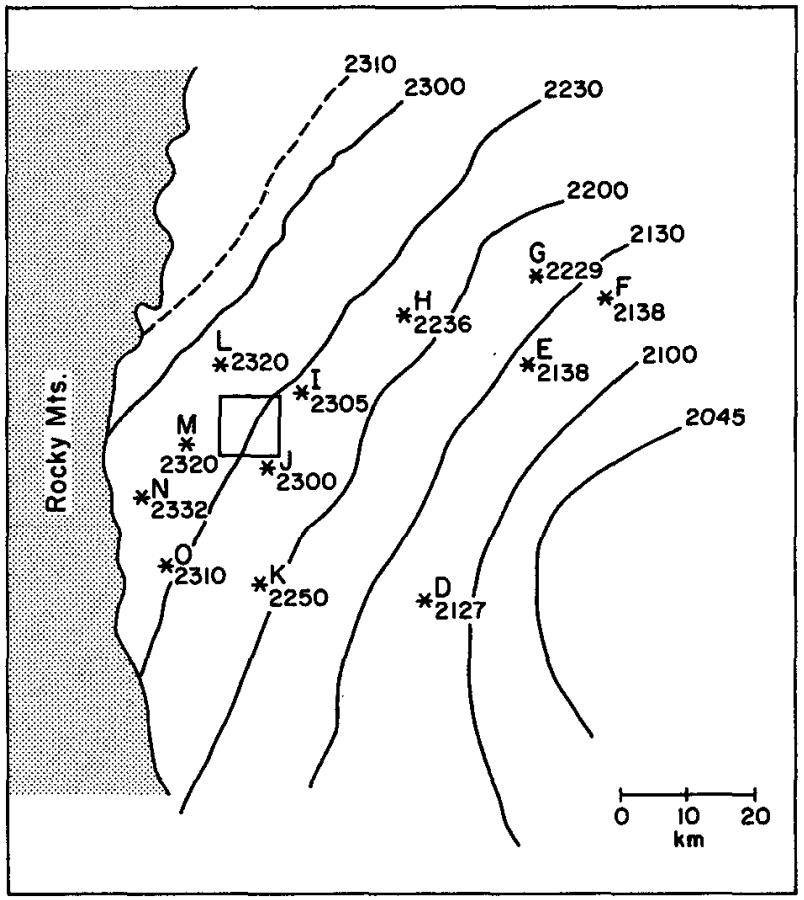

FIG. 3. The gust front location at 30 min intervals and the location of the first precipitation echo of cells that were initiated in the region behind the gust front. The time of detection is indicated. The box indicates the location of the dual-Doppler analyses.

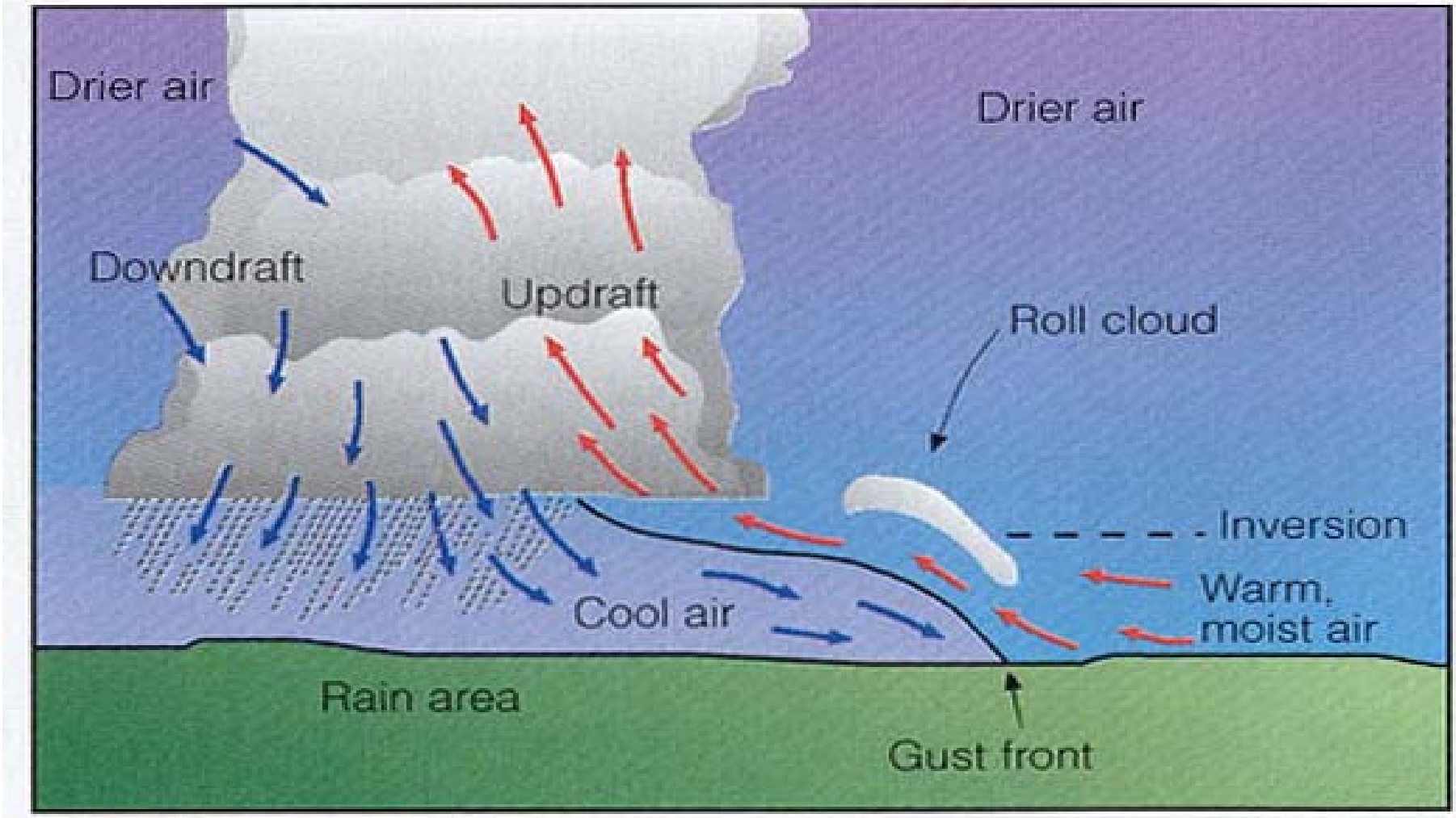

Figure 10.5
The lower half of a severe squall-line-type thunderstorm and some of the features associated with it.

Schematic features for the gust front

(Droegemeier and Wilhelmson 1987)

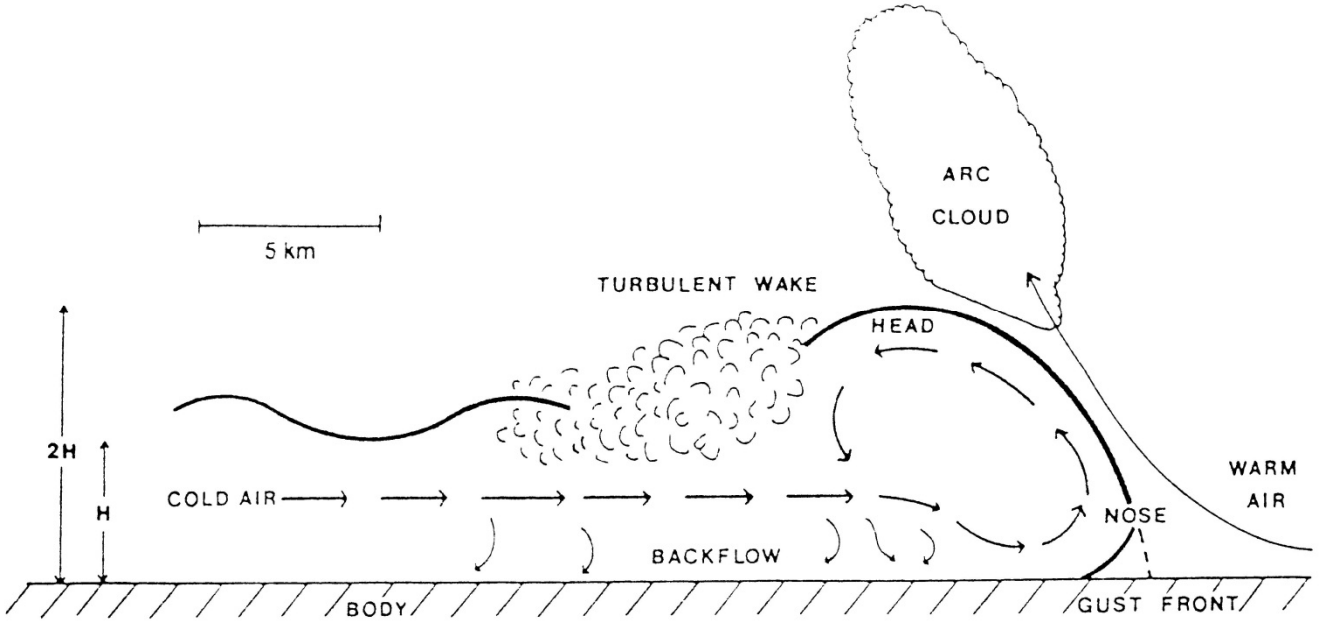

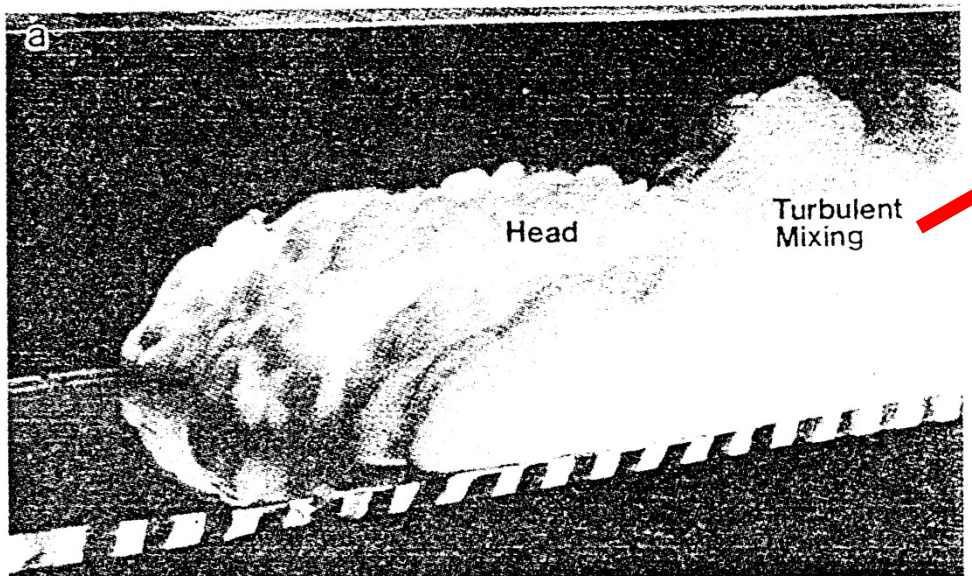

Density current observed in laboratory tanks (Simpson 1969)

Density current movie in the lab.

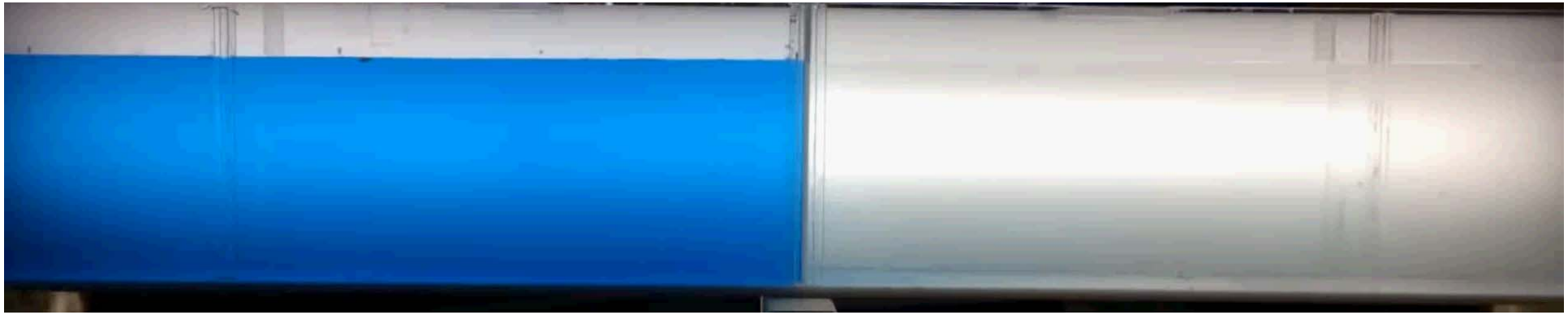

Simpson and Britter (1980) showed the density current velocity can be approximated by the expression:

$$u = k\left[\frac{gh(T_1 - T_2)}{T_2}\right]^{1/2} + bu_0$$

***T_1:* Warm airmass temperature*; T_2:* Cold airmass temperature**

***h:* the depth of the cold air**

***U_0:* Cross-density-current velocity (negative for a wind toward the cold air)**

***b*~0.6*; K*~0.9 (constant)**

Taking T_1~288.7 K, T_2~286.7 K, u_0~2.4 m s^{-1} and *h*~2000 m, *u*~9 m s^{-1}

Chong et al. (1987) 熱帶颱線低層水平雷達回波結構

(Low-level horizontal structure of a tropical squall line)

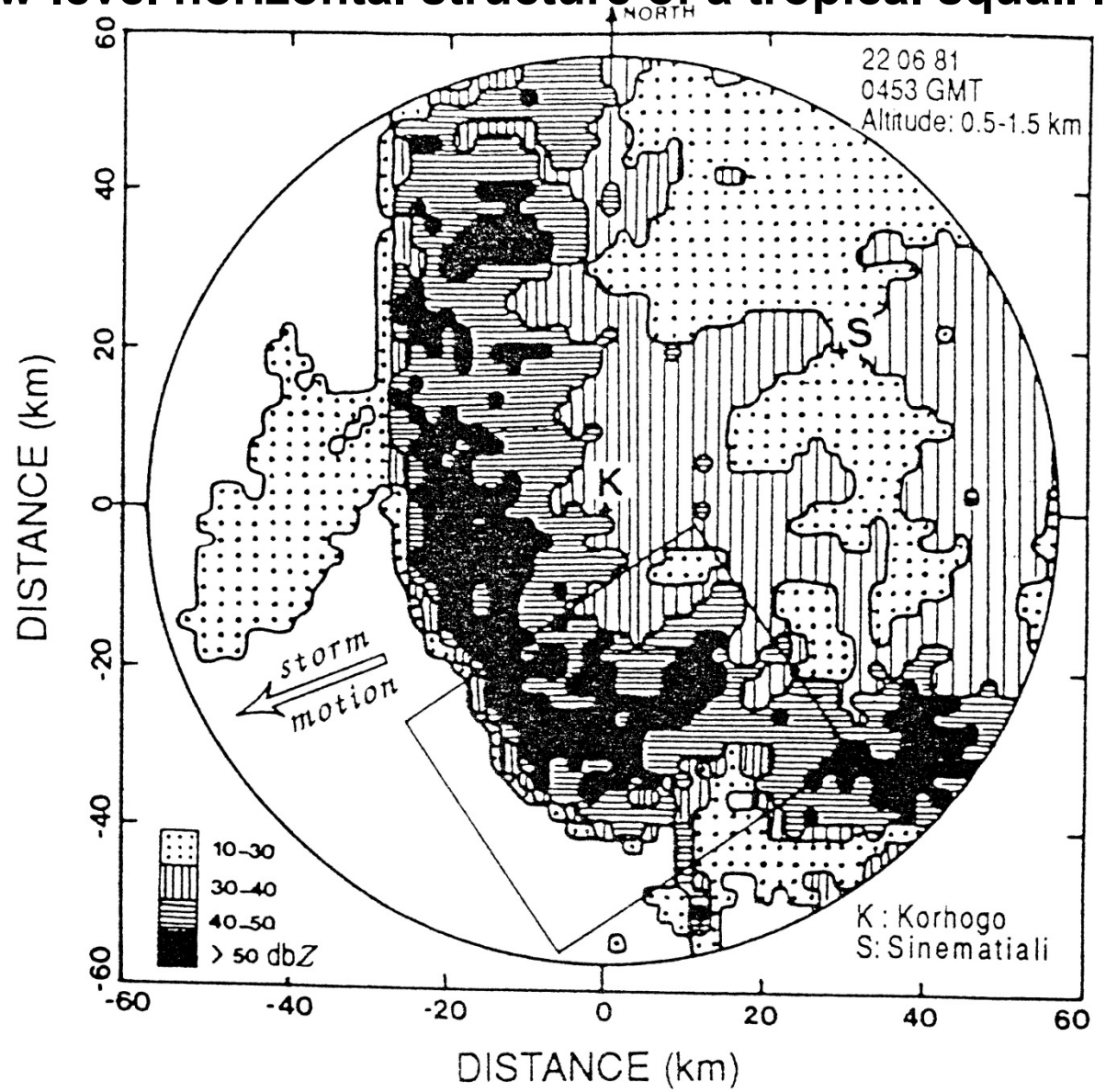

熱帶颱線垂直回波結構 (Chong et al. 1987)

Vertical structure of the tropical squall line

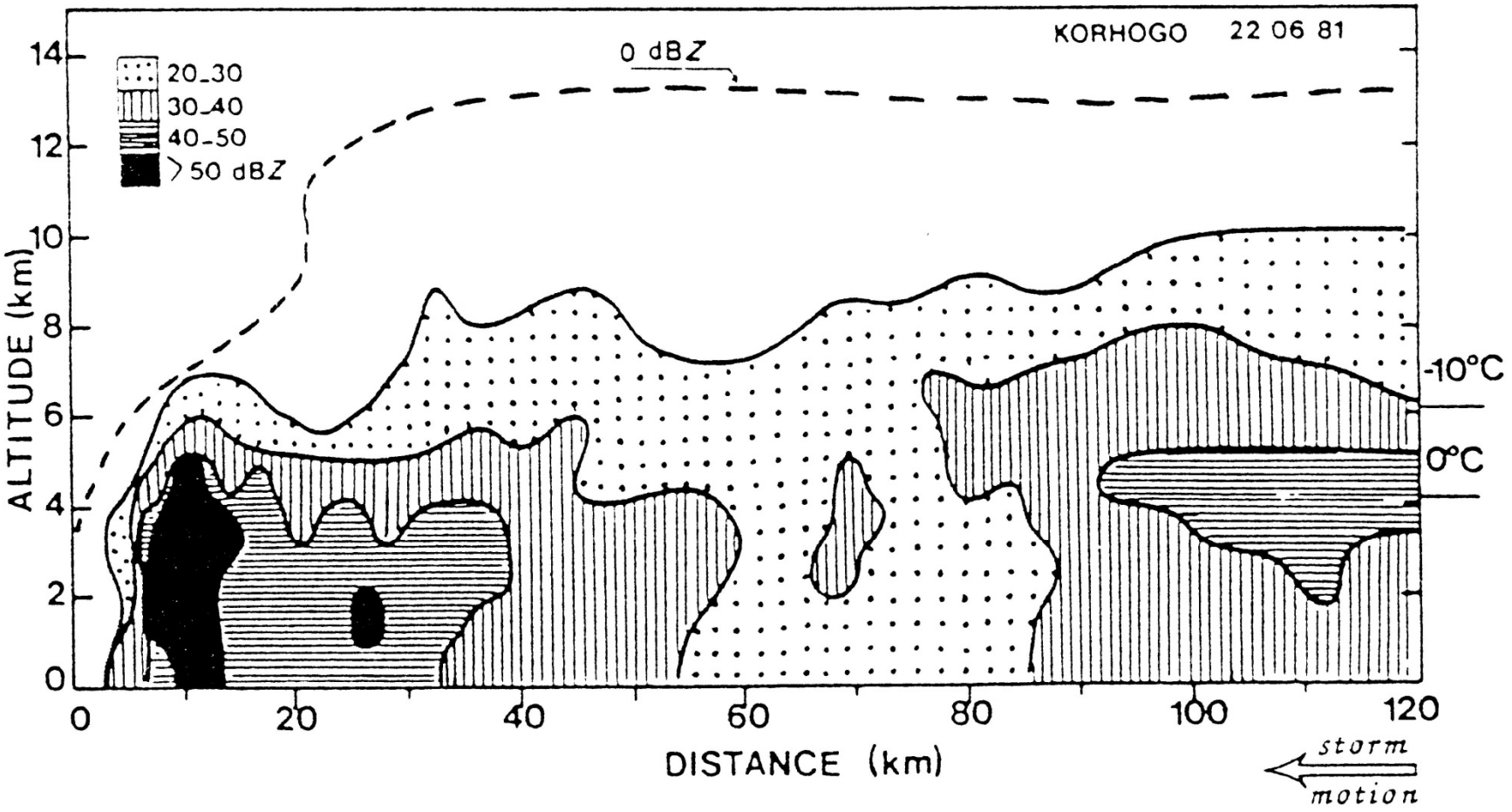

Bright-band signatures seen from airborne Doppler radar (Yu et al. 1999)

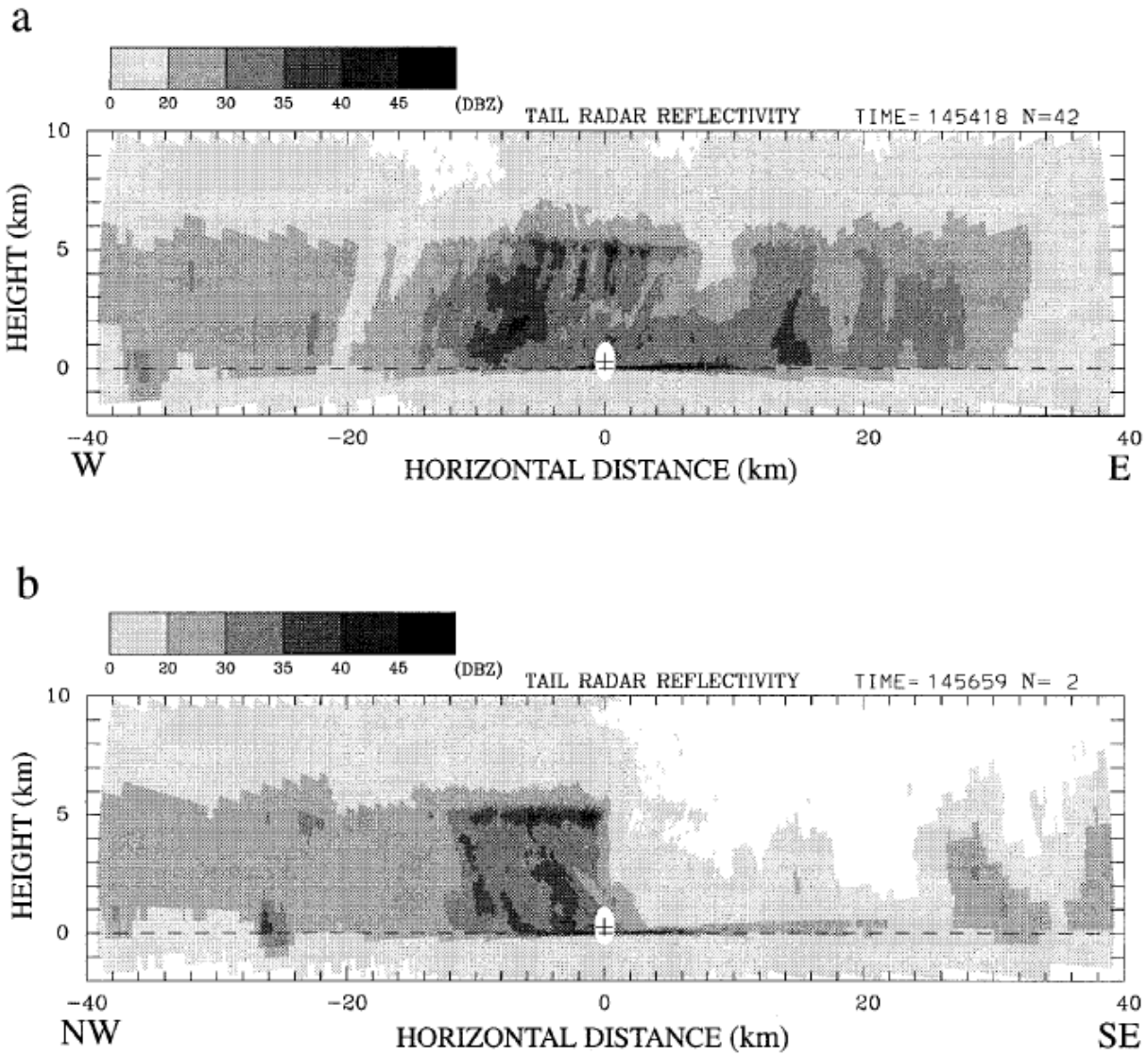

FIG. 9. As in Fig. 8 except for cross sections C and D displayed in (a) and (b), respectively. The altitude of the aircraft is approximately equal to 300 m for these two cross sections.

東北季風影響臺灣期間微波降雨雷達所觀測到之雷達回波及雨滴落速

(Right panel: Time-height cross section of Micro Rain Radar for a precipitation event during northeasterly monsoon flow)

(2006年2月25日19時到24時)

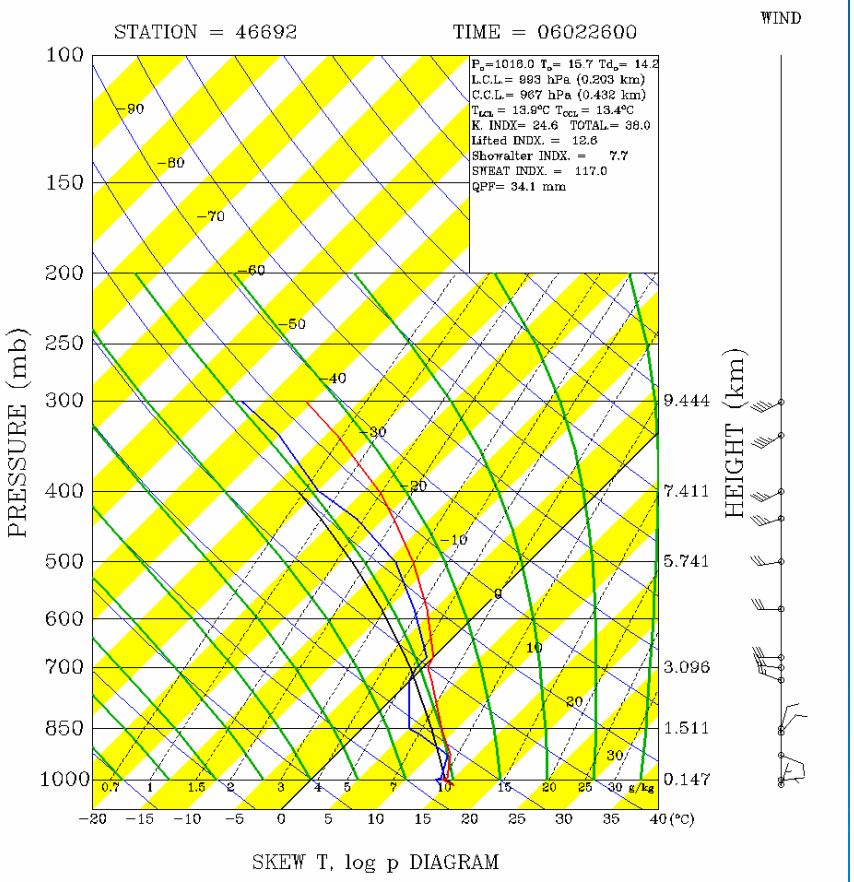

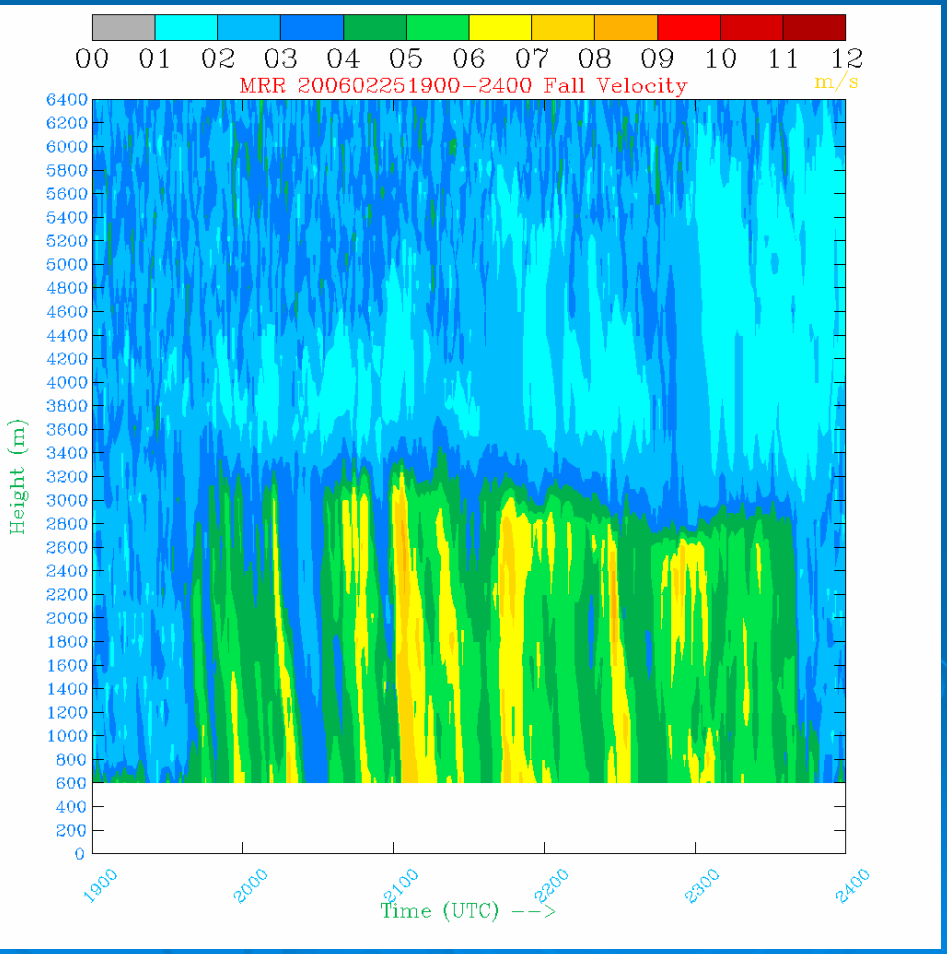

06022600Z 0℃ 3355m 677.8mb

Houze et al. (1990)

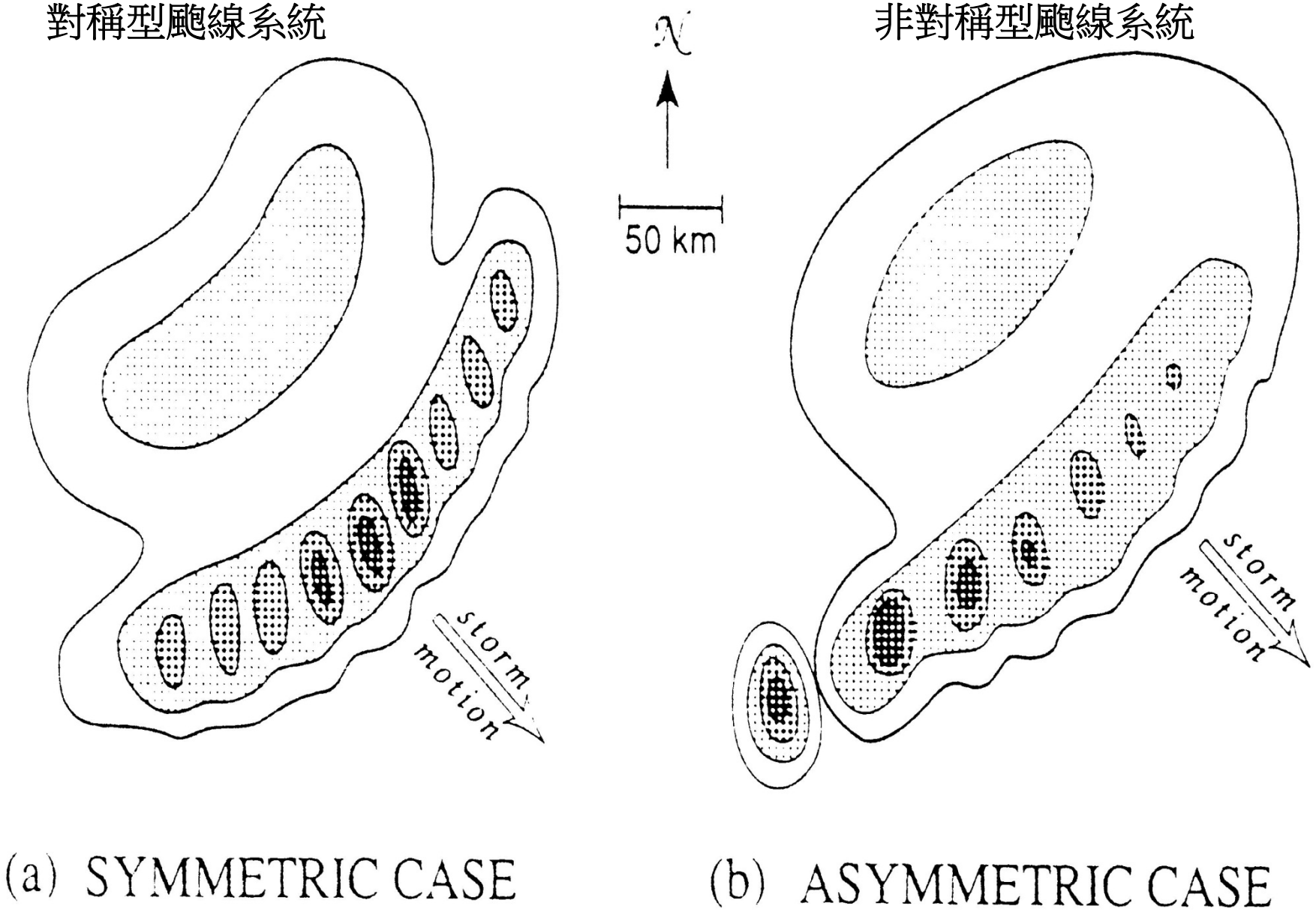

Houze et al. (1990)

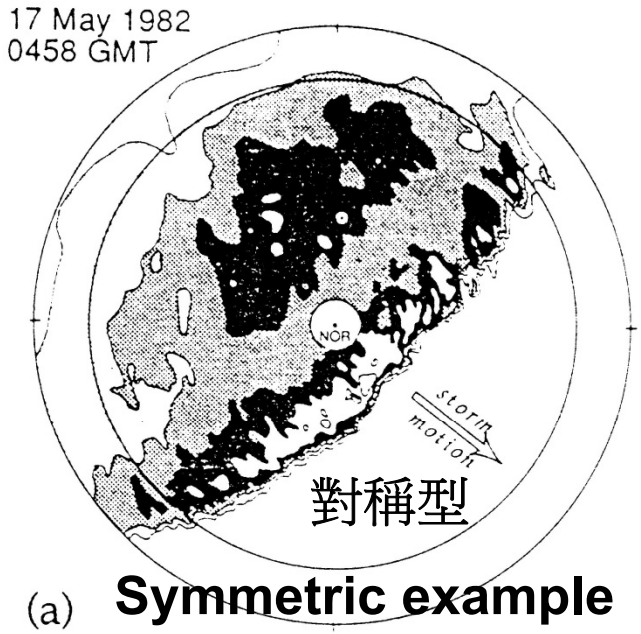

對稱型

(a) **Symmetric example**

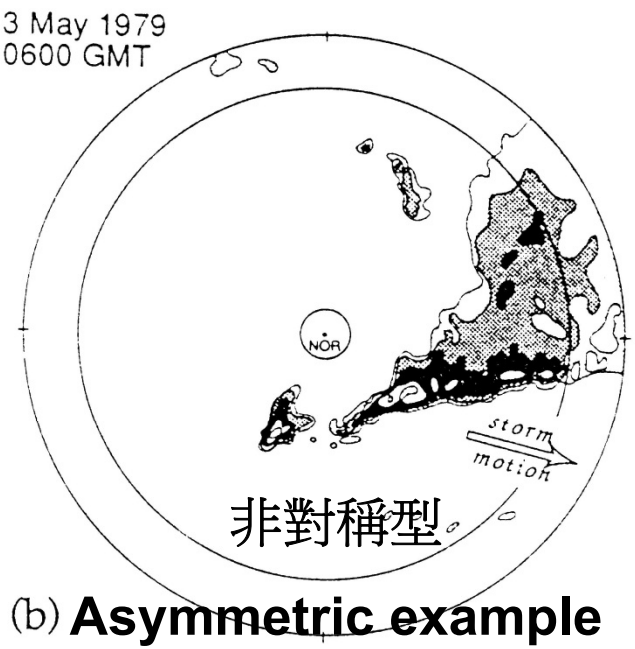

非對稱型

(b) **Asymmetric example**

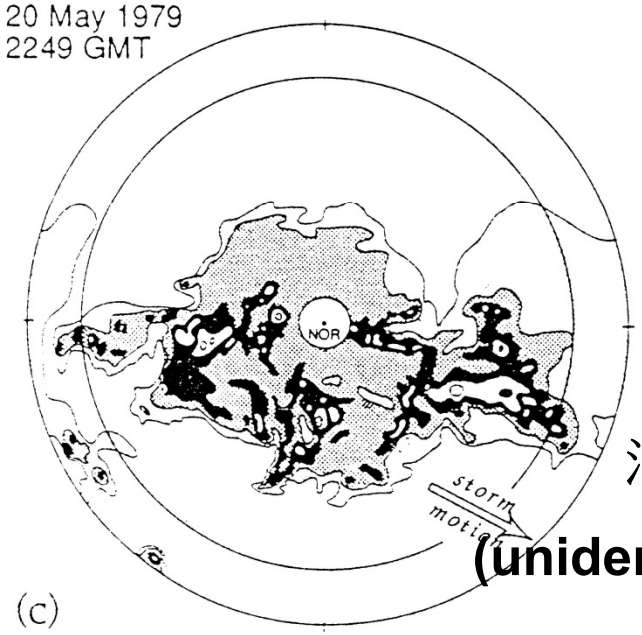

(c)

混亂型(佔**1/3**)

(unidentified example)

Parker and Johnson (2000) 對流線與層狀降水區之相關位置

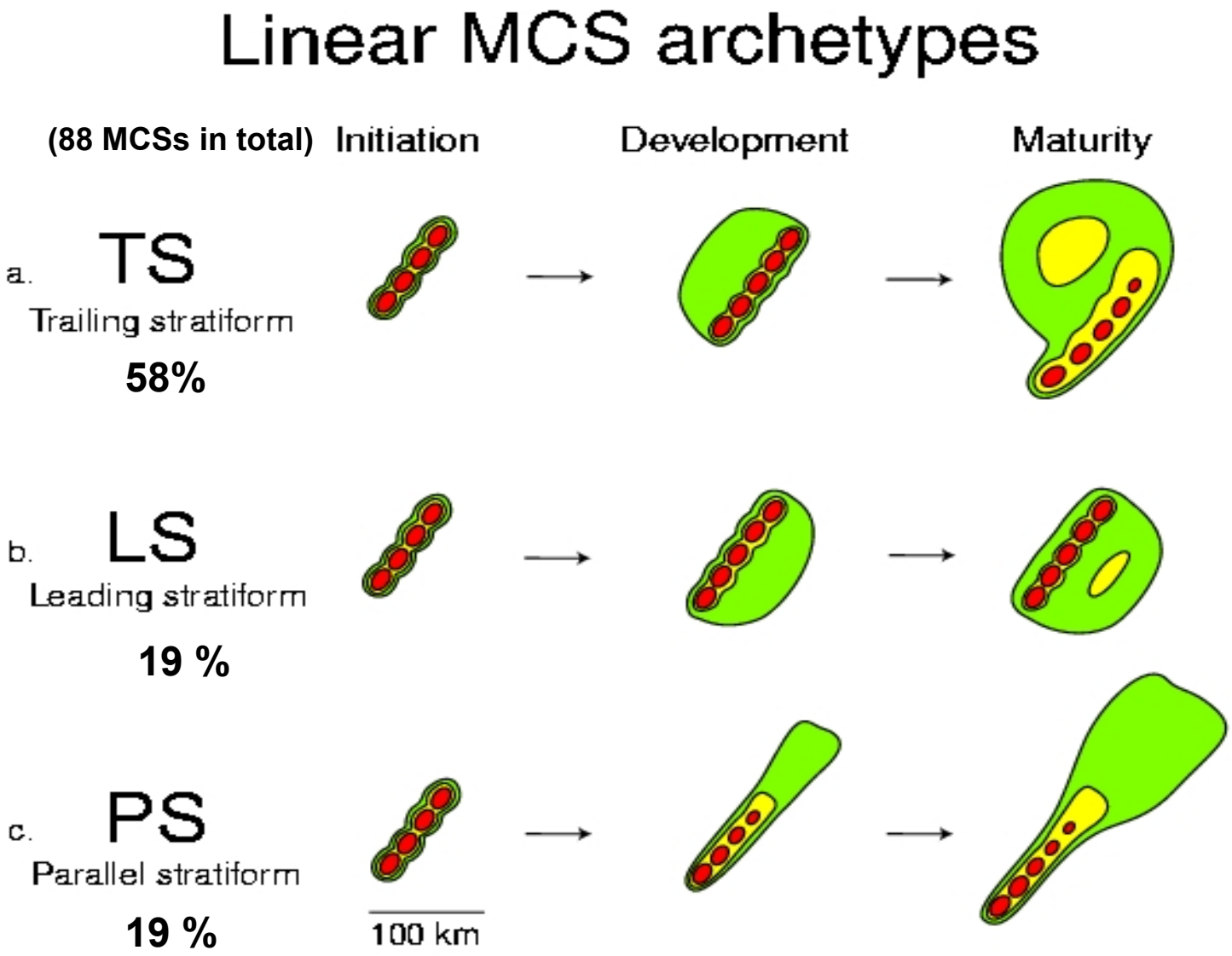

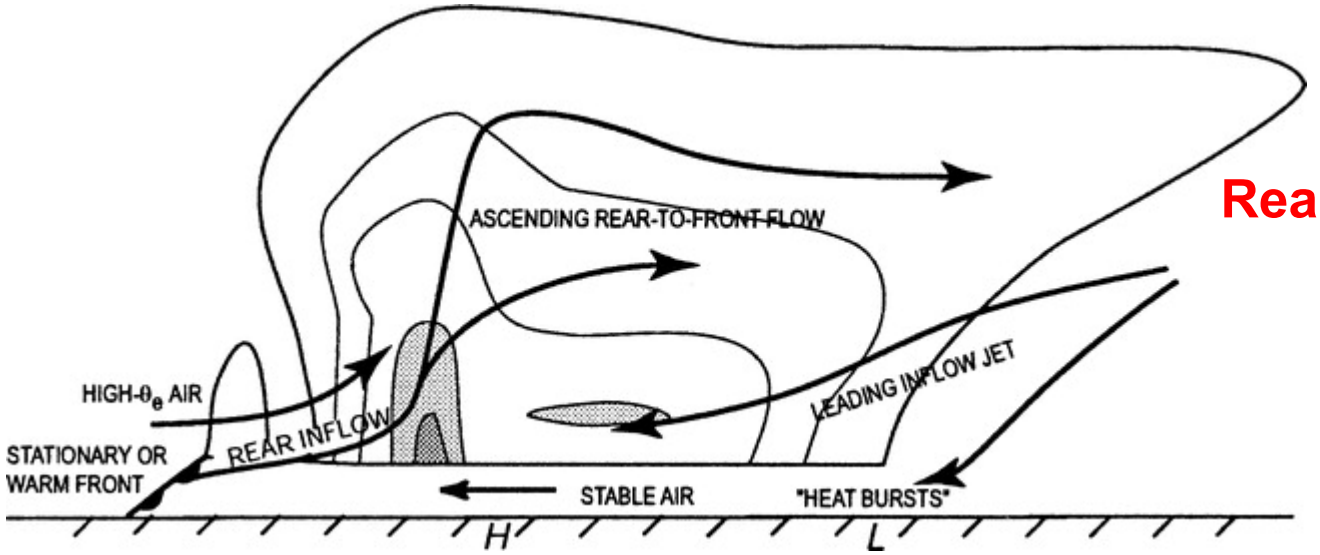

Rear-fed LS MCS

Front-fed LS MCS

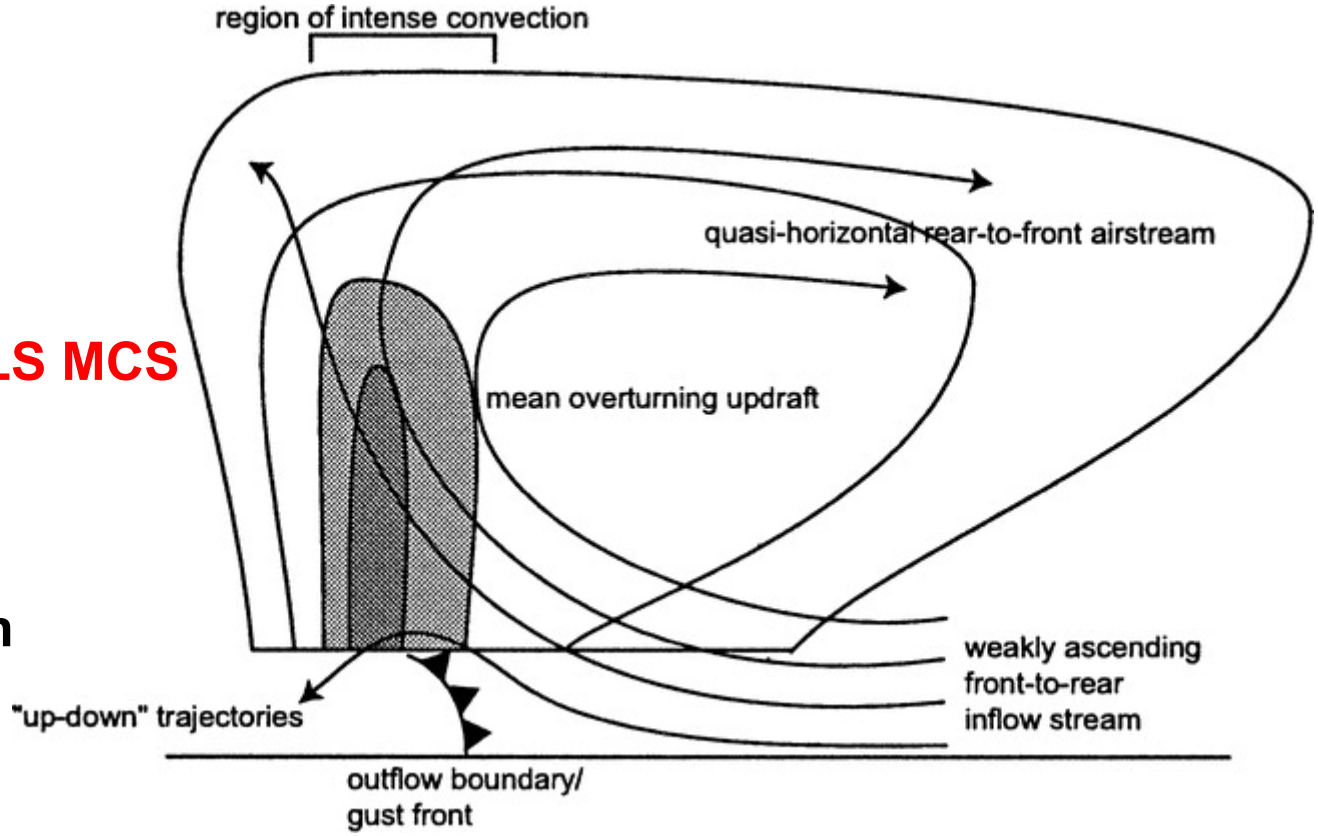

Parker and Johnson (2004)

中尺度對流系統之雷達回波演化 (Leary and Houze 1979)

Evolution of radar echoes associated with a MCS

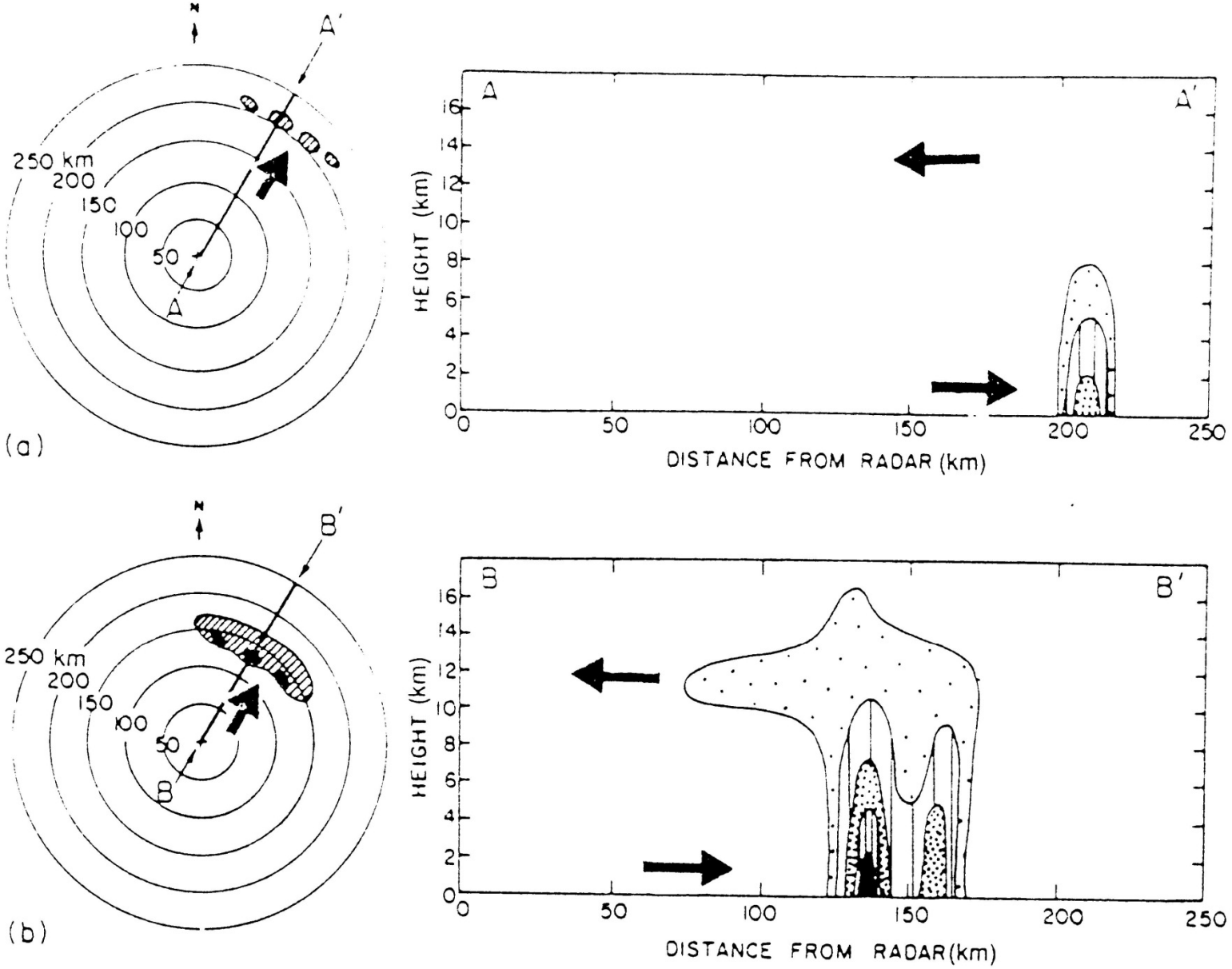

(續, continued)

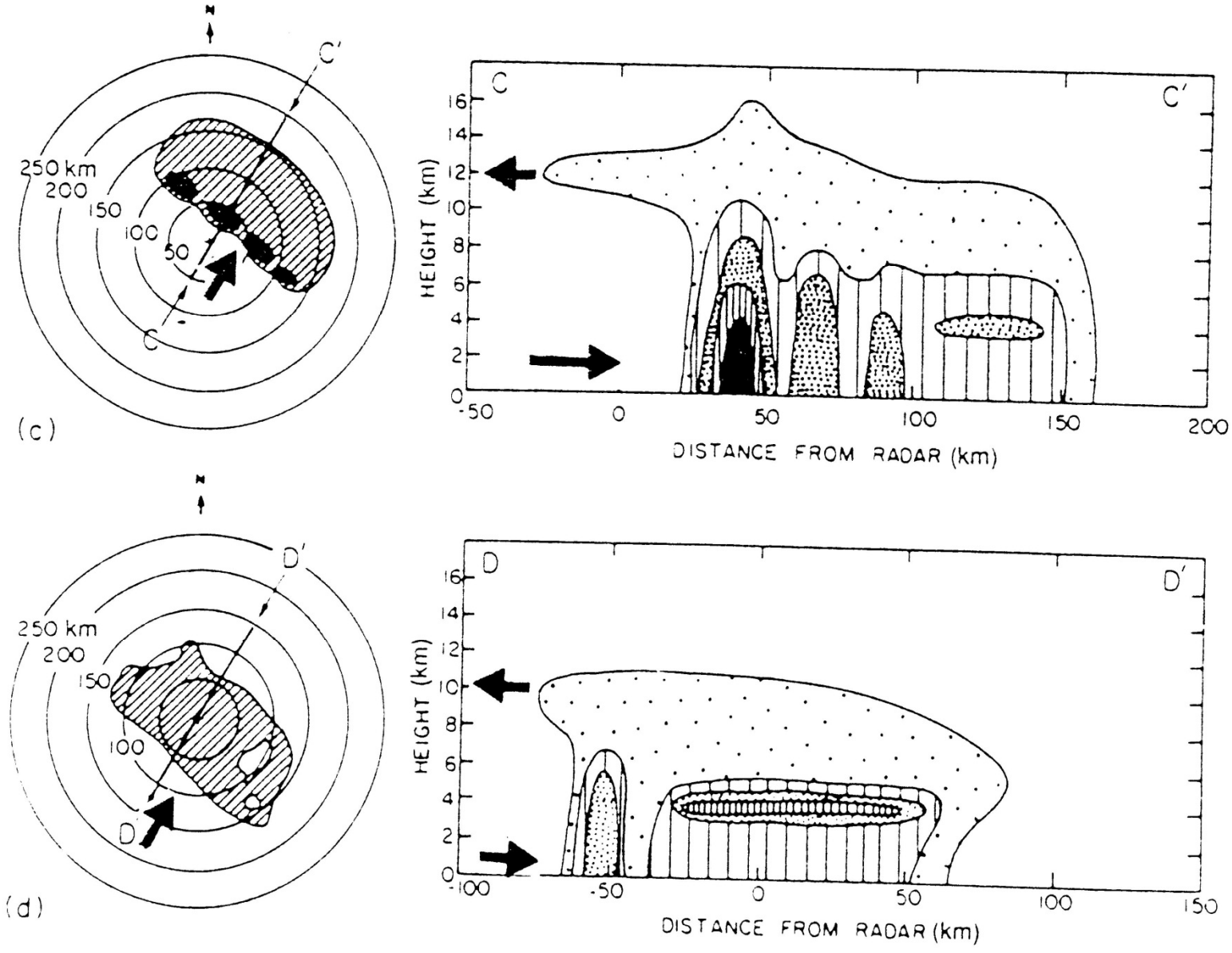
C'
250 km
200
150
100
50
C
(c)
C
C'
HEIGHT (km)
DISTANCE FROM RADAR (km)
D'
D
(d)
D
D'
HEIGHT (km)
DISTANCE FROM RADAR (km)

颱線系統內部對流區與層狀區降水量隨時間的變化 (Houze 1977)

Temporal variation of the convective vs. stratiform rainfall of a squall line

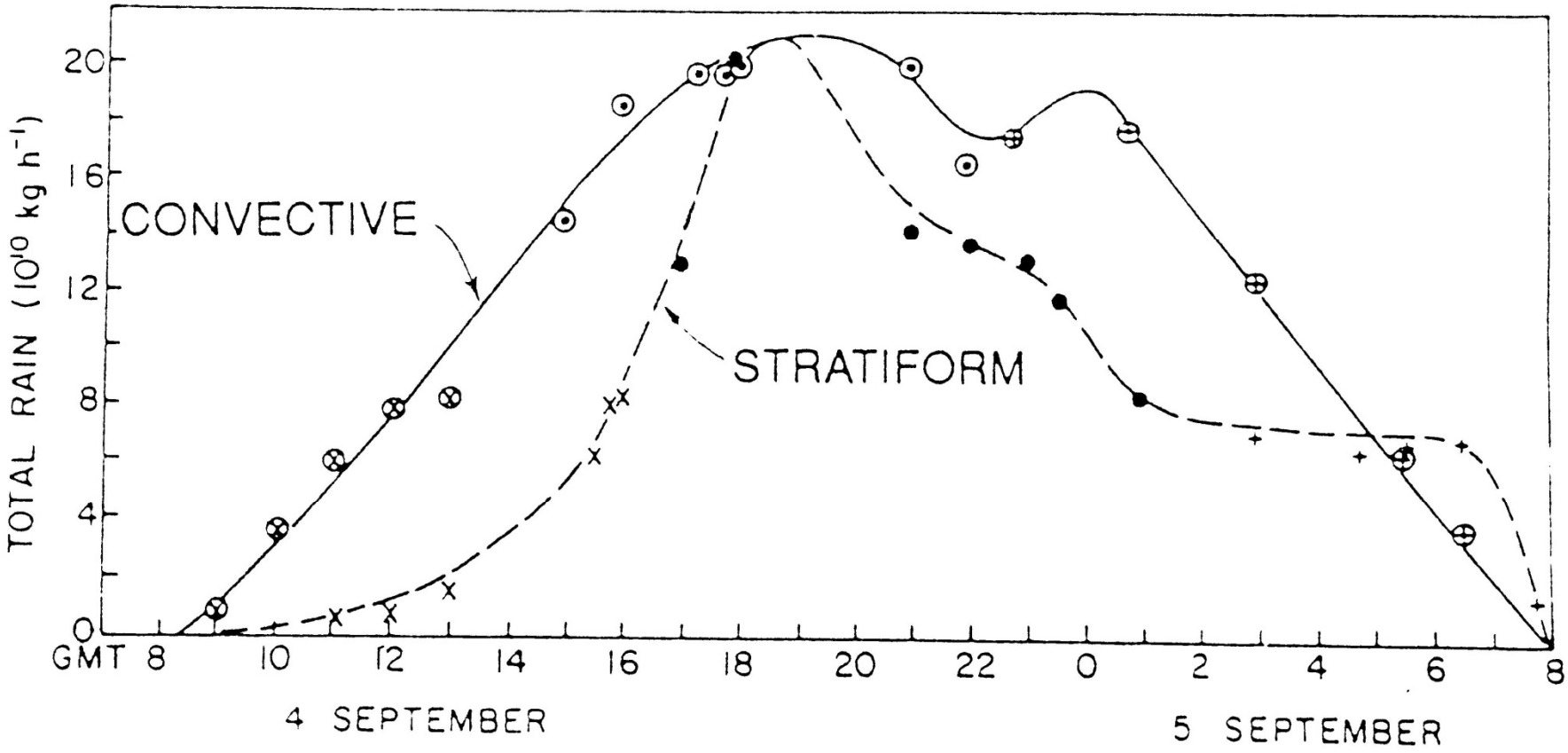

颱線發展形式的分類 (Bluestein and Jain 1985)

(Developing types of squall line systems)

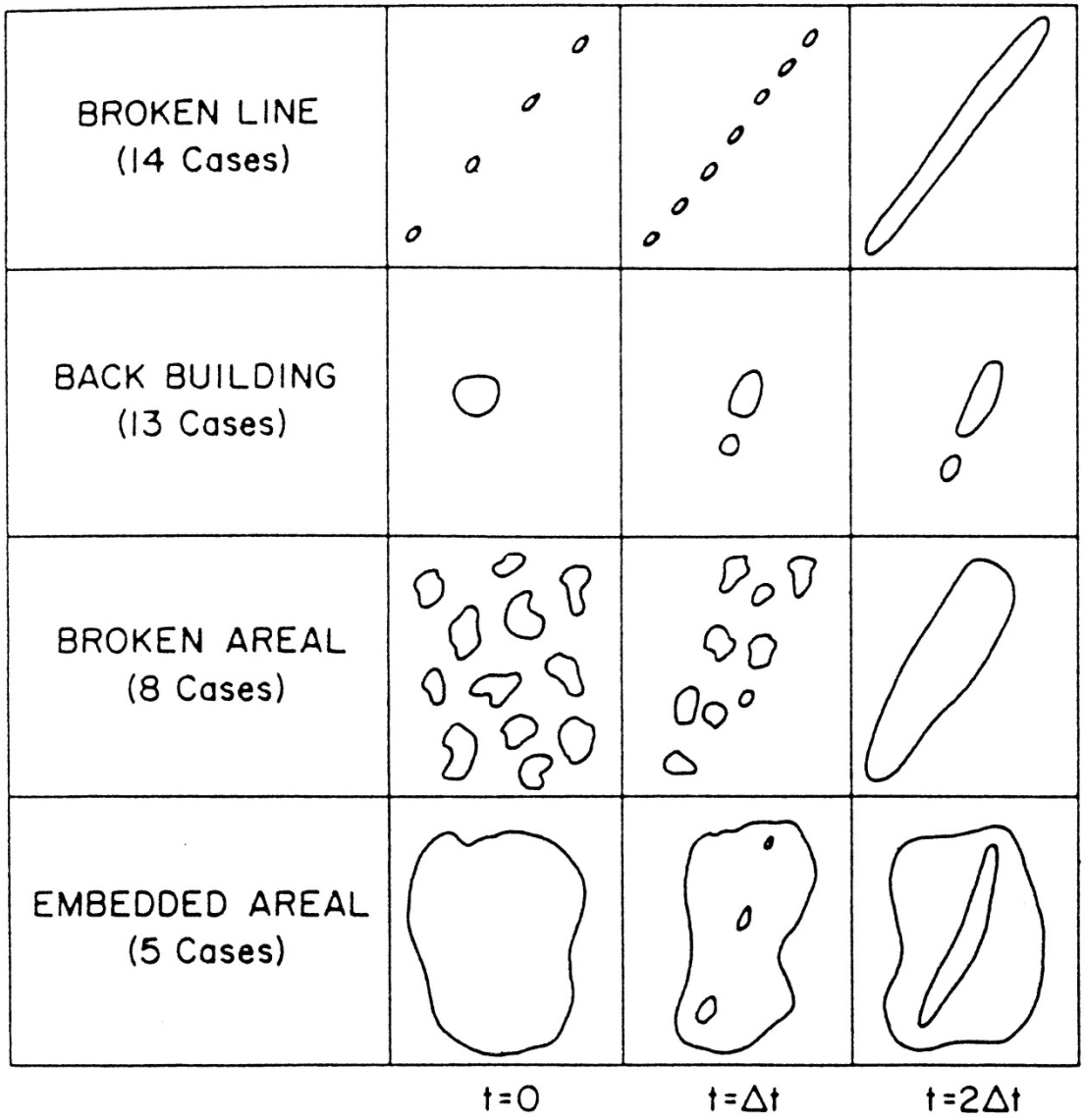

熱帶颱線的水平回波結構 (0.5 degree PPI) (Roux 1988)

Horizontal structure of precipitation for a tropical squall line

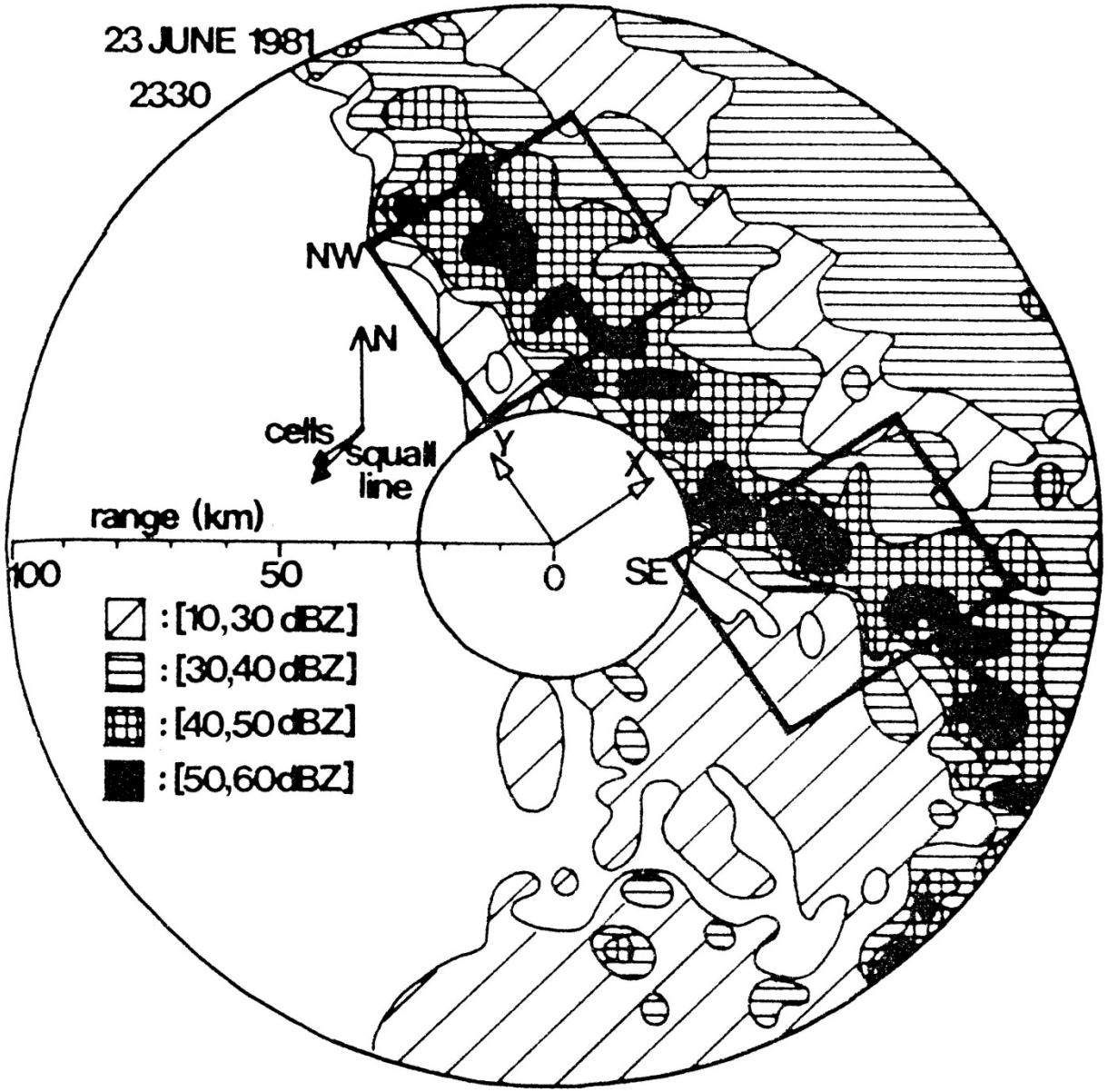

颱線水平風場與回波結構 (Roux 1988)

Horizontal structure of airflow and precipitation of a tropical squall line

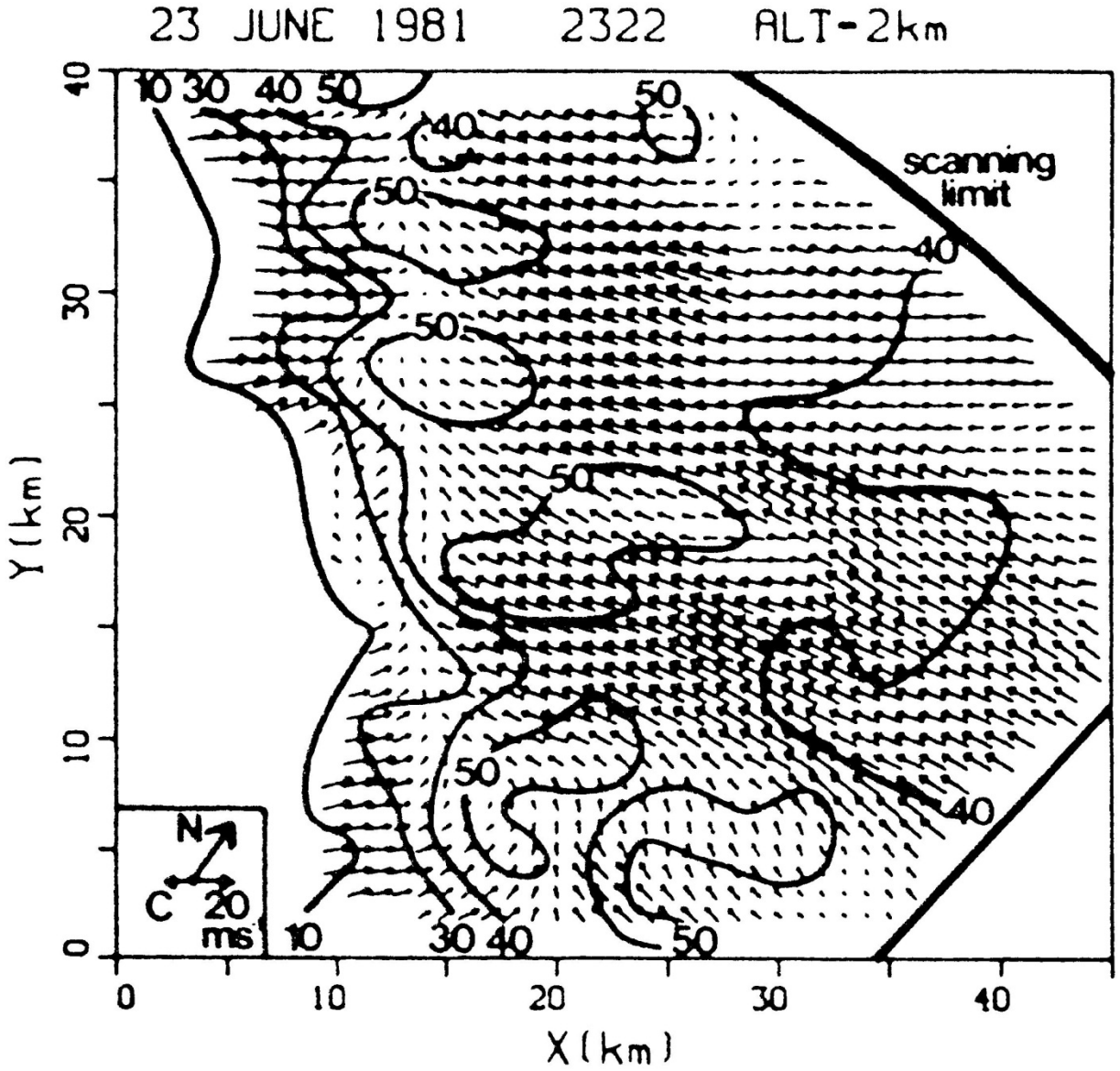

颱線風場與回波垂直結構 (Roux 1988)

(Vertical structure of airflow and precipitation of a tropical squall line)

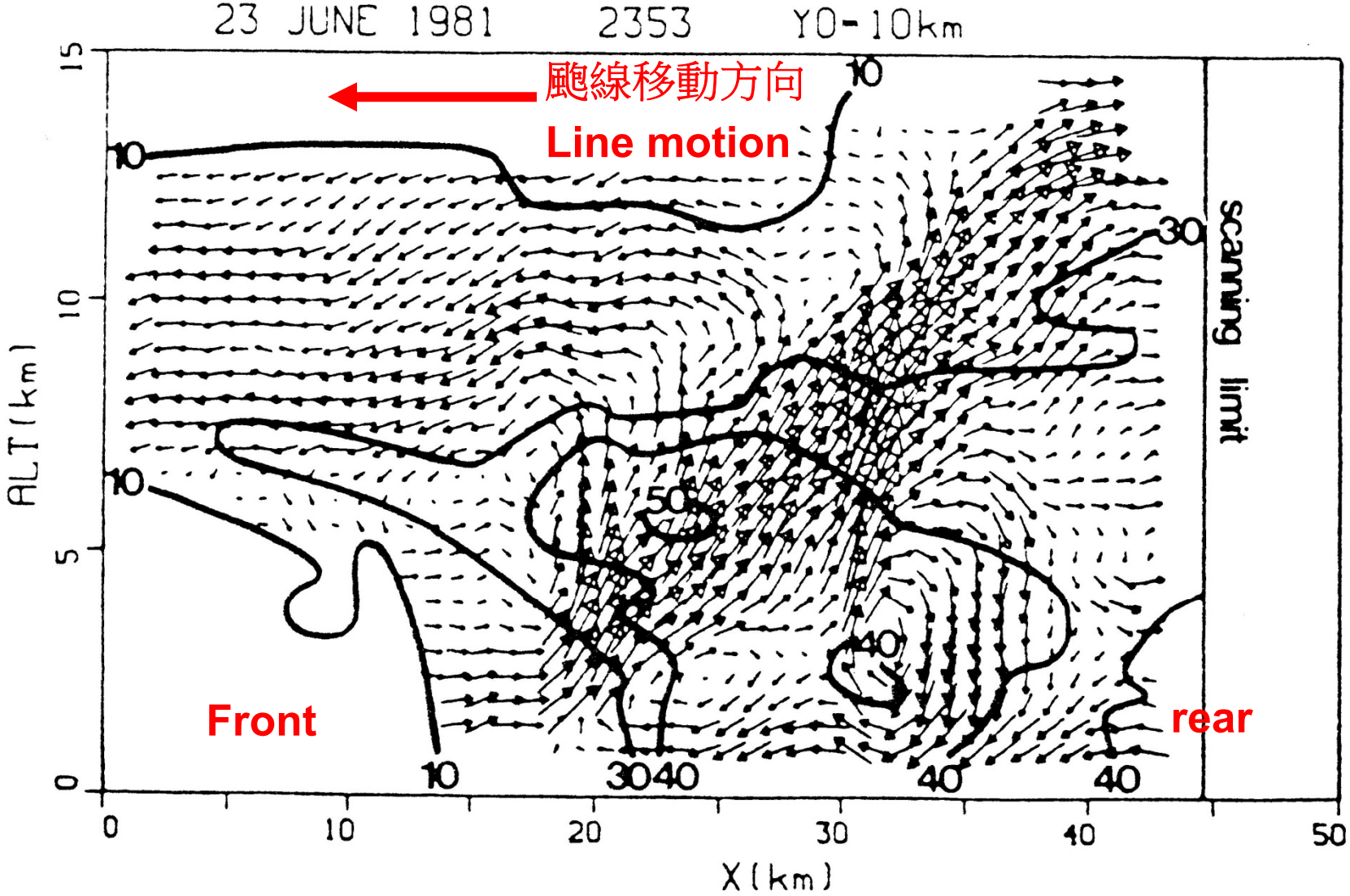

垂直速度(vertical velocity)

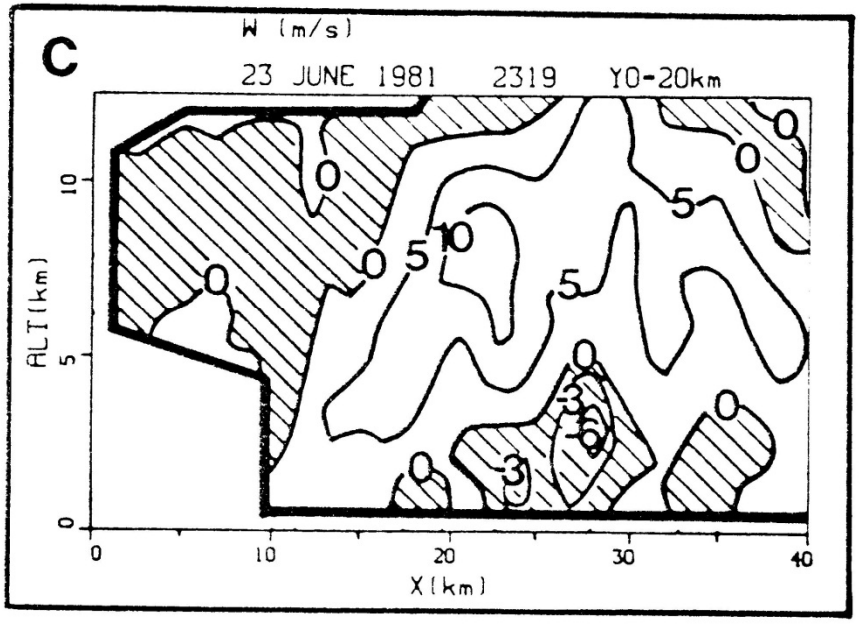

雷達回波 (radar reflectivity)

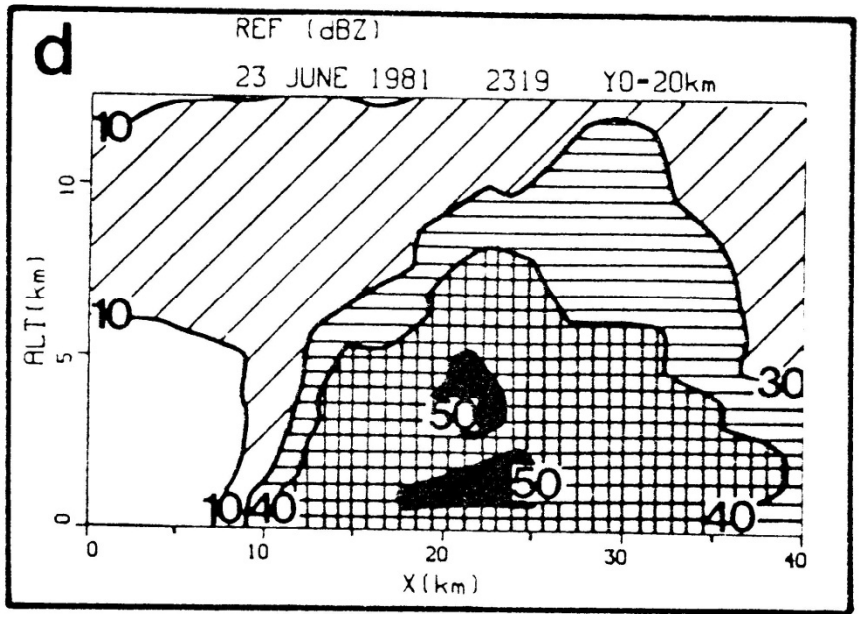

擾動溫度場 (perturbation T)

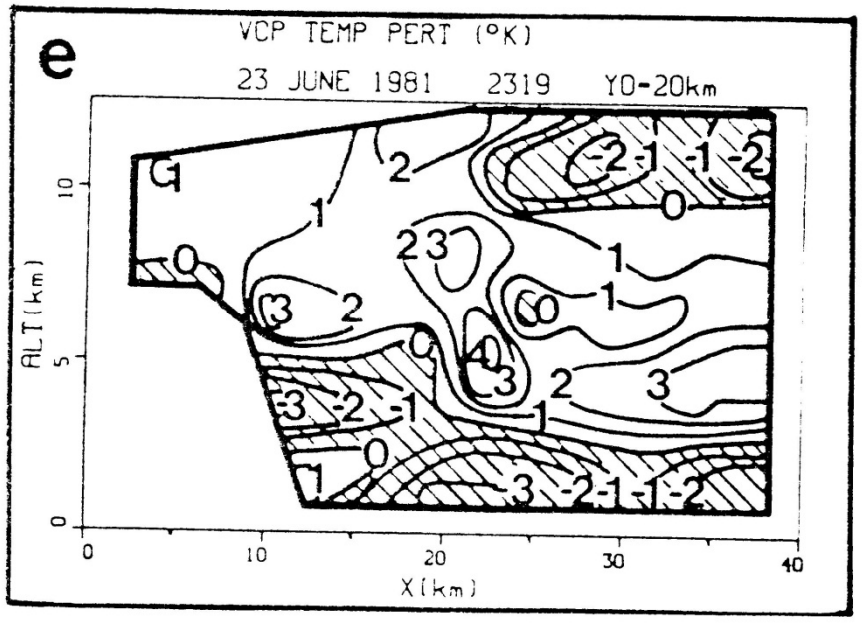

擾動氣壓場 (perturbation P)

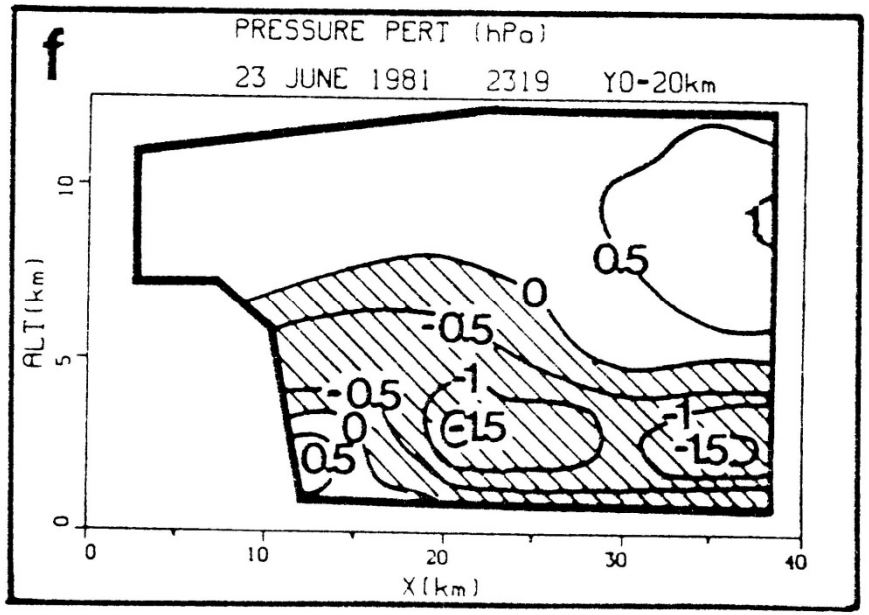

飛機觀測的颱線擾動氣壓場 (LeMone et al. 1984)

Vertical structure of perturbation pressure associated with a squall line derived from airborne in-situ measurements

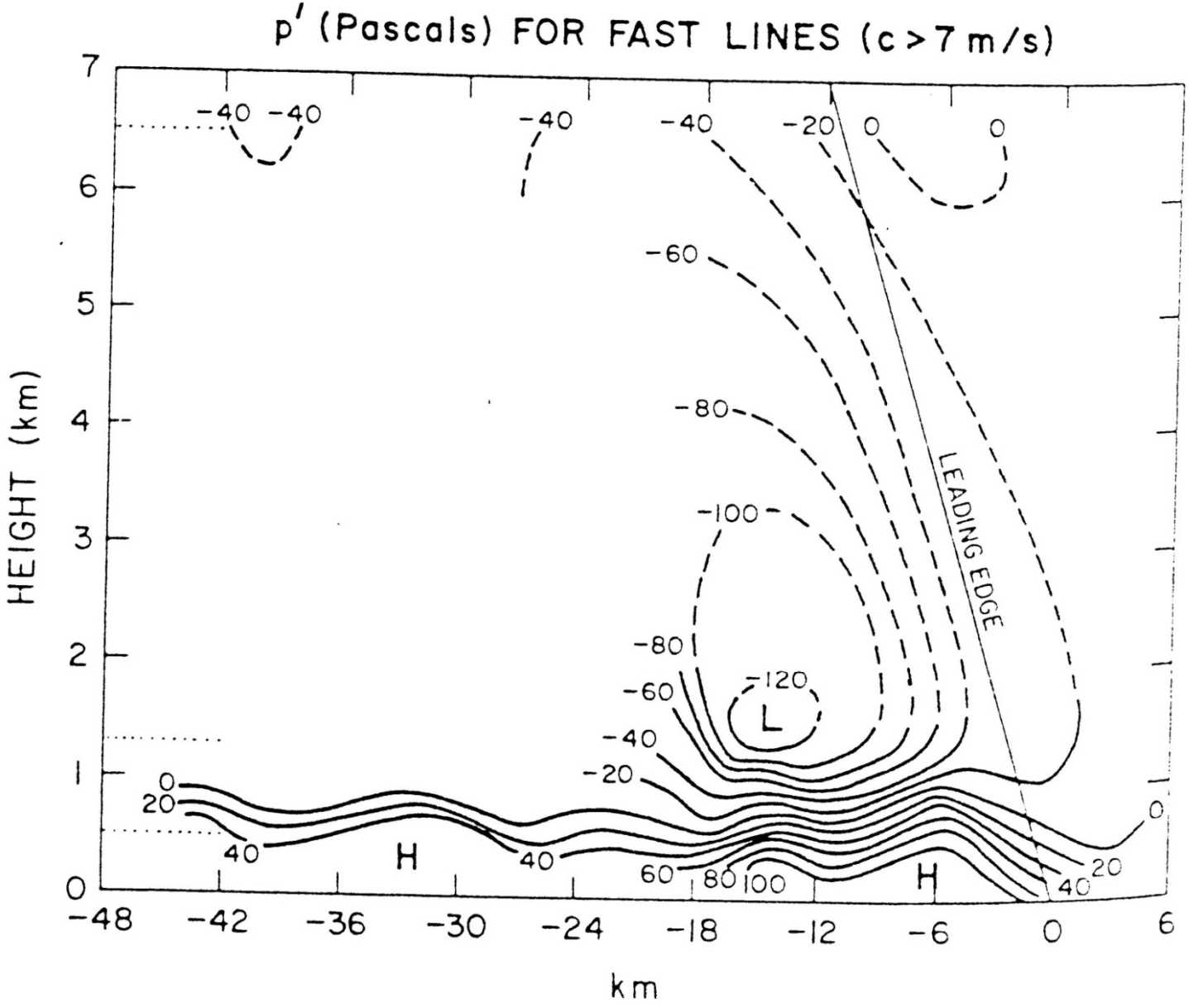

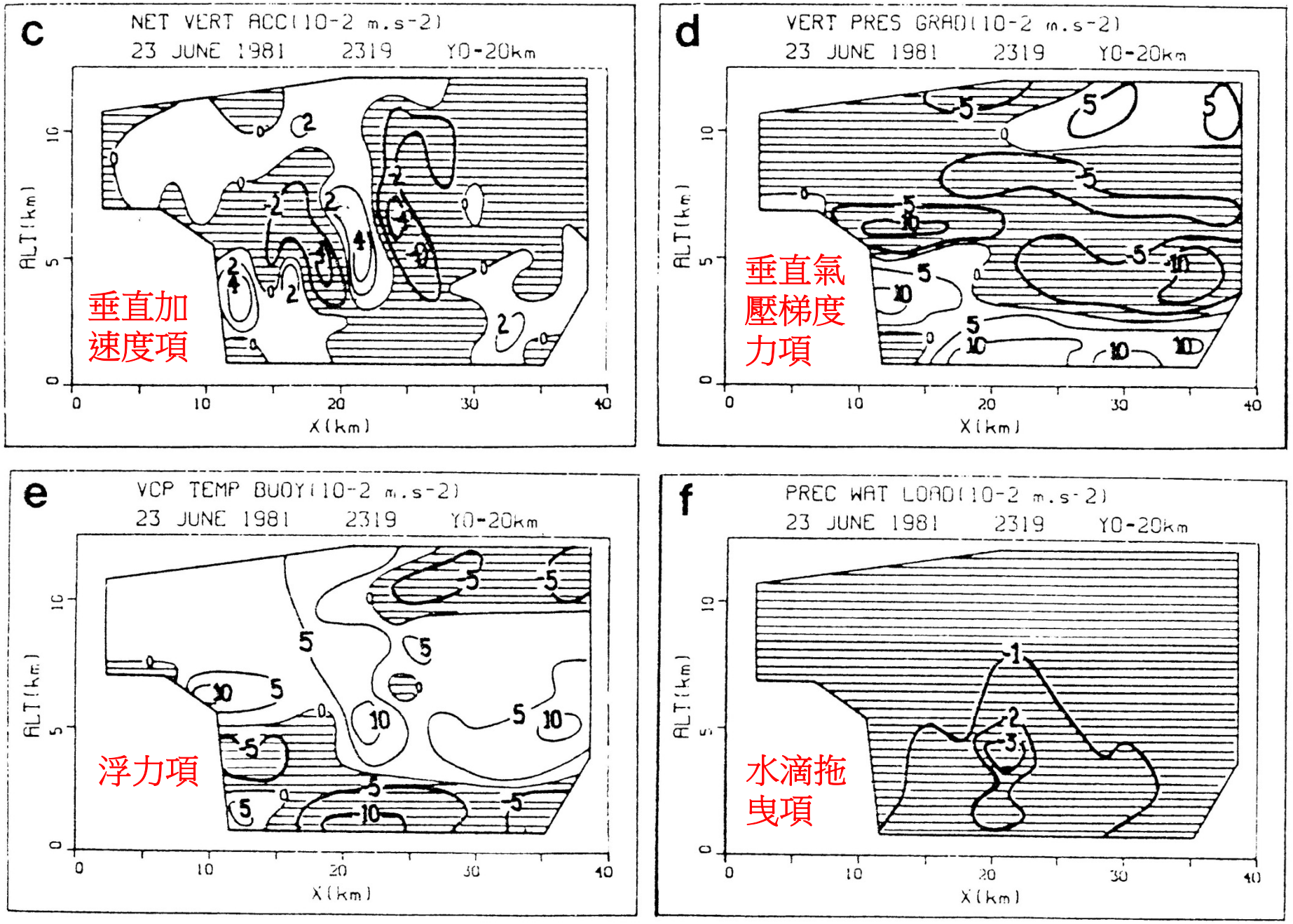
c
NET VERT ACC(10-2 m.s-2)
23 JUNE 1981 2319 Y0-20km
垂直加速度項
d
VERT PRES GRAD(10-2 m.s-2)
23 JUNE 1981 2319 Y0-20km
垂直氣壓梯度力項
e
VCP TEMP BUOY(10-2 m.s-2)
23 JUNE 1981 2319 Y0-20km
浮力項
f
PREC WAT LOAD(10-2 m.s-2)
23 JUNE 1981 2319 Y0-20km
水滴拖曳項
ALT(km)
X(km)

中緯度颱線系統內部氣流結構特徵 (Smull and Houze 1985)

Airflow features of a mid-latitude squall line from a larger scale view

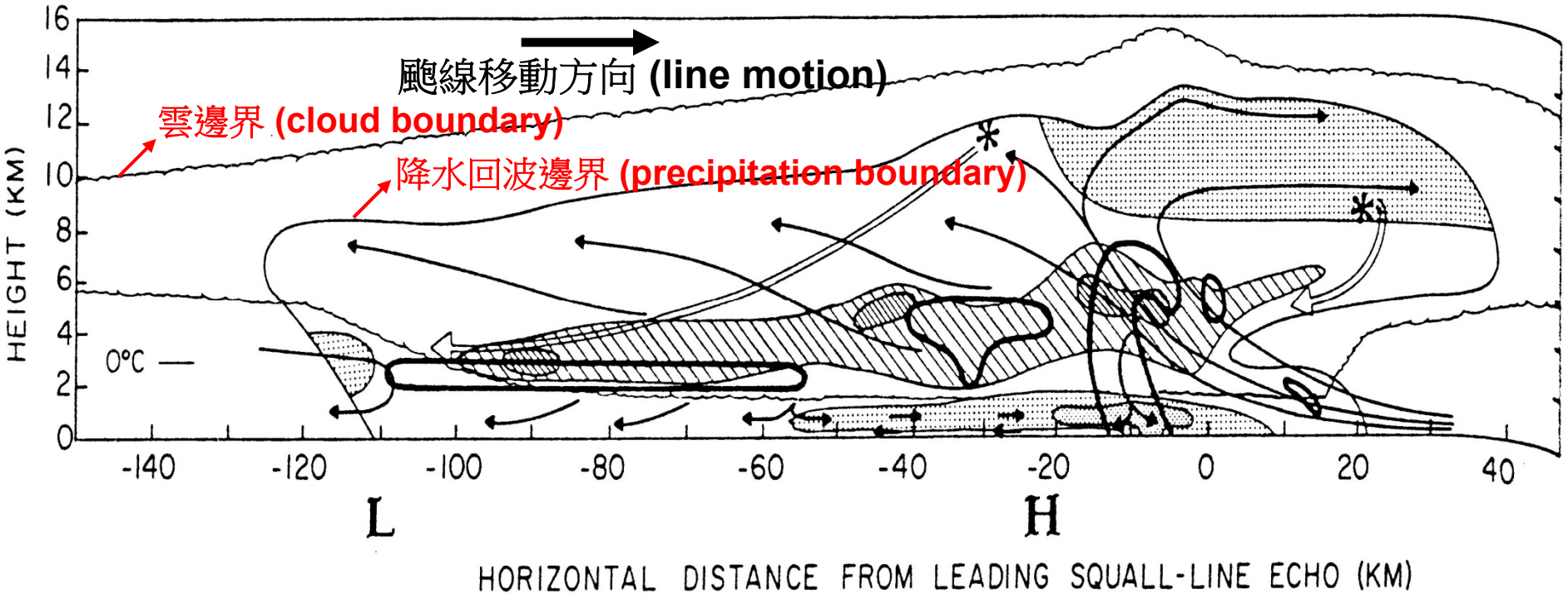

颱線層狀降水區平均輻散, 渦度及垂直速度隨高度的變化 **(Jorgensen and Smull 1993)**

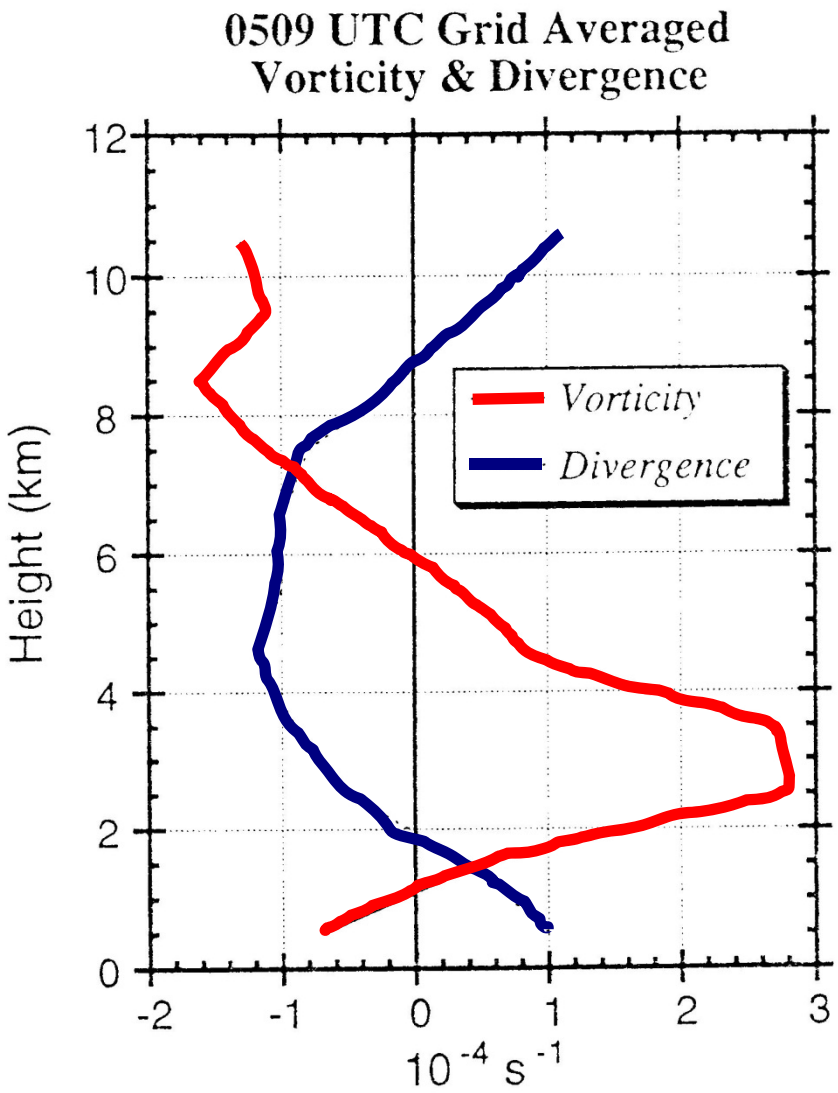

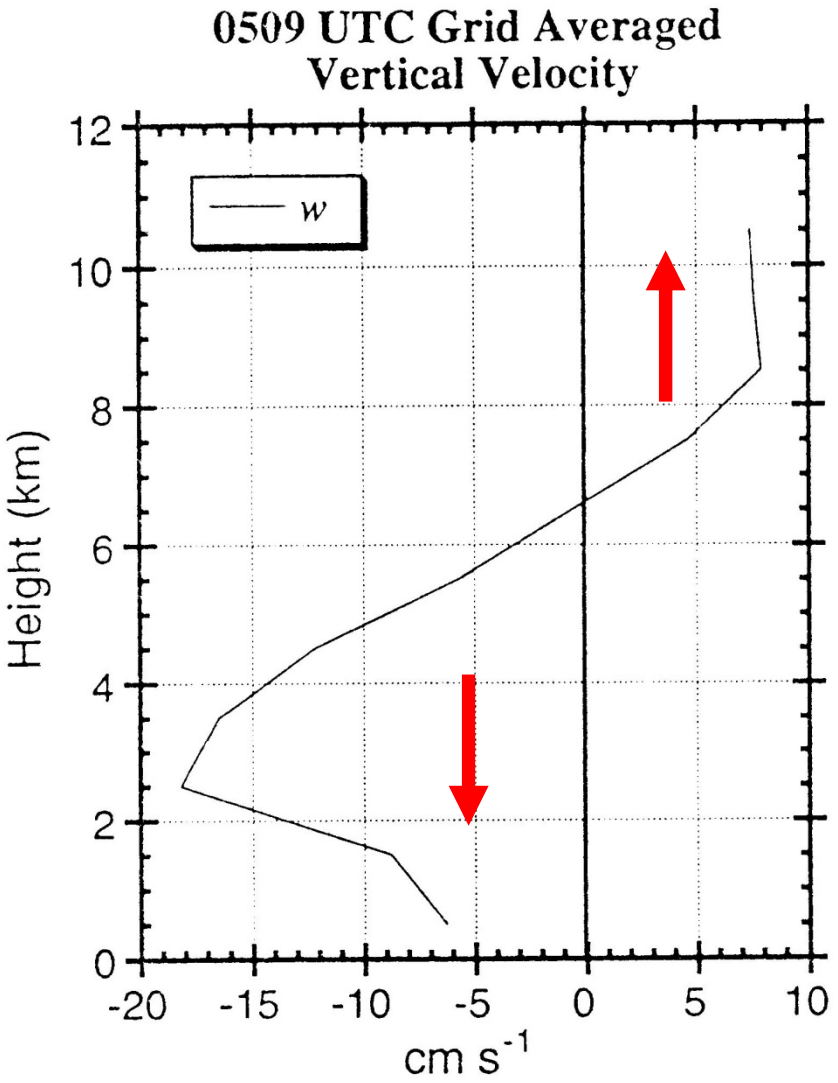

颱線對流降水區與層狀降水區內平均垂直速度隨高度變化之比較

Mean vertical velocity calculated over the convective and stratiform region of a squall line (Biggerstaff and Houze 1991)

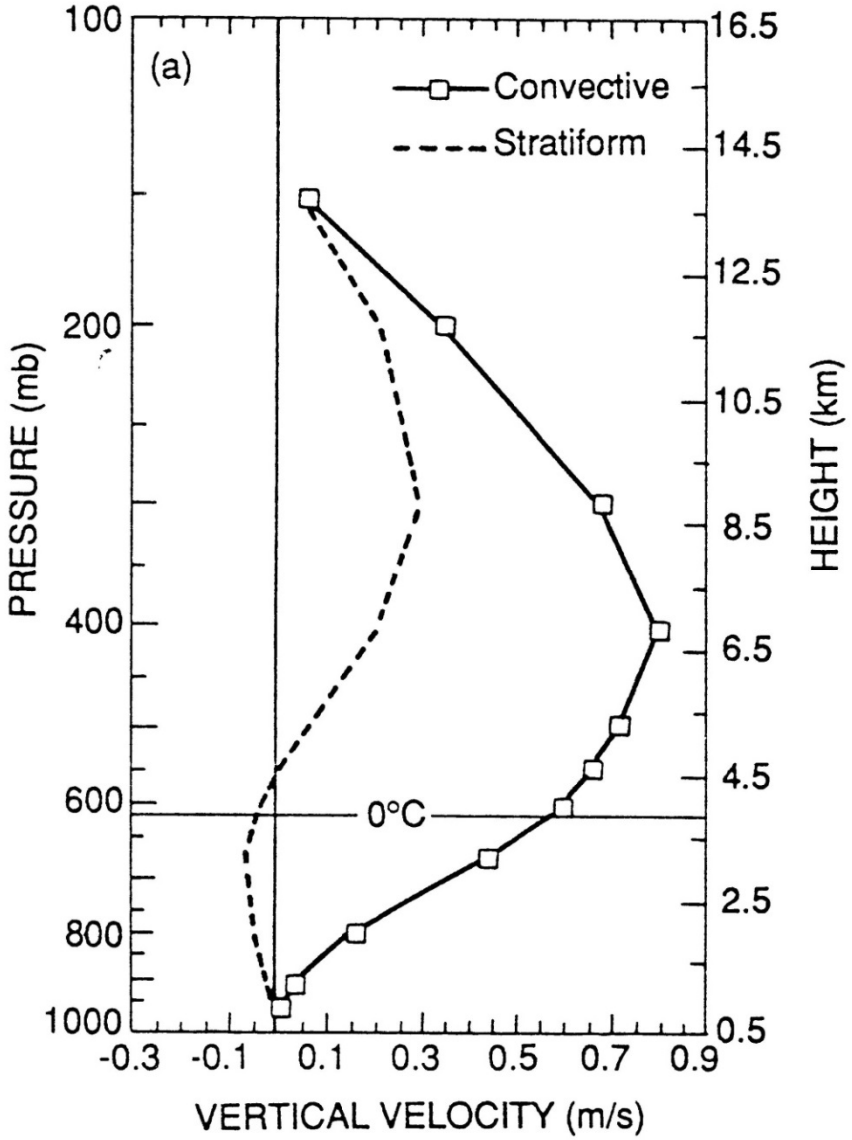

颮線內部水(冰)粒子軌跡線之示意圖 (Biggerstaff and Houze 1991)

(Trajectories of hydrometeors inside a squall line system)

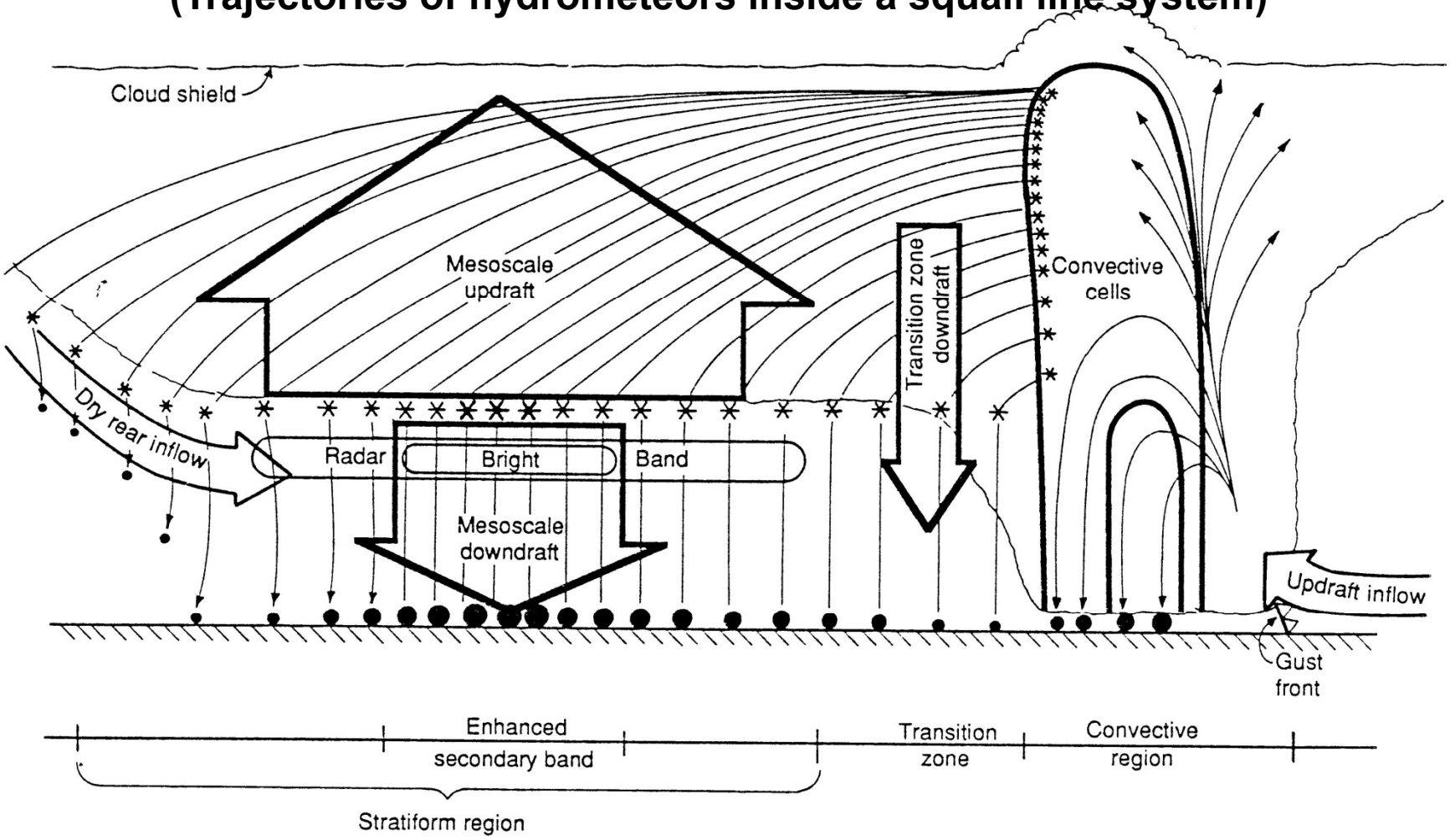

FIG. 18. Conceptual model of the two-dimensional hydrometeor trajectories through the stratiform region of a squall line with trailing stratiform precipitation. See text for further explanation.

颮線系統內部氣流與氣壓場結構之概念模式 (Houze et al. 1989)

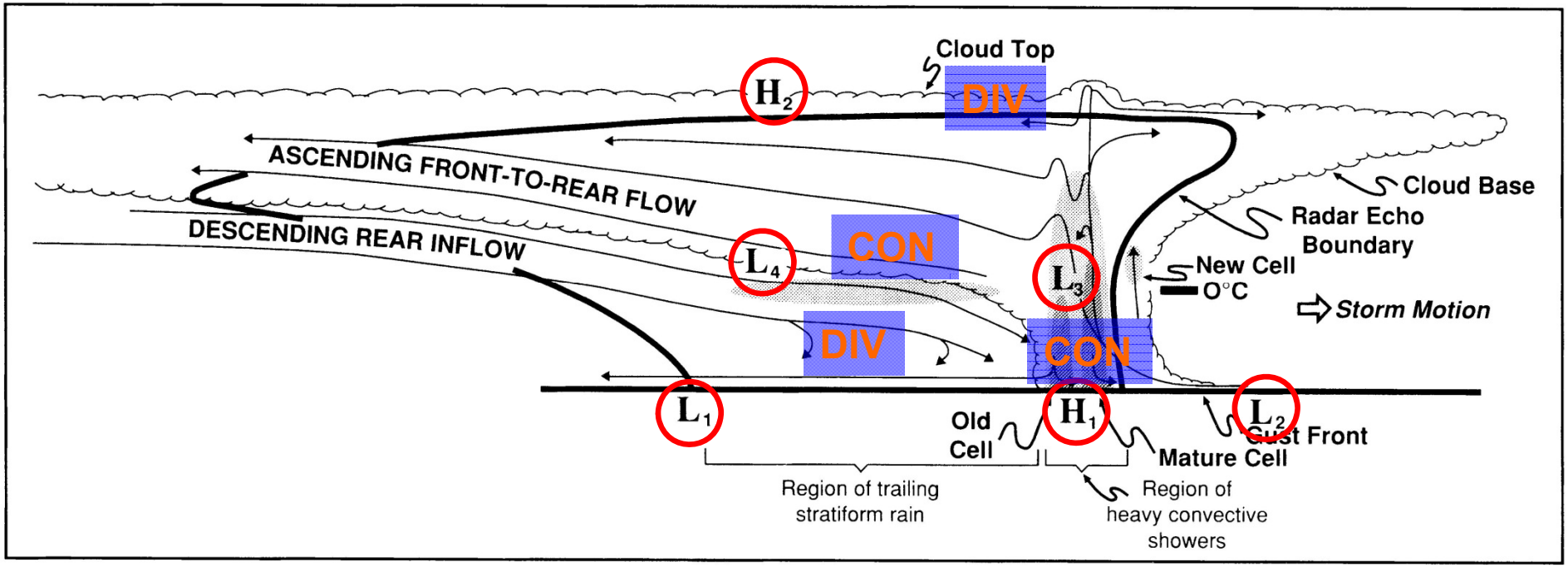

H1: 中尺度高壓, 常發生在對流降水區之低層 (產生原因: 水滴拖曳與降水蒸發冷卻)

H2: 系統高層之中尺度高壓 (產生原因: 可能與 (1) 對流系統高層雲頂輻射冷卻 (2) 中高層潛熱加熱 (3) 中尺度上衝流之絕熱膨脹冷卻等等有關)

L1: 後緣低壓 (**wake Low**), 常發生在接近地面層, 層狀降水區之後側邊緣 (產生原因: 未飽和下降增溫)

L2: 對流線前面之低壓 (產生原因: 補償性下沉增溫)

L3: 傾斜對流上衝流下方之低壓 (產生原因: 潛熱釋放增溫)

L4: 層狀區接近溶解層高度之低壓, 尺度比**L3**大 (產生原因: 可能與伴隨中尺度上衝之潛熱釋放增溫有關)

Roles of MCVs in contributing to tropical cyclogenesis (Houze 2010)

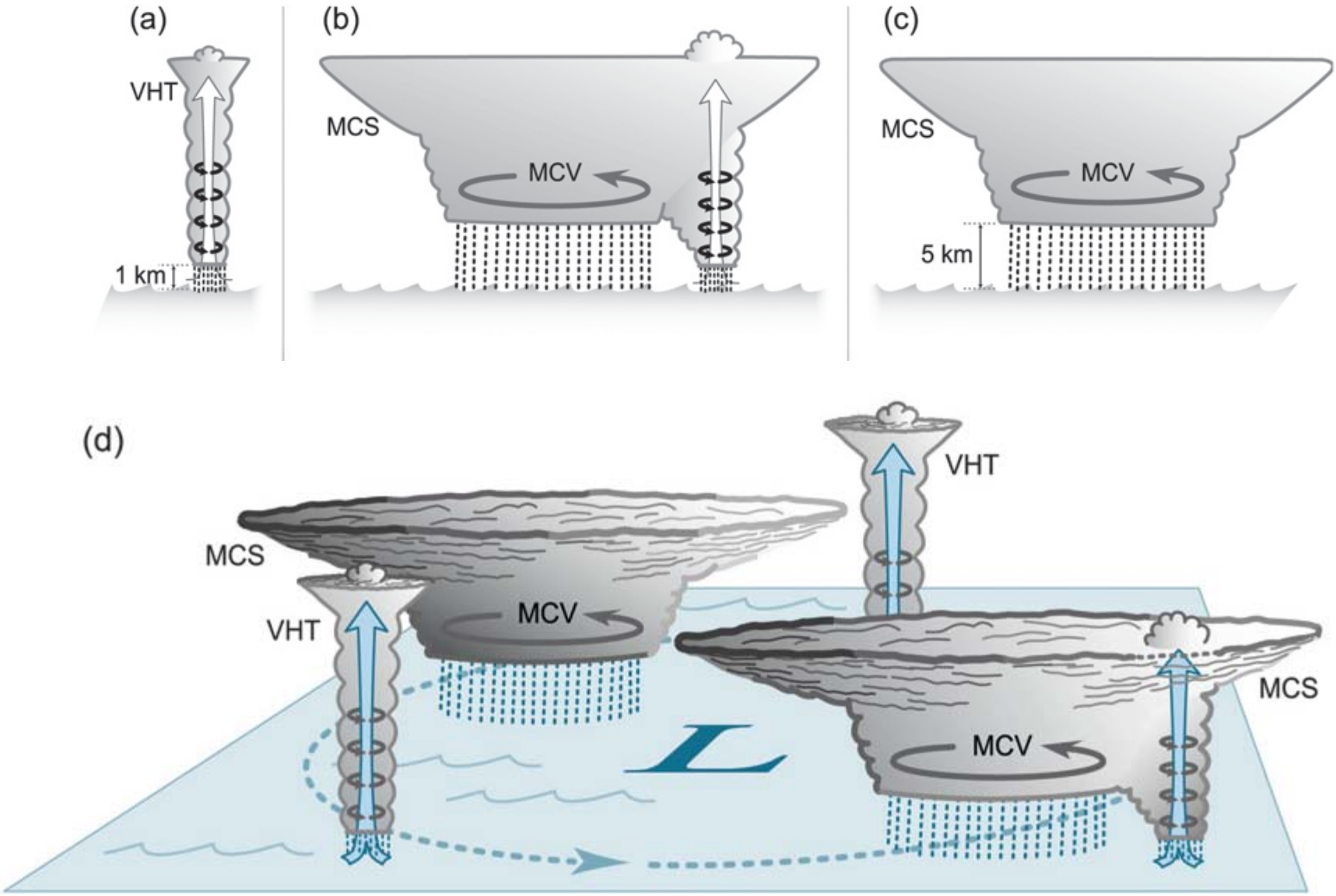

對稱型與非對稱型颱線地面氣壓場之分佈 (Loehrer and Johnson 1995)

Surface pressure distribution of symmetric and asymmetric squall lines

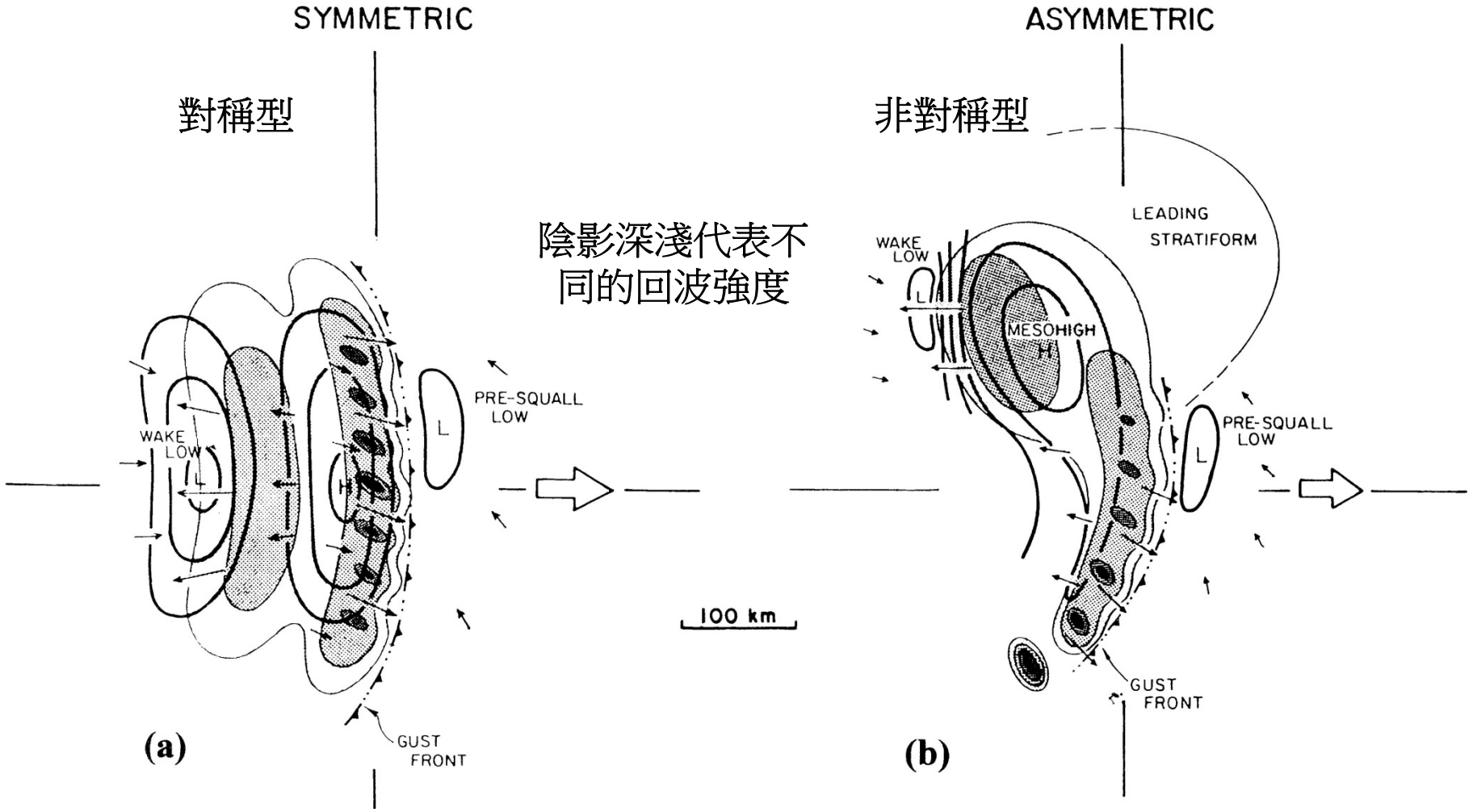

中尺度對流複合體 **(Mesoscale Convective Complex, MCC)** 所引發的高層**(200-mb)**反氣旋環流 **(Fritsch and Brown 1982)**

Upper-level MCC-induced anticyclonic circulation

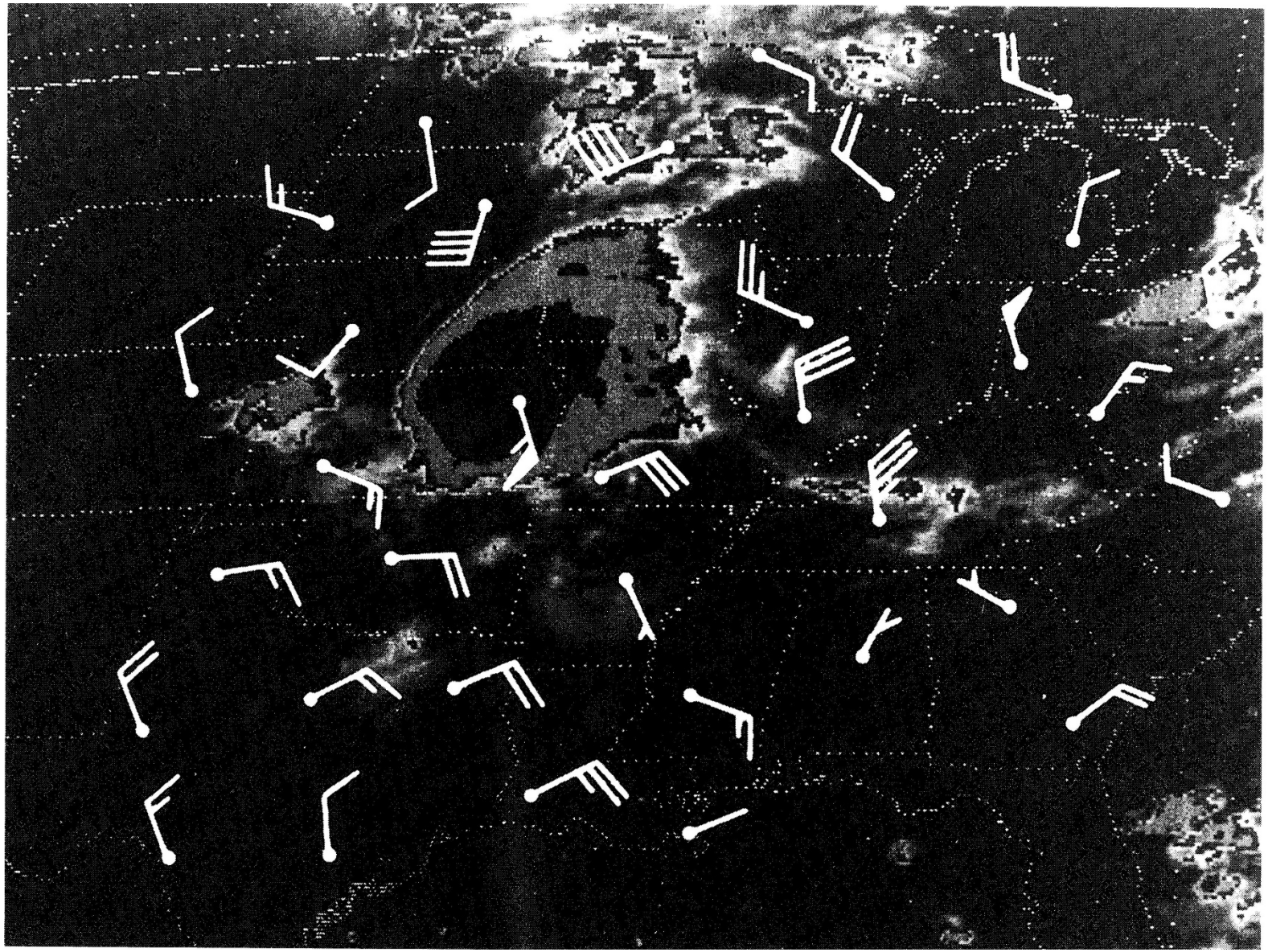

伴隨對稱型與非對稱型颮線系統中對流層氣流之概念模式 **(Houze et al. 1989)**

(Conceptual model of mid-level airflow patterns associated with symmetric and asymmetric squall lines)

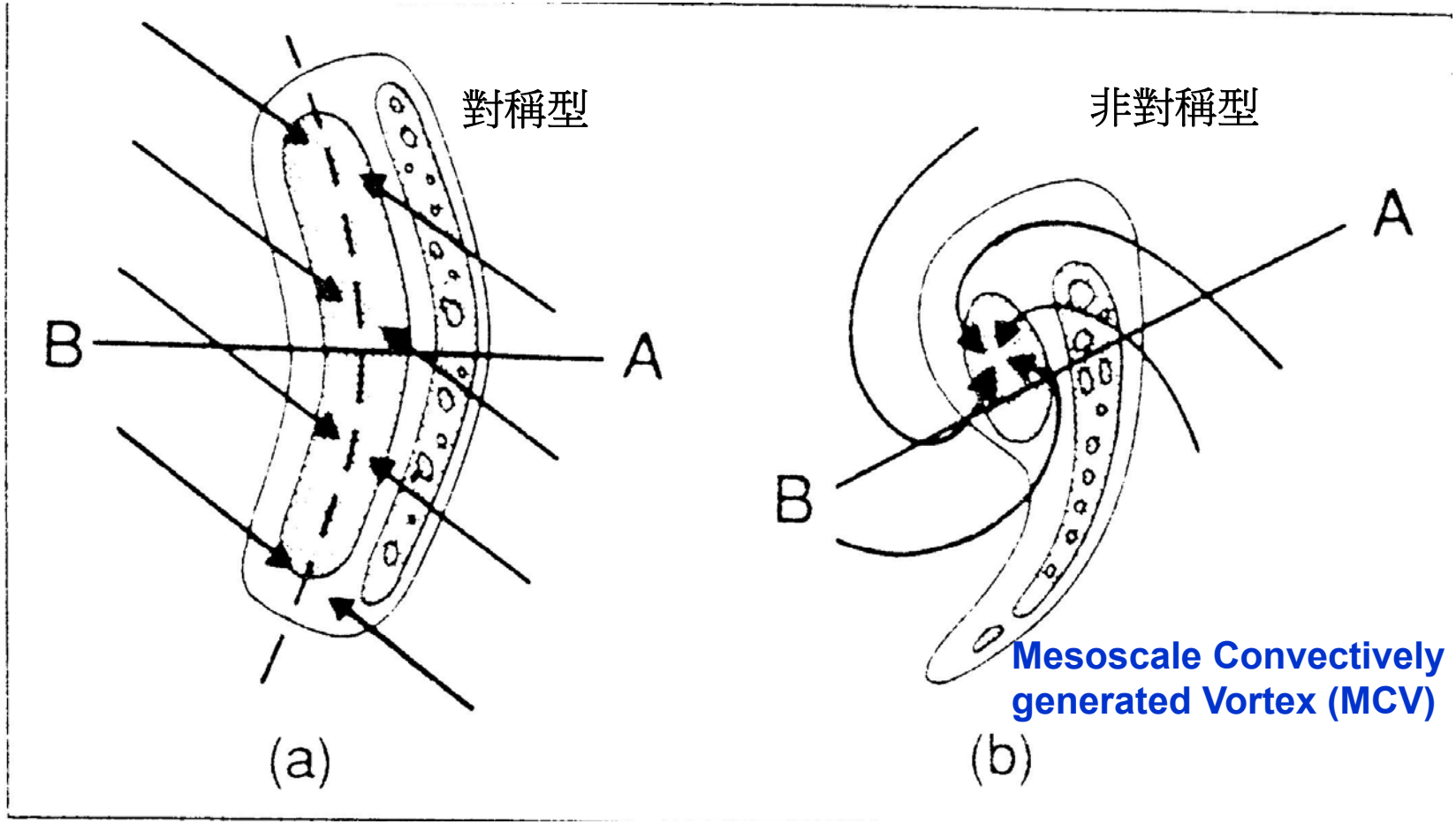

發生在美國中部中尺度渦旋環流(MCV)之可見光雲圖 **(Menard and Fritsch 1989)**

Visible satellite image showing evidence of MCV embedded within a MCS

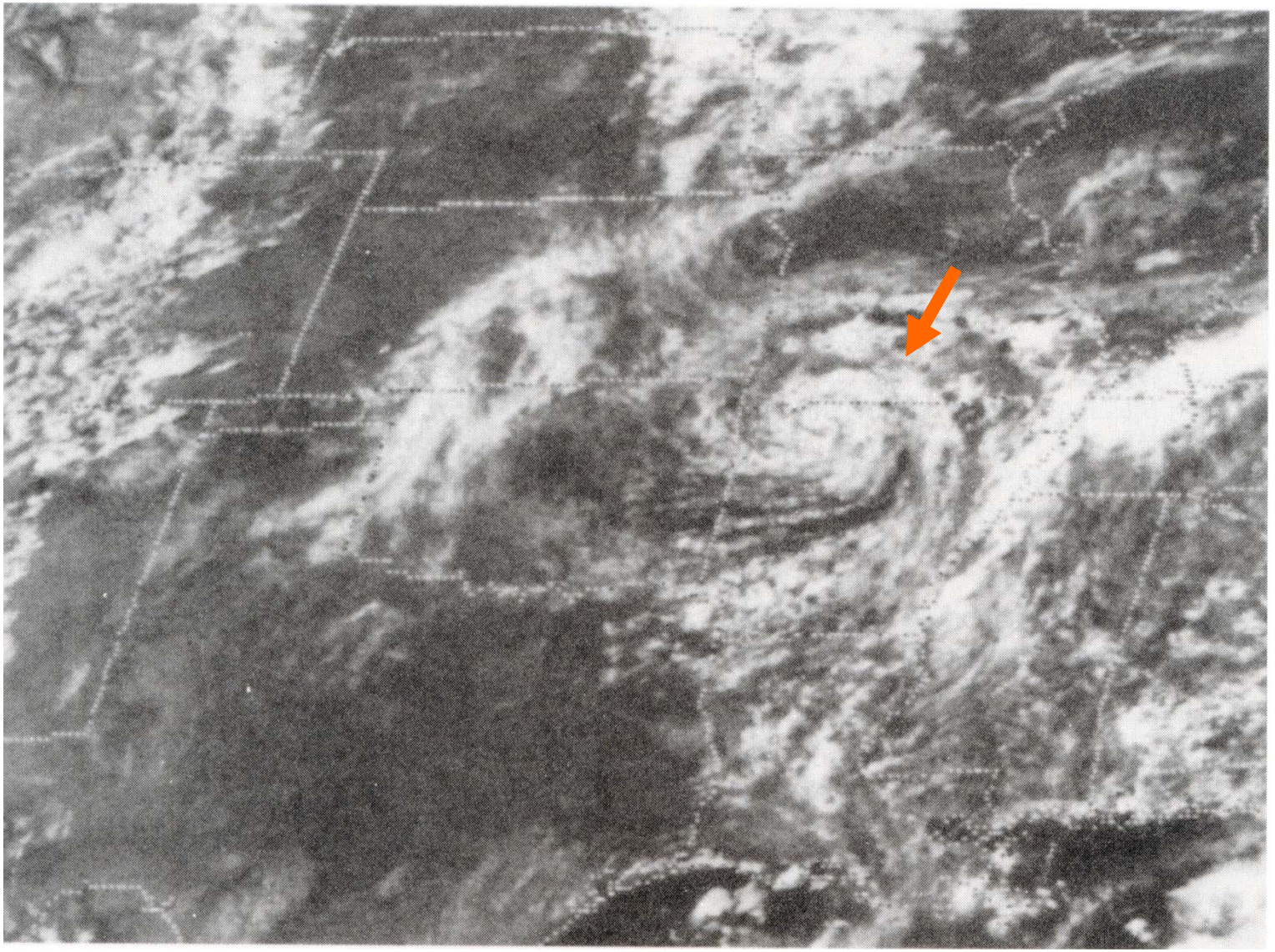

中緯度颱線系統後緣層狀降水區之中層 **(600 mb)**中尺度渦旋

A MCV located in the stratiform region of a mid-latitude squall line (Smull and Houze 1985)

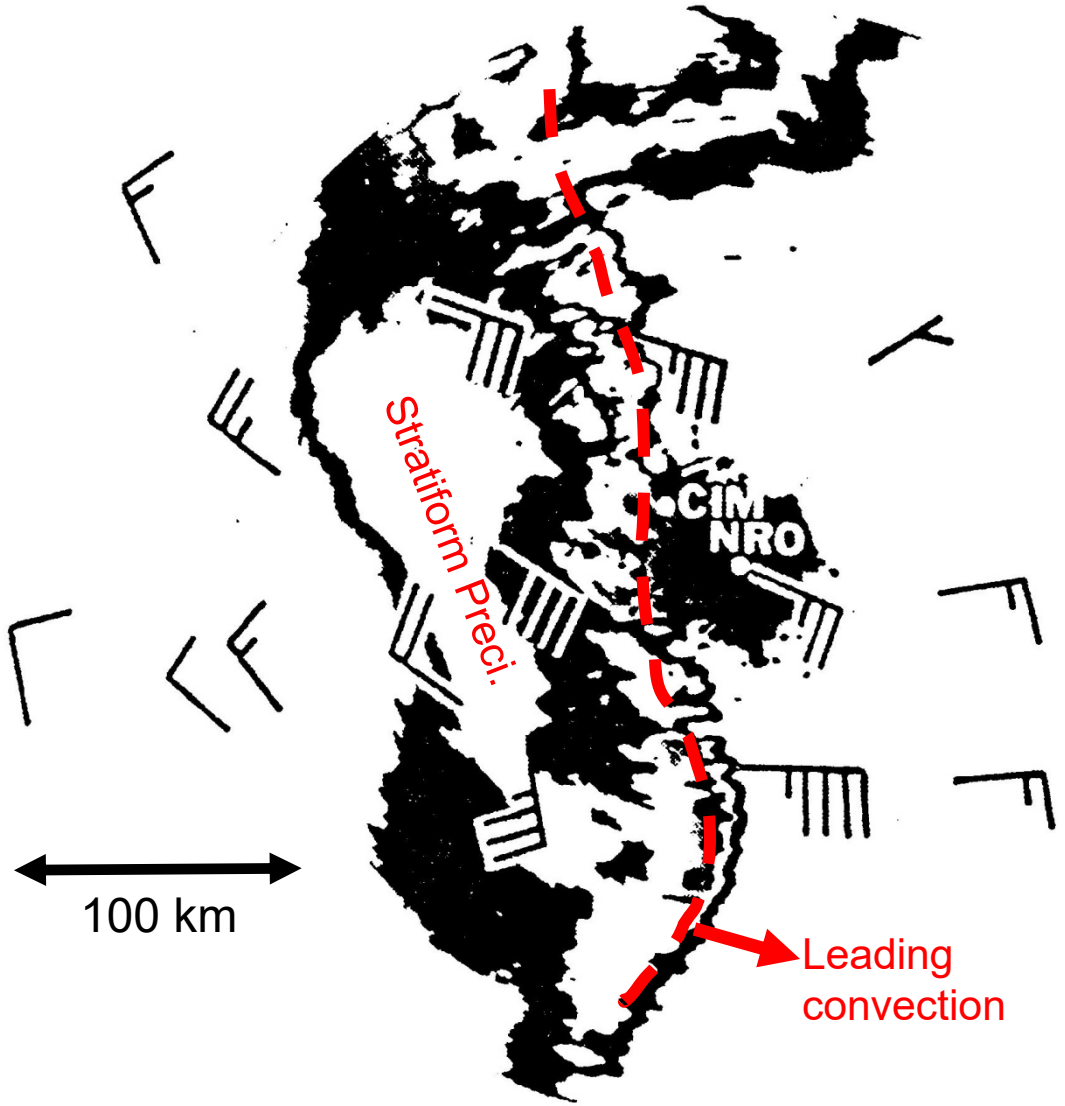

在台灣東南方海面所觀測到的副熱帶中尺度渦旋

A subtropical MCV observed in southeastern Taiwan (Yu et al. 1999)

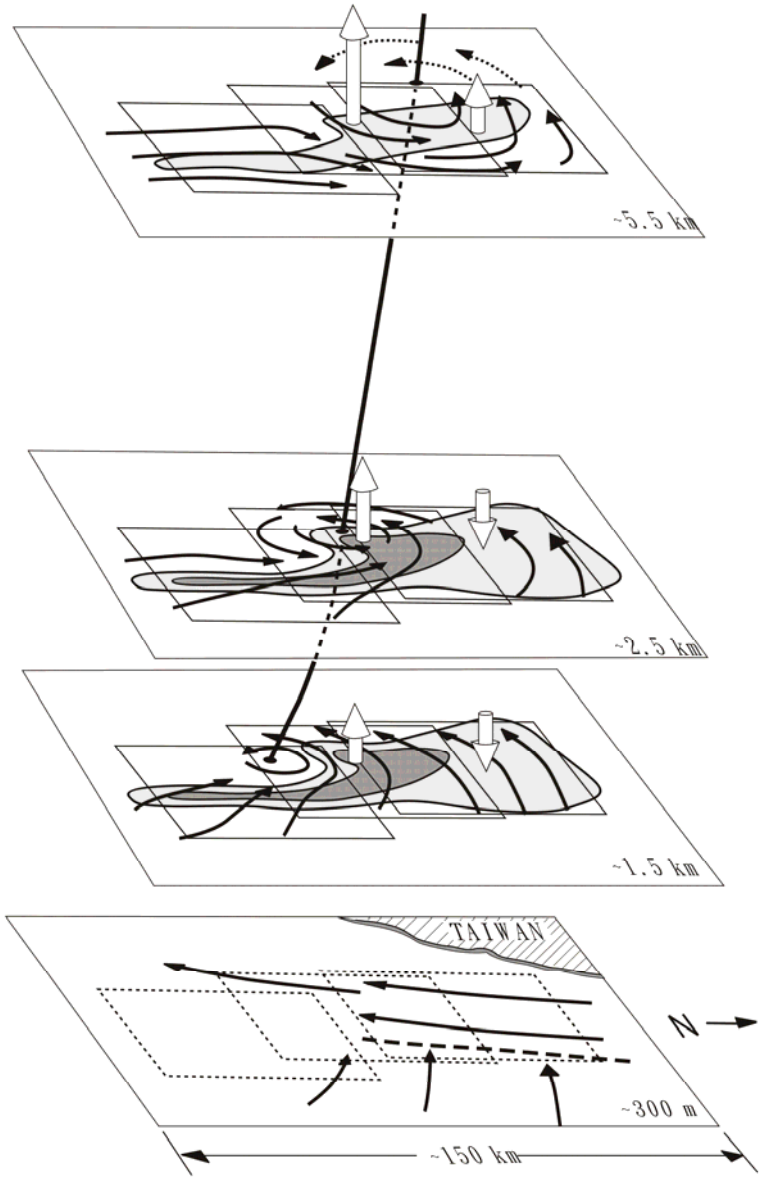

熱帶颱線北側邊緣尺度較小之MCV

A MCV observed near the northern end of a tropical squall line (Jorgensen et al. 1997)

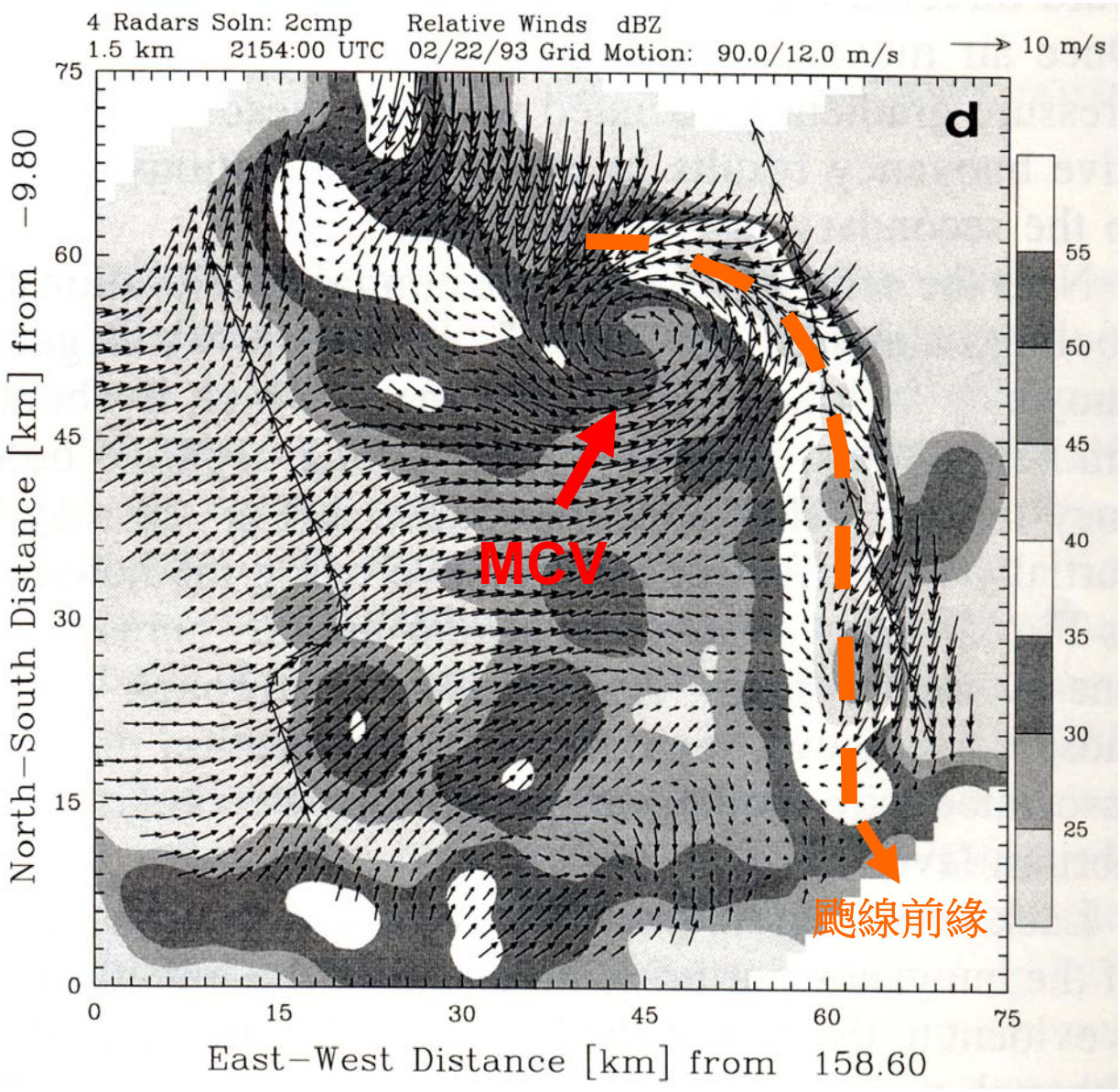

存在於對流前緣後方之尺度較小MCV (Verlinde and Cotton 1990)

A relatively small MCV observed in the rear side of the leading convective line

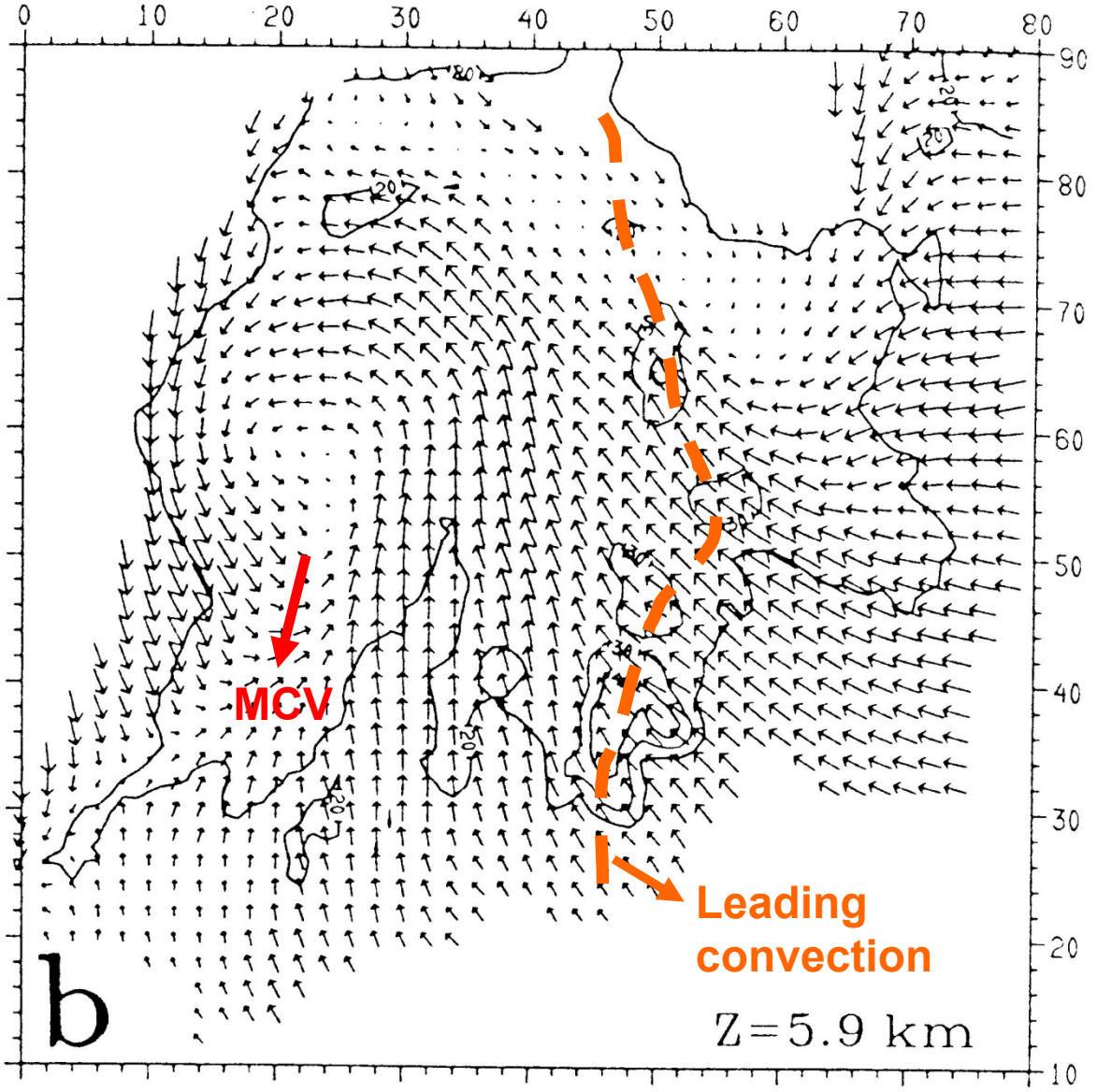

紅外線衛星雲圖顯示許多積雲簇存在於熱帶與低緯地區

Many cloud clusters exist over low-latitude regions

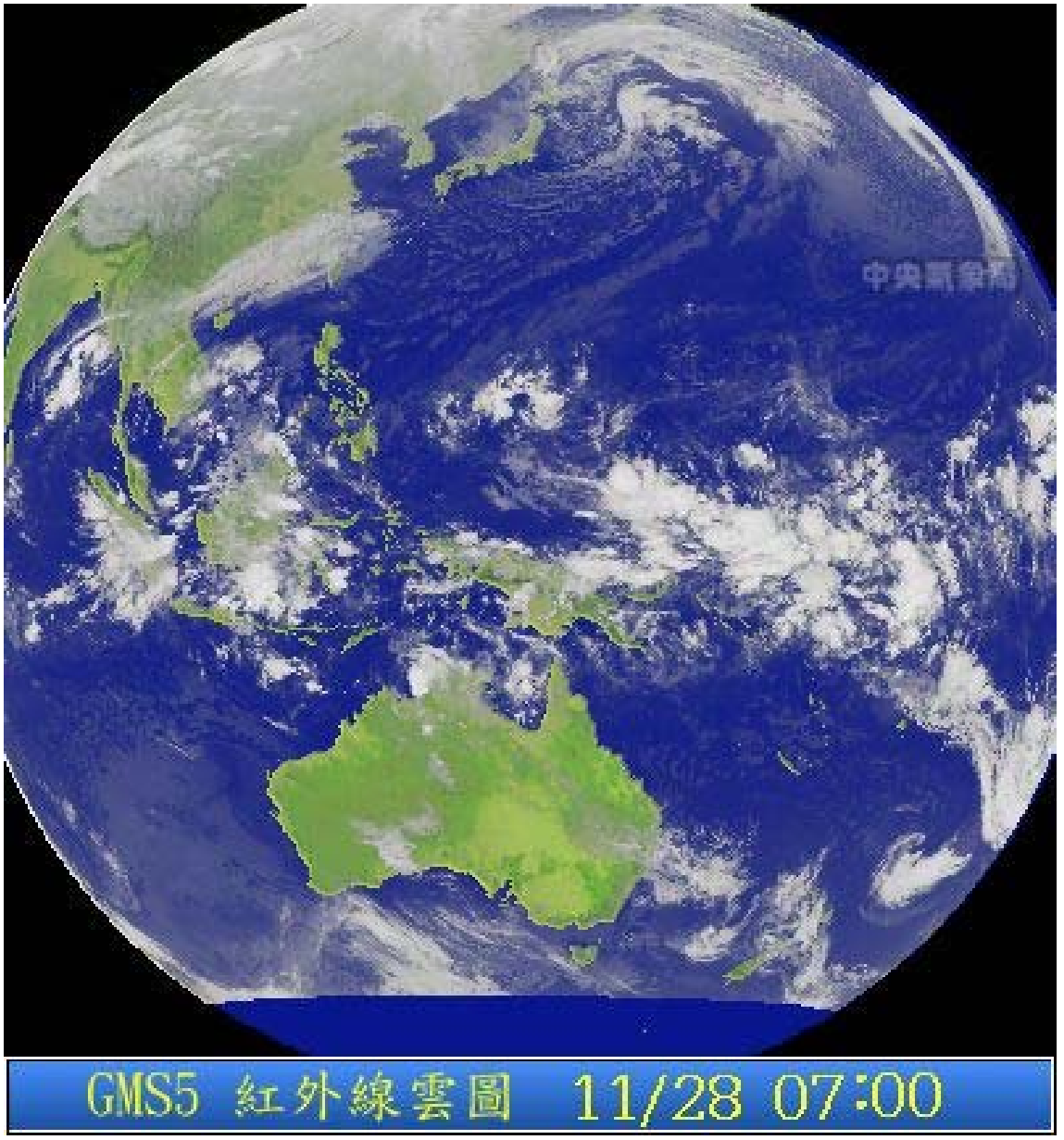

透過傾側效應將水平渦度轉成垂直渦度示意圖 **(Holton 1992)**

(Schematic showing the tilt of horizontal vorticity into vertical)

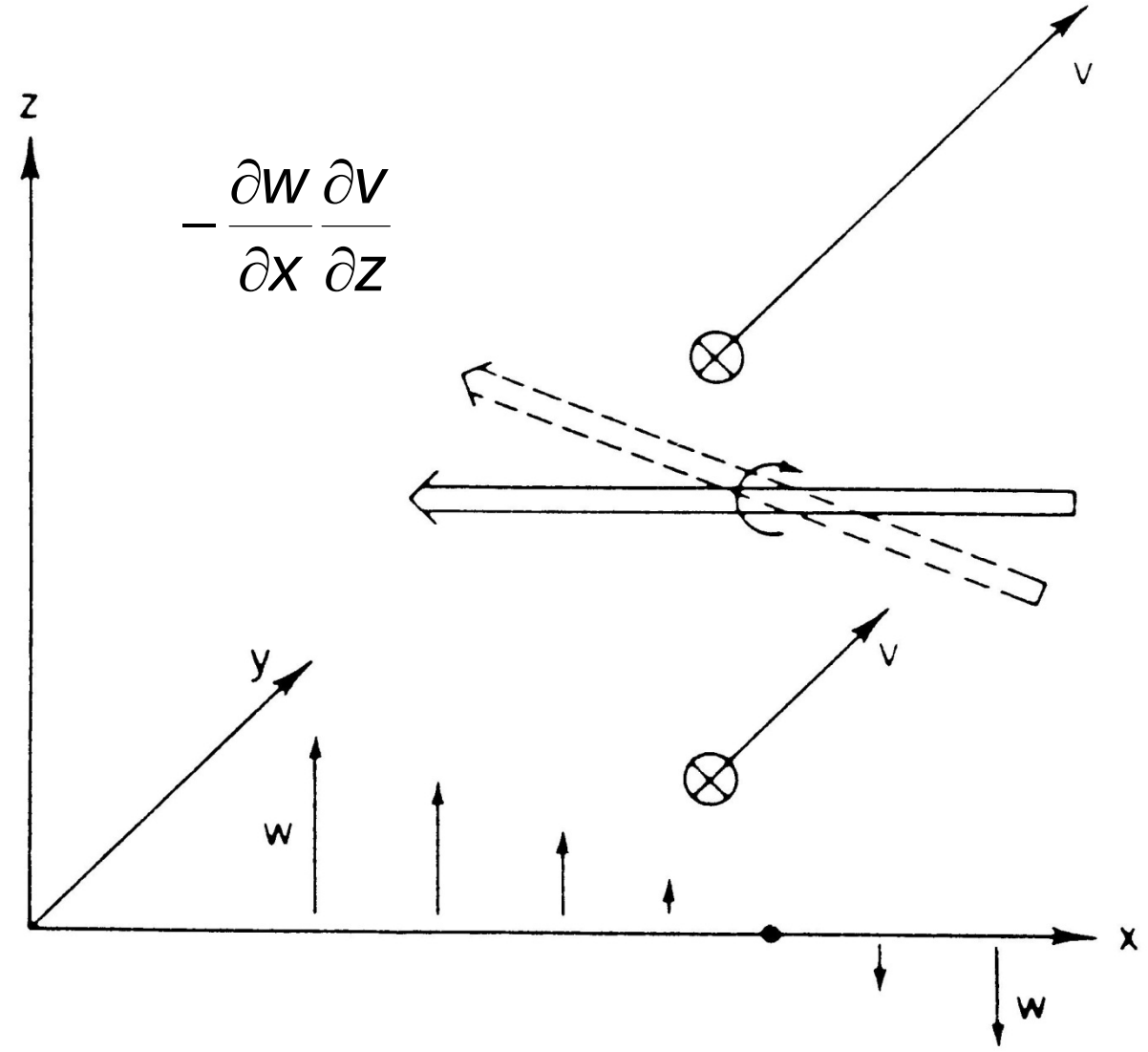

環境水平渦管與一對流胞交互作用所產生垂直渦度之示意圖 **(Klemp 1987)**

Schematic showing interaction of a convective cell with environmental vorticity

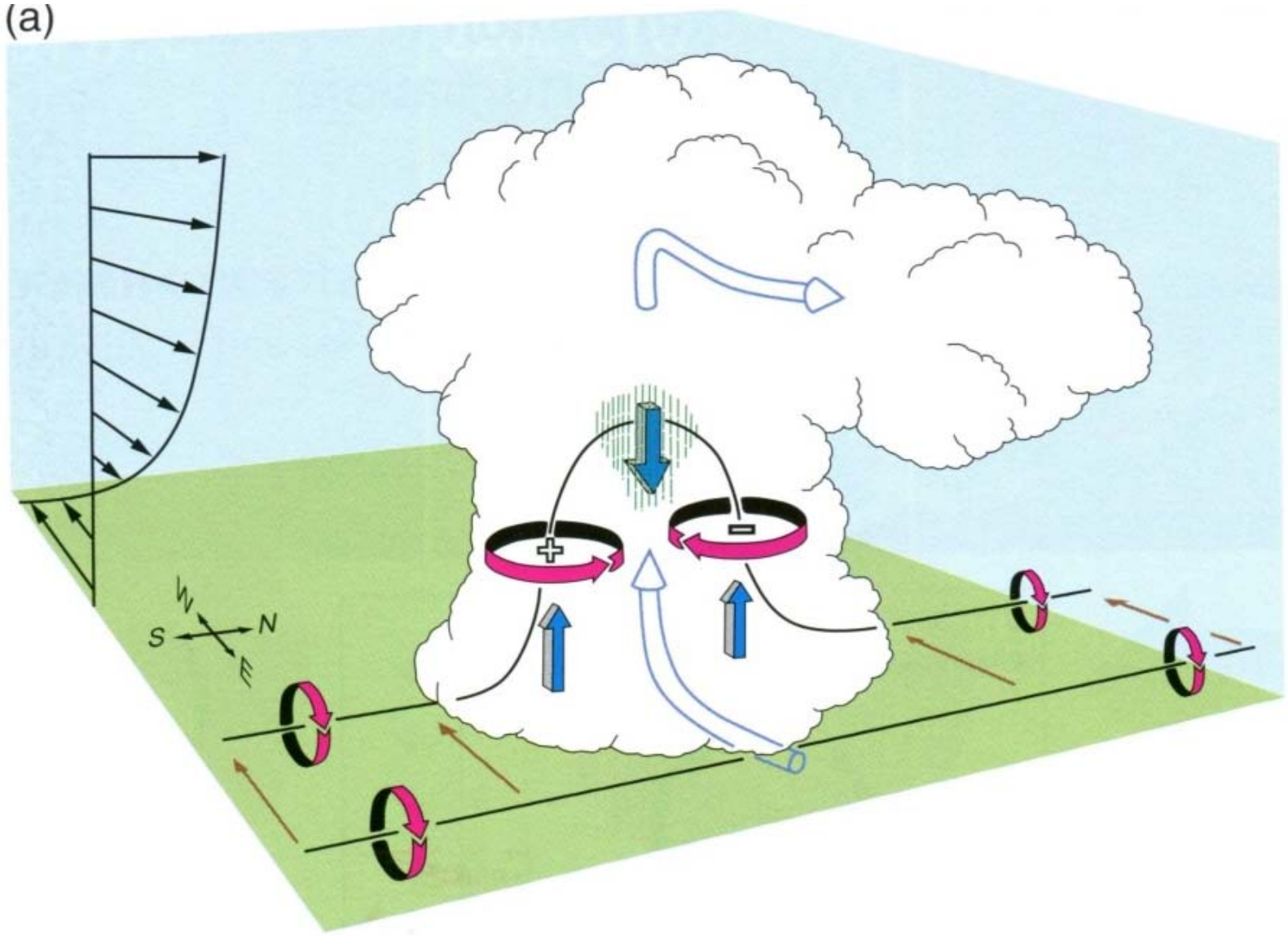

環境水平渦管進一步與對流胞之下衝流交互作用所產生垂直渦度之示意圖 **(Klemp 1987)**

Schematic showing patterns of vertical vorticity as the convective downdraft further interacts with environmental shear (vorticity)

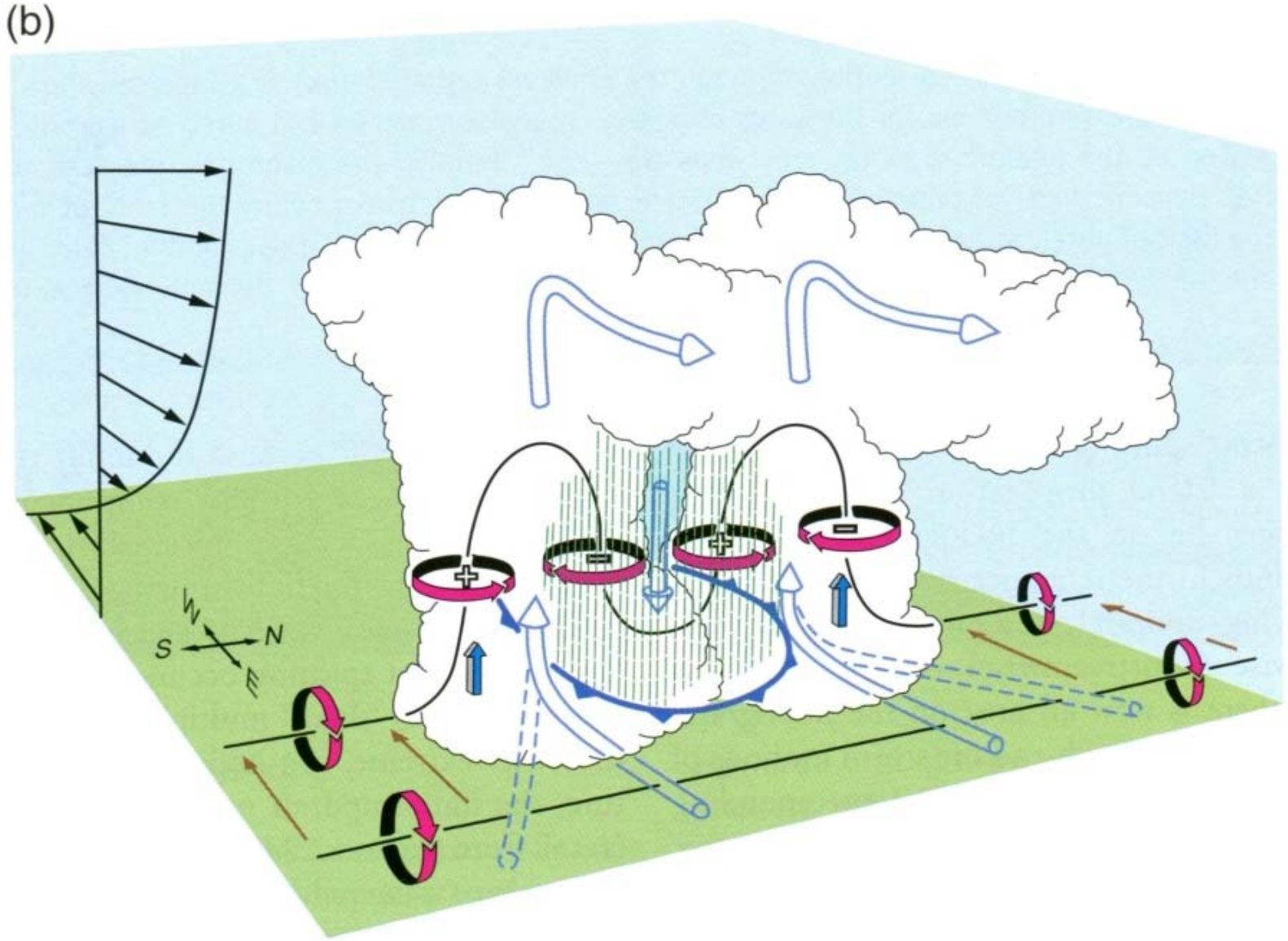

氣旋式渦旋與反氣旋渦旋同時分別存在於颱線北側後緣及南側邊緣 **(Scott and Rutledge 1995)**

(A pair of vortices exist in the northern and southern flank of a squall line)

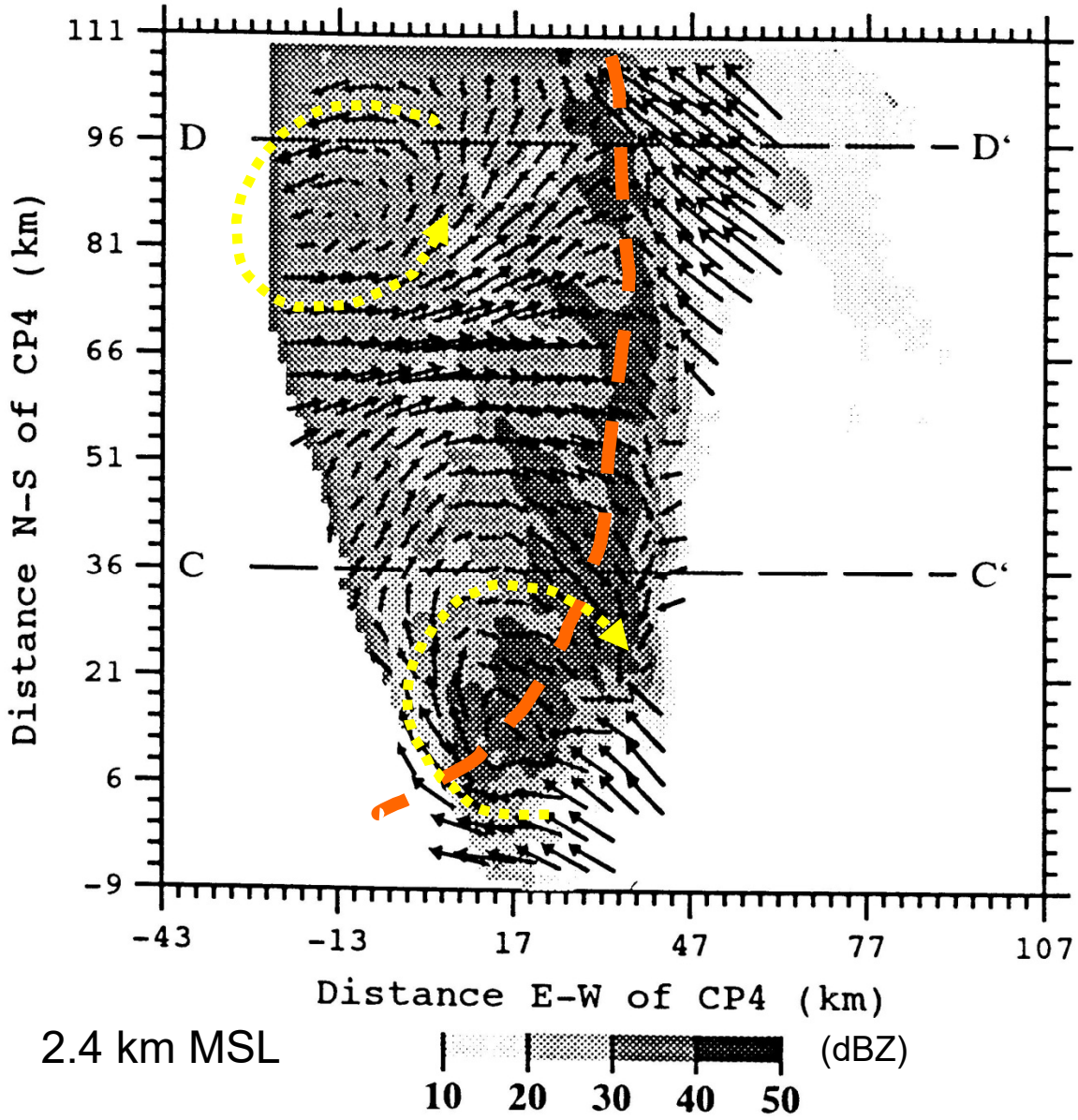

透過對流上衝流與中尺度上(下)衝流對環境水平渦管的傾側效應所產生垂直氣旋式 (與反氣旋) 渦度之概念圖 **(Biggerstaff and Houze 1991)**

Distribution of vertical vorticities produced by the interaction between mesoscale updraft/downdraft and environmental shear/vorticity

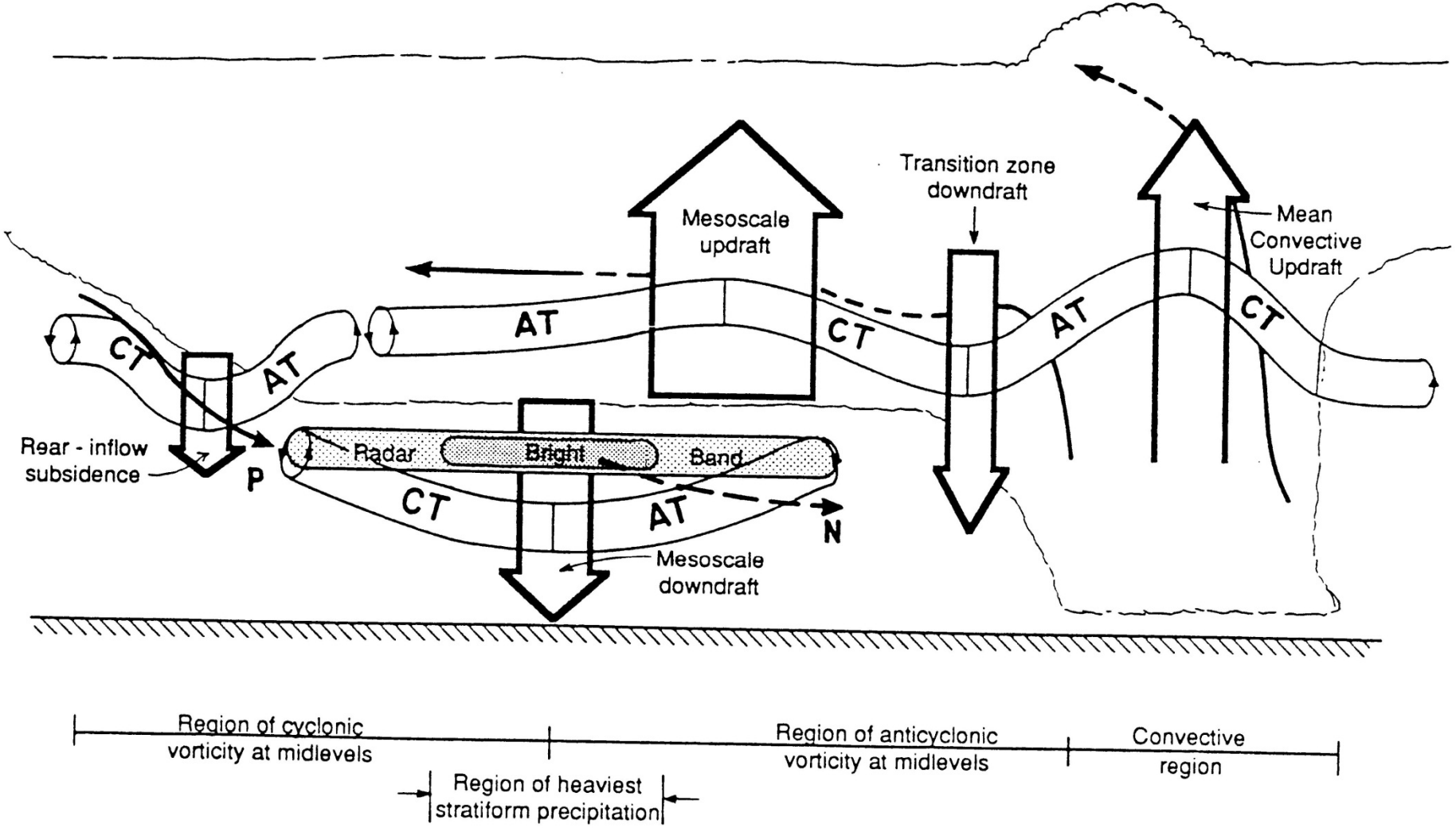

颮線系統內部相對垂直渦度分佈之概念圖 (Biggerstaff and Houze 1991)

Distribution of vertical vorticity inside a squall line system

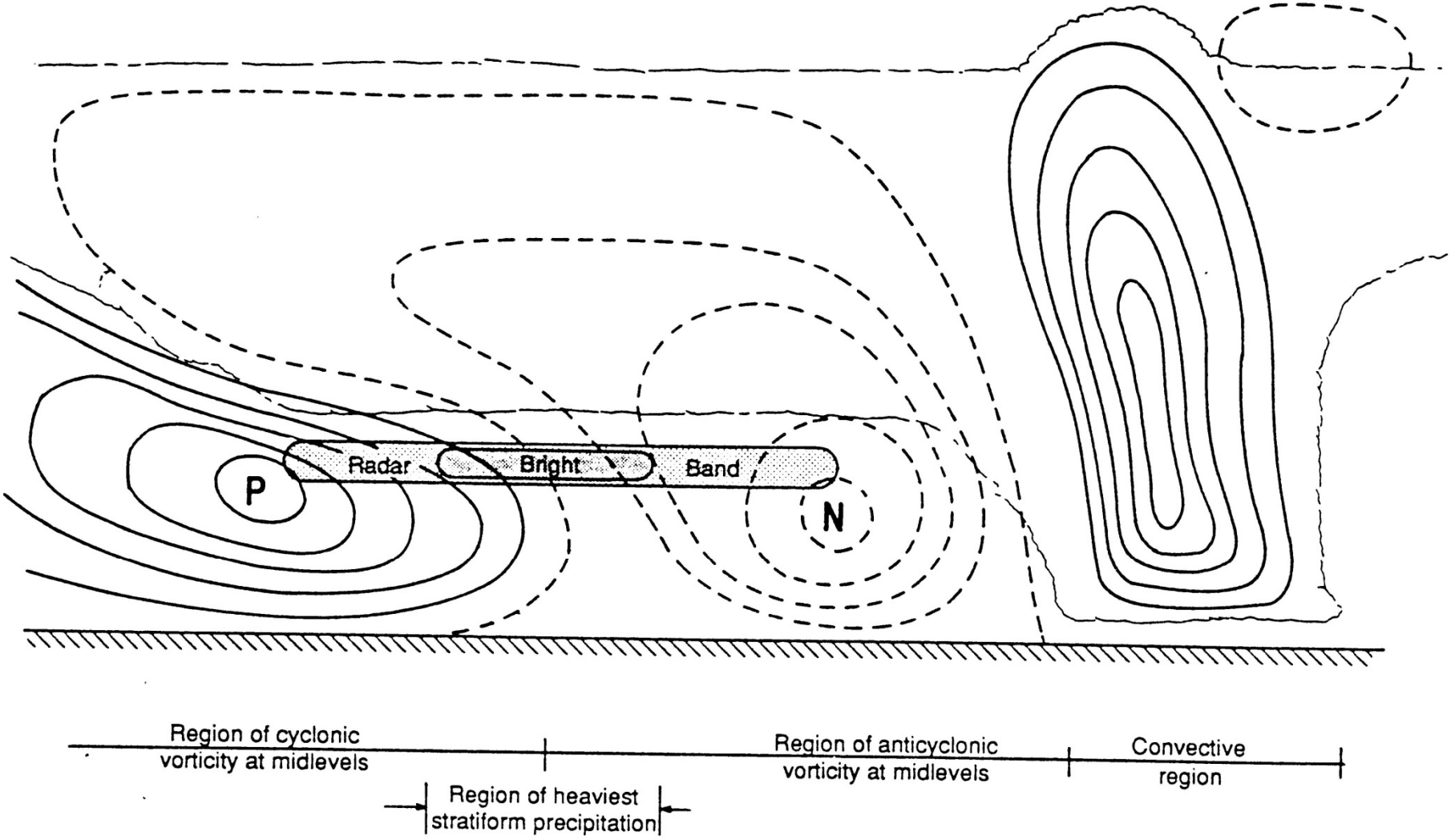

The tilting of ambient horizontal vorticity by vertical motions within a MCS (Wakimoto et al. 2015)

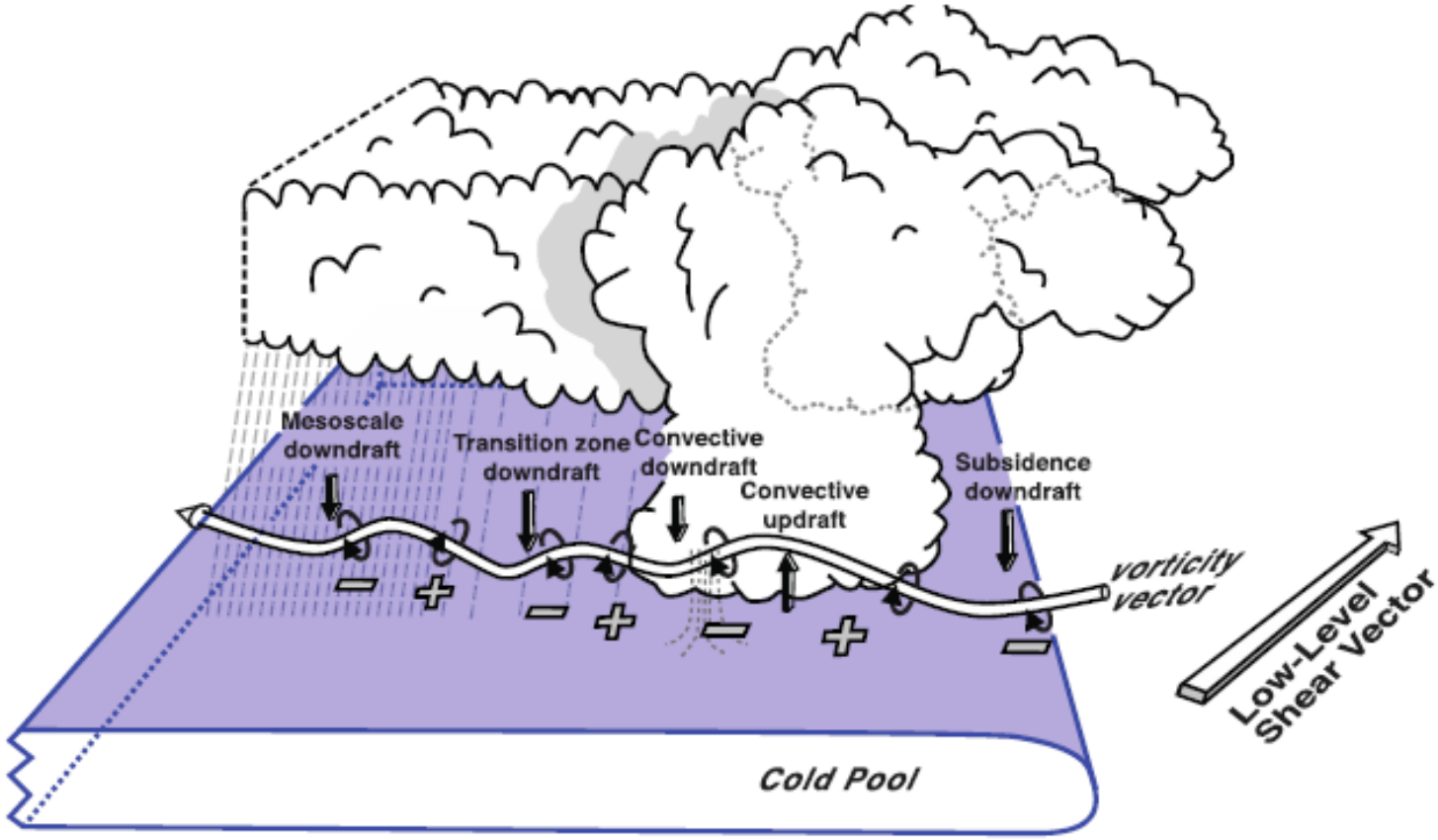

Fig. 16. Schematic model summarizing the tilting of ambient horizontal vorticity by the vertical motions within a mesoscale convective system during the early stage of development. The plus and minus signs denote the sign of vertical vorticity that are created.

Importance of the tilting of cold-pool-generated horizontal vorticity on contributing to the counterrotating circulations (Wakimoto et al. 2015)

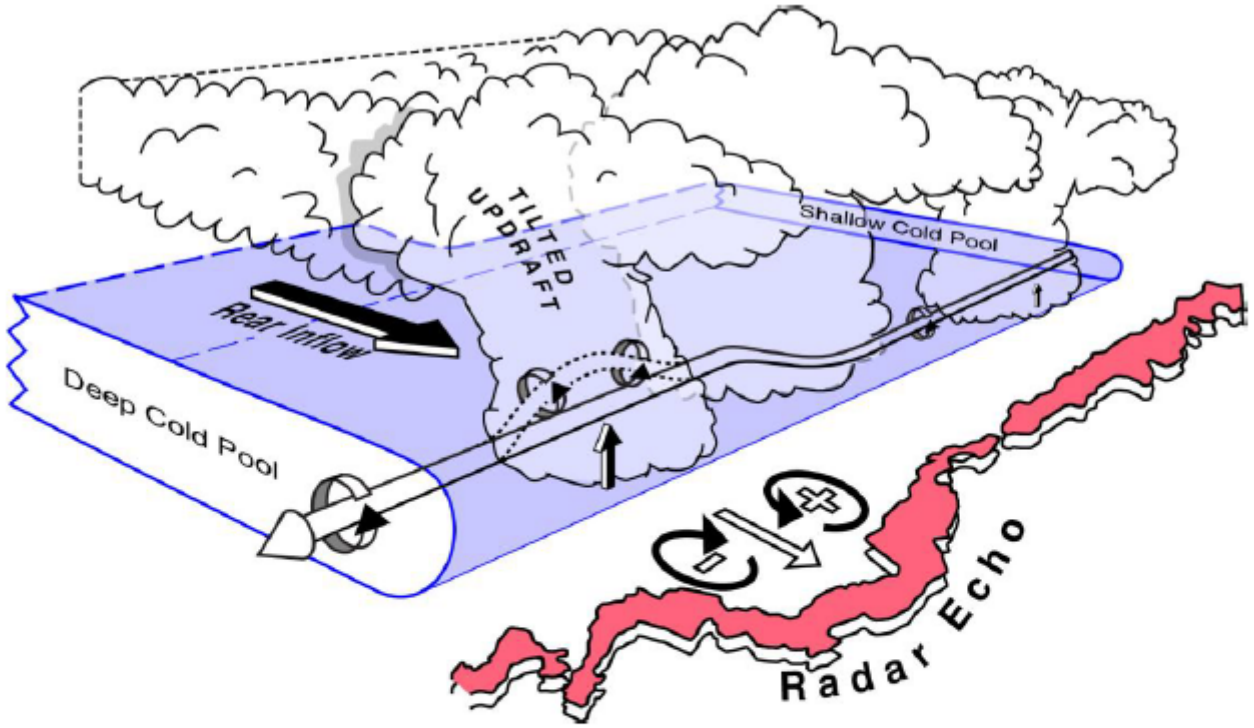

Fig. 17. Schematic model illustrating the development of the counterrotating circulations that contribute to the development of a subsystem or embedded bow echo. These circulations preferentially form at a local region where the cold pool is deep. Updrafts tilt the horizontal vorticity produced within the leading edge of the cold pool producing the counterrotating circulations. The circulations promote the development of a rear-inflow jet that is also augmented by the upshear-tilted updraft. Radar echo depiction of the embedded bow echo that develops is shown by the red shaded region in the schematic.

現階段關於中尺度對流系統內部MCV可能之垂直渦度來源概念圖 (Yu 1995)

Schematic showing different sources of vorticity contributing to the formation of MCV

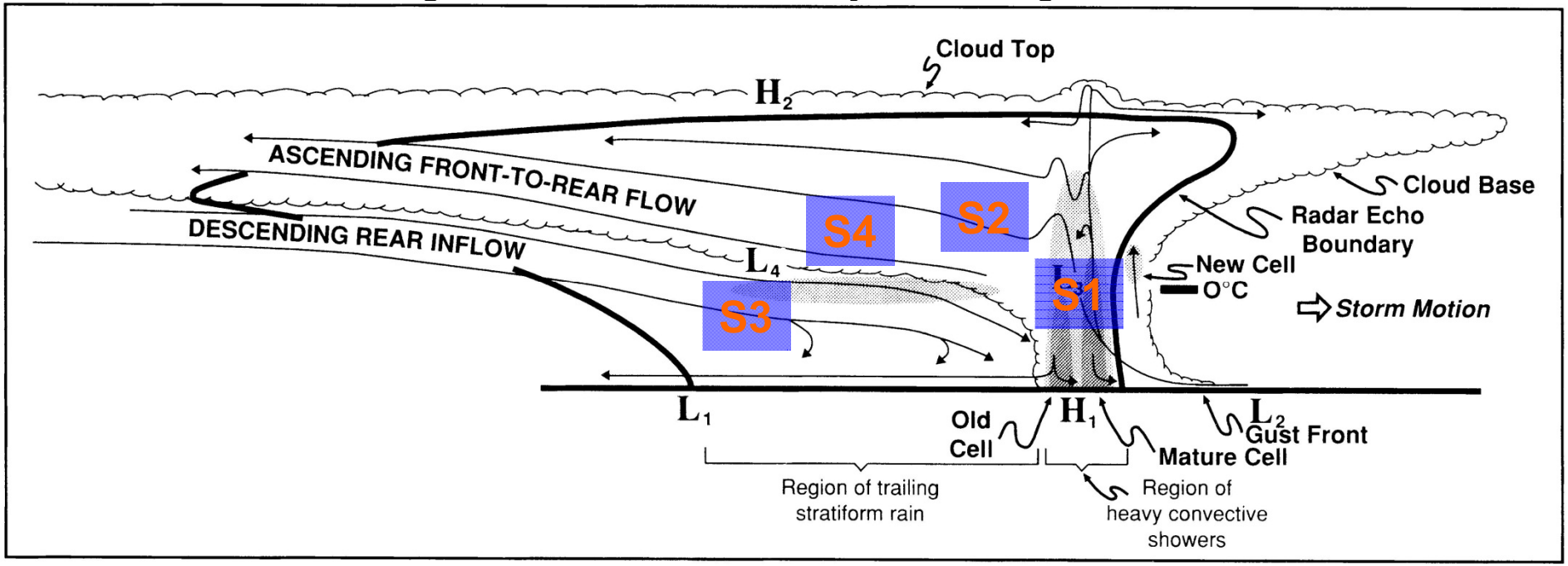

Source 1 (S1): 對流上(下)衝流之傾側效應 **(Yu et al. 1999; Weisman 1993)**

Source 2 (S2): 對流區所產生的垂直渦度向系統後緣傳送 **(Verlinde and Cotton 1990)**

Source 3 (S3): 透過中尺度下衝流之傾側效應 **(Brandes and Ziegler 1993; Biggerstaff and Houze 1991)**

Source 4 (S4): 透過中對流層輻合將原先存在的行星渦度與相對渦度增強 **(Johnson and Bartels 1992)**